

# This is to certify that the thesis entitled

# Biophysical and Structural Studies of HrpA, a Type III Secretion Pilin from Gamma-proteobacterial Plant Pathogens

presented by

Jason M. Criscione

has been accepted towards fulfillment of the requirements for the

M.S. degree in Chemistry

Major/Frofessor's Signature

11 August 2006

MSU is an Affirmative Action/Equal Opportunity Institution

LIBRARY Michigan State University

# PLACE IN RETURN BOX to remove this checkout from your record. TO AVOID FINES return on or before date due. MAY BE RECALLED with earlier due date if requested.

DATE DUE	DATE DUE	DATE DUE
<u>.</u>		

2/05 p:/CIRC/DateDue.indd-p.1

# BIOPHYSICAL AND STRUCTURAL STUDIES OF HRPA, A TYPE III SECRETION PILIN FROM GAMMA-PROTEOBACTERIAL PLANT PATHOGENS

Ву

Jason M. Criscione

# A THESIS

Submitted to
Michigan State University
in partial fulfillment of the requirements
for the degree of

MASTER OF SCIENCE

Department of Chemistry

2006

#### **ABSTRACT**

# BIOPHYSICAL AND STRUCTURAL STUDIES OF HRPA, A TYPE III SECRETION PILIN FROM GAMMA-PROTEOBACTERIAL PLANT PATHOGENS

Bv

#### Jason M. Criscione

The type III secretion system plays a vital role for the virulence of Gram-negative bacteria [8]. Gamma-proteobacterial plant pathogens utilize type III secretion to transport cytosolic effector proteins across the cell wall of its target host cell [24]. This essential cytosol-to-cytosol interaction is accomplished through the assembly of the type III secretion apparatus (TTSA). The TTSA in proteobacterial plant pathogens is comprised of a membrane-embedded base and a hollow extracellular filament termed the Hrp pilus [16]. The base features a complex basal body that spans the periplasm and is associated with both the inner and outer membranes (of the Gram-negative bacteria) [28]. The Hrp pilus elongates through addition of protein monomers (pilins) in helical repeat at its tip, to invade the plant host cell and serve as a conduit for transport of effector proteins [24]. The pilus is considered an attractive pharmaceutical target, both because it is extracellular and because its elimination renders the bacteria non-virulent.

This work focuses on determining the structure and biophysical properties of two unrelated HrpA pilins from proteobacterial plant pathogens, *Erwinia amylovora* and *Pseudomonas syringae*.

#### **ACKNOWLEDGMENTS**

I would like to express my gratitude to my research advisor, Dr. William Wedemeyer. As a research mentor, scientist, penseur, and friend, I hold you in the highest regard. You are a person of true intellect, passion, and wisdom. You have served as a beacon to guide me through my seemingly ever-winding journey through the world of science. I have taken a great deal away from this relationship, and it has been my pleasure to work with you.

I would like to thank my thesis committee members, Dr. Michael Feig and Dr. John McCracken, for their support and a challenging final examination.

I would like to thank the Wedemeyer laboratory for their support. Special thanks go to Terry Ball, Russell LaClair, and Joel Lwande. Terry provided me with essential instruction on several biochemical techniques and methods. He also performed some of the preliminary TEM and analytical ultracentrifugation experimentation. Russell contributed to the project by collecting some of the preliminary CD and HN-HSQC data. Joel provided me with information from his experience with several molecular biology techniques. He also collected the initial data for thermal melt analysis.

I would like to thank several laboratories that facilitated the experiments performed within this work. I am grateful to Dr. Babak Borhan and Marina Tanasova for the use of their CD instrument. The analytical ultracentrifugation data were collected at the MSU

Macromolecular Structure, Sequencing and Synthesis Facility, with the assistance of Dr. Joseph Leykam. The TEM images were taken at the MSU Center for Advanced Microscopy, with the assistance of Dr. Alicia Pastor-Lecha. The protein crystallization was a collaborative effort with Dr. Jennifer Ekstrom. We would like to thank Dr. R. M. Garavito and Dr. Nicole Webb for the use of their crystal screening robot. The solid-state NMR spectra were obtained during my tenure in Dr. David Weliky's laboratory. I would like to thank both Dr. Weliky for his guidance and expertise and the senior member of the group, Dr. Michele Bodner, for her instruction on experimental solid-state NMR techniques and for collecting some of the spectra displayed in this work.

# **TABLE OF CONTENTS**

LIST OF TABLES	vii
LIST OF FIGURES	viii
I. Introduction to Type III Secretion and the Role of the Hrp Pilus	1
I.A. Probing the Structure and Function of HrpA from P. syringae and E. amylovora	4
II. Computational Modeling of HrpA	5
II.A. Multiple Sequence Alignment (MSA)	5
II.B. Secondary-structure Predictions	7
II.C. Three-dimensional Modeling of the Hrp Pilus	8
III. Protein Preparation	12
III.A. Plasmid Constructs	12
III.A.i. Truncated, Wild-type HrpA from P. syringae pv. tomato [DC3000]	12
III.A.ii. Full-length, Wild-type HrpA from E. amylovora	13
III.B. Expression of Wild-type HrpA Pilins	13
III.C. Expression of the Truncated, Wild-type <sup>15</sup> N-labeled HrpA from <i>P. syringae</i>	14
III.D. Expression of Single-Residue-Labeled HrpA from P. syringae	15
III.E. Purification of HrpA Pilins	15
III.F. Cleavage of the N-terminal (His) <sub>6</sub> Tag on HrpA from P. syringae	21
IV. In Vitro Preparation of the Hrp Pilus	26
IV.A. Two Forms of HrpA: Monomer and Multimer	26
IV.A.i. 2,2,2-trifluoroethanol (TFE)	27

IV.A.ii. Salts	29
IV.A.iii. Stable Multimers of Uniform Dimensions	33
IV.A.iii.a. Adenosine Diphosphate (ADP)	33
IV.A.iii.b. Dickerson-Drew Dodecamer of DNA	. 34
V. Secondary and Tertiary Structure of Monomeric and Multimeric HrpA	. 37
V.A. Analytical Ultracentrifugation	. 38
V.B. Size Exclusion Chromatography	. 43
V.C. Solution-state 2D-NMR and HN-Heteronuclear Single Quantum Correlation (HN-HSQC)	44
V.D. Thermal Folding Transitions by UV Spectroscopy	. 46
V.E. Circular Dichroism (CD)	51
V.F. Solid-state NMR (SSNMR)	59
VI. Conclusions	72
VII. Works in Progress	74
VII.A. Unfolding/Dissociation Kinetics of Multimeric HrpA from P. syringae	74
VII.B. Preparation, Expression, Purification, and Fluorescence Microscopy of an N-terminal GFP-tagged HrpA Construct	
VII.C. Proline Mutations	. <b>77</b>
VII.D. Atomic-resolution Structural Studies: X-ray Crystallography and Electron Fiber Diffraction	. 81
VII.D.i. Crystallization of Monomeric HrpA and X-ray Diffraction	. 81
VII.E. Fiber Diffraction Studies of Multimeric HrpA	. 83
Appendix. Buffers and Stock Solutions	87
Bibliography	. 88

# LIST OF TABLES

Table 3.1	Gradient elution scheme from 0% to 100% NiB buffer	16
Table 3.2	Composition of % NiB in the eluted fractions	17
Table 3.3	SDS-PAGE sample preparation	17
Table 3.4	Size exclusion gel filtration system parameters	19
Table 5.1	JASCO J-810 acquisition parameters	52

# **LIST OF FIGURES**

Figure 1.1 Model of the TTSA of a proteobacterial plant pathogen where (A) is the Hrppilus, (B) is the membrane-embedded base, (C) is the plant host cell, (D) is the extracellular space, (E) is the outer bacterial membrane, (F) is the peptidoglycan layer, (G) is the periplasmic space, (H) is the inner bacterial membrane, (I) is the bacterial cytosol, (J) is the translocator protein, HrpA, chaperone complex, (K) is the effector protein, HrpZ, chaperone complex, (L) is the unstructured HrpA monomer, and (M) is the folded HrpA monomer associating with the tip of the growing pilus
Figure 2.1 Multiple Sequence Alignment (MSA) of HrpA from Pseudomonas syringae pv. maculicola (PSPVM), Pseudomonas syringae pv. tomato (PSPVTOM), Pseudomonas syringae pv. actinidiae (PSPVA), Pseudomonas syringae pv. delphinii (PSPVD), Pseudomonas syringae pv. magnoliae (PSPVM_1), Pseudomonas syringae pv. theae (PSPVTH), Pseudomonas syringae pv. tagetis (PSPVTA), Pseudomonas syringae (HRPA_PS), Pseudomonas syringae pv. oryzae (PSPVO), Erwinia pyrifoliae (ERW_PYR), Erwinia amylovora (ERW_AM and HRPA_ERWAM), Pantoea stewartii subsp. stewartii (PSSST), Pectobacterium carotovorum subsp. carotovorum (ERW_PC). Highly conserved, moderately conserved, and unconserved residues are represented by an outlined grey background with a white letter, an outlined white background with a boldface black letter, and a colorless background with a black letter, respectively 6
Figure 2.2 Predicted secondary structure of HrpA from P. syringae using SAM-T2K, where H and C represent Helix and Coil, respectively, and the intensity relates to the probability
Figure 2.3 Model for the self-assembly of the Hrp pilus
Figure 2.4 For a α-helix, contributions from polarized amide groups along the peptide backbone generate a net dipole moment (P) which points from the C-terminus to the N-terminus, neglecting side chain contribution. The direction of the induced electric field (E) is depicted by the dashed arrows
Figure 2.5 The electrostatic and hydrophobic clusters of the C-terminal helices of HrpA
Figure 3.1 Coomassie-stained SDS-PAGE gel of purified HrpA from (a) P. syringae and (b) E. amylovora
Figure 3.2 MALDI-TOF-MS spectrum of the truncated, wild-type HrpA from P. syringae. The peak centered at 9.8 kDa represents the truncated, wild-type HrpA and the peak centered at 7.9 kDa is a consistently observed degradation product of

Figure 3.3 Typical size exclusion chromatogram for HrpA from P. syringae20
Figure 3.4 Size exclusion chromatogram for isolation of cleaved HrpA22
Figure 3.5 SDS-PAGE gel depicting the time evolution of the thrombin digestion. Land 1 contains molecular weight standards. Lane 2 contains HrpA diluted in the 1X cleavage buffer pH 8.4. The band at 14.5 kDa represents the uncleaved HrpA and the band at ~8 kDa represents the consistently observed degradation product of HrpA that is consistent in weight with the (His)6 tag cleaved HrpA. Lanes 3 and 4 contains the contents from Lane 2 in the presence of thrombin (5 units/mg) at time t=0 and t=2 hours, respectively Lanes 5, 6, and 7 represent purified (His)6 tag cleaved HrpA collected from size exclusion fractions 10-12
Figure 3.6 HPLC chromatogram of purified, cleaved HrpA from P. syringae 24
Figure 3.7 MALDI-TOF-MS spectrum of cleaved HrpA from P. syringae25
Figures 4.1 (a,b) TEM images of <i>in vitro</i> Hrp pilus assembly for (a) uncleaved and (b (His) <sub>6</sub> tag cleaved wild-type, truncated HrpA from <i>P. syringae</i> in the presence of TFE
Figures 4.2 (a-h) TEM images of truncated, wild-type HrpA from <i>P. syringae</i> in the presence of 50 mM NaH <sub>2</sub> PO <sub>4</sub> buffer pH 5.5 with (a) no salt (b) 300 mM NaF, (c) 300 mM Na <sub>2</sub> SO <sub>4</sub> , (d) 300 mM NaCl, (e) 300 mM NaNO <sub>3</sub> , (f) 300 mM NaBr, (g) 300 mM NaI, and (h) 300 mM NaSCN
Figures 4.3 (a,b) TEM images of truncated, wild-type HrpA from P. syringae in the presence of 50 mM NaH <sub>2</sub> PO <sub>4</sub> buffer pH 5.5 doped with ADP
Figures 4.4 (a-b) TEM images of truncated, wild-type HrpA from <i>P. syringae</i> in the presence of 50 mM NaH <sub>2</sub> PO <sub>4</sub> buffer pH 5.5 doped with the Dickerson-Drew dodecame of DNA
Figure 5.1 Sedimentation velocity of truncated, wild-type HrpA from  P. syringae
Figure 5.2 Sedimentation equilibrium of truncated, wild-type HrpA from  P. syringae
Figure 5.3 HSQC spectrum of <sup>15</sup> N-labeled truncated, wild-type HrpA from <i>P. syringae</i> F1 and F2 correspond to <sup>15</sup> N and <sup>1</sup> H chemical shifts, respectively

Figure 5.4 Protein folding is observed by monitoring the absorbance differences exhibited by the tyrosine chromophore at 287 nm as the tyrosine transitions from being folded, or unexposed to the solvent (dotted line) to being unfolded, or exposed to the solvent (solid line)
Figure 5.5 Thermal melt analysis for the truncated, wild-type HrpA monomer from P. syringae
Figure 5.6 Thermal melt analysis for the uncleaved truncated, wild-type Hrp pilus from P. syringae
Figure 5.7 Thermal melt analysis for the (His) <sub>6</sub> tag cleaved truncated, wild-type Hrp pilus from P. syringae
Figure 5.8 (a) CD spectrum of the truncated, wild-type HrpA monomer from P. syringae in 50 mM NaH <sub>2</sub> PO <sub>4</sub> buffer at pH 5.5
Figure 5.8 (b) CD spectrum of the truncated, wild-type HrpA monomer from P. syringae in 10% TFE and 50 mM NaH <sub>2</sub> PO <sub>4</sub> buffer at pH 5.5
Figure 5.8 (c) CD spectrum at 5°C of the truncated, wild-type HrpA monomer from P. syringae in 50 mM NaH <sub>2</sub> PO <sub>4</sub> buffer pH5.5 with (A) 25 mM NaF, (B) 100 mM NaF, (C) 300 mM NaF, and (D) 600 mM NaF.
Figure 5.9 (a) CD spectrum at 5°C of the truncated, wild-type HrpA from P. syringae incorporated into the pilus in the presence of 10% TFE in 50 mM NaH <sub>2</sub> PO <sub>4</sub> buffer at pH 5.5
Figure 5.9 (b) CD spectrum at 5°C of the truncated, wild-type HrpA from P. syringae incorporated into the pilus in the presence 50 mM NaH <sub>2</sub> PO <sub>4</sub> buffer at pH 5.5 containing (A) no salt, (B) 10 mM NaF, (C) 50 mM NaF, (D) 100 mM NaF, and (E) 150 mM NaF.
Figure 5.10 (a) Increasing temperature ramp from 5-60°C and its associated pilus stability observed at (A) 5°C, (B) 10°C, (C) 20°C, (D), 40°C, and (E) 60°C
Figure 5.10 (b) Decreasing temperature ramp from 60-5°C and the refolding of the dissociated pilus at (A) 5°C, (B) 10°C, (C) 20°C, (D), 40°C, and (E) 60°C
Figures 5.11 (a-g) CPMAS signals for single isotopically labeled, truncated, wild-type HrpA from E. amylovora (a-c) and P. syringae (d-g) pili. HrpA from E. amylovora was labeled with <sup>13</sup> C=O (a) Ala, (b) Gly, and (c) Leu, and HrpA from P. syringae was labeled with <sup>13</sup> C=O (d) Ala, (e) Gly, (f) Lys, and (g) Met

Figure 5.12 REDOR-filtered signal from the 1-13C Ile-15N Leu unique pair in the
truncated, wild-type HrpA from P. syringae prepared pili
Figure 5.13 Local 2° structure information of multimeric HrpA by homology. Fo HrpA from $E$ . amylovora, the "*" and the "-" indicate residues involved in (1) an α-helix and (2) an α-helix or β-sheet, respectively. For HrpA from $P$ . syringae, the "+" indicate residues involved in an α-helix. The "^" indicates residues involved in an α-helix that occur at the same position in both sequences. Finally, the ">" indicates residues having the same sequence position in both pilins, but are involved in (1) an α-helix or (2) an α helix or β-sheet in $P$ . syringae or $E$ . amylovora, respectively
Figure 7.1 First-order exponential decay of Hrp pilus unfolding
Figures 7.2 (a-d) TEM images of (a) I89P mutant HrpA, (b) 1:1 molar ratio of I89P mutant and truncated, wild-type HrpA, (c) I101P mutant HrpA, and (d) 1:1 molar ratio of I89P mutant HrpA, and (d) 1:1 molar ratio of I8P mutant HrpA, and (d) 1:1 molar ratio of I8P mutant HrpA, and (d) 1:1 mol
I101P mutant and truncated, wild-type HrpA in the presence of 50 mM NaH <sub>2</sub> PO <sub>4</sub> buffe pH 5.5 with 300 mM NaF
Figure 7.3 Photograph of needle-like crystals of (His) <sub>6</sub> tag cleaved, truncated, wild-type HrpA from <i>P. syringae</i> obtained after two days of incubation at 5°C in 200 mN ammonium sulfate and 30% PEG 4000
Figure 7.4 TEM image for truncated, wild-type HrpA from <i>P. syringae</i> in the presence of 200 mM ammonium sulfate and 30% PEG 4000
Figure 7.5 Electron diffraction image for the TEM sample area in Figure 7.485

# I. Introduction to Type III Secretion and the Role of the Hrp Pilus

The type III secretion system plays a vital role in the virulence of many Gram-negative bacteria [8]. Both animal (e.g. Yersinia, Shigella, and Salmonella) and plant (e.g. Pseudomonas syringae and Erwinia amylovora) pathogenic bacteria utilize the type III secretion to transport effector proteins from their cytosol to that of their eukaryotic host cell [24]. These effector proteins suppress the innate immune response of the eukaryotic host to benefit the propagation of the Gram-negative bacteria [11]. Though these effectors vary greatly across bacterial species, the molecular transport machinery, the type III secretion apparatus (TTSA), is structurally and functionally conserved. More than 20 conserved translocation proteins are involved in constructing this macromolecular structure that spans the inner bacterial membrane, the periplasmic space, the peptidoglycan layer, the outer bacterial membrane, the extracellular space, and the host barrier [44] (Figure 1.1). Thus, virulence relies upon this essential cytosol-to-cytosol interaction mediated by the assembly of the TTSA [8].

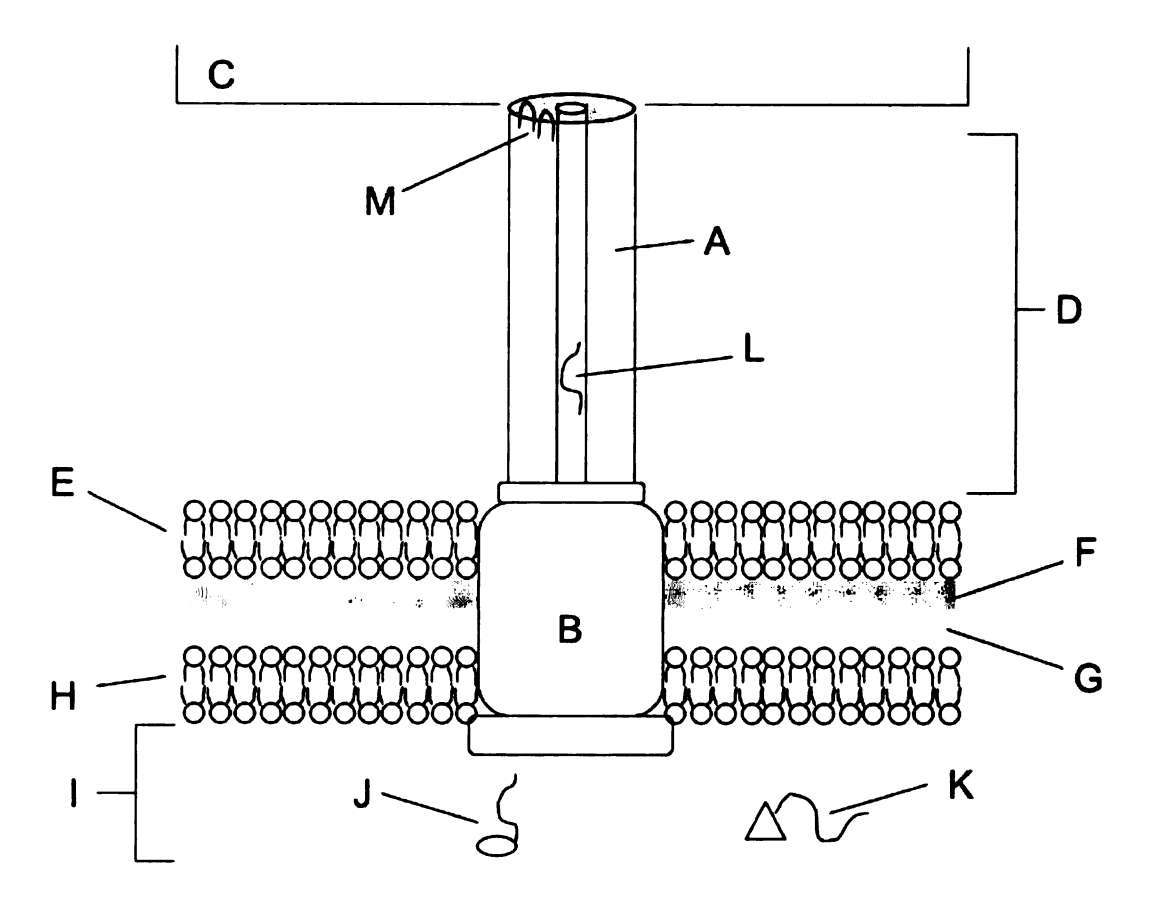


Figure 1.1 Model of the TTSA of a proteobacterial plant pathogen where (A) is the Hrp pilus, (B) is the membrane-embedded base, (C) is the plant host cell, (D) is the extracellular space, (E) is the outer bacterial membrane, (F) is the peptidoglycan layer, (G) is the periplasmic space, (H) is the inner bacterial membrane, (I) is the bacterial cytosol, (J) is the translocator protein, HrpA, chaperone complex, (K) is the effector protein, HrpZ, chaperone complex, (L) is the unstructured HrpA monomer, and (M) is the folded HrpA monomer associating with the tip of the growing pilus.

The TTSA is termed a "needle complex" [28] and is comprised of (1) a membrane-embedded base and (2) a hollow extracellular filament, termed either a needle or a hypersensitive response and pathogenticity (Hrp) pilus in animal or plant pathogens, respectively [16]. The Hrp pilus and the needle are structurally and functionally similar, sharing outer diameters of roughly 8 nm and small structural proteins (7-9 kDa). Although both filaments have been shown to elongate through assembly of monomeric

subunits [12] induced by bacterium-host cell-to-cell contact [6], a distinct difference is observed in their lengths. This is probably because of the differences in cell barriers of plant and animal cells, specifically the >100 nm thickness of plant cell wall [16].

The major structural protein of the Hrp pilus is encoded by the HrpA gene, an essential gene for the type-III-mediated hypersensitive response and pathogenicity [8]. The expressed and purified translocator protein, the HrpA pilin from *Pseudomonas syringae pathovar tomato* strain [DC3000], has been shown to reassemble into Hrp pili *in vitro* [36]. Immunocytochemistry has shown that the Hrp pilus elongates by addition of HrpA pilin subunits at its distal end and that the effector protein HrpZ is only secreted from the tip of the pilus [24]. Thus, the Hrp pilus is thought to penetrate the plant cell wall [5] and serve as a conduit for transport of effector proteins [17].

The mechanism for the association of HrpA monomers to form the pilus is not well-understood. In this work, we hypothesize that HrpA, albeit natively unstructured as a monomer, adopts a stable fold that is predominantly α-helical upon incorporation into the Hrp pilus. This hypothesis is consistent with the existing evidence that Hrp pilus assembly requires that the translocation of HrpA to the membrane-embedded base be assisted by a chaperone [33]. Dissociation of the chaperone upon reaching the base enables the natively unfolded HrpA to flow through the 2 nm inner diameter of the forming pilus. Upon reaching the tip of the pilus, the HrpA monomer folds to continue the assembly [24]. It is important to elucidate this mechanism because the pilus is considered to be an attractive pharmaceutical target, both because it is extracellular and

because its elimination renders the bacteria non-virulent. The development of a small-molecule inhibitor would serve to prevent the spread of crop diseases, including wilting, blight, and leaf spots.

#### I.A. Probing the Structure and Function of HrpA from P. syringae and E. amylovora

This work focuses on two unrelated HrpA pilins from plant pathogens, *Erwinia amylovora* and *Pseudomonas syringae pv. tomato* [DC3000]. Conventional structure-determination methods, such as X-ray crystallography and solution-state NMR, have so far failed to obtain a structure for these proteins. We wish to overcome this obstacle and determine the three-dimensional structure of both the HrpA pilin and Hrp pilus to aid in drug design. This work will attempt to address several fundamental questions regarding the structure and function of both the pilin and the self-assembled pilus: (1) What is the structure of the HrpA monomer? (2) What is the structure of the Hrp pilus? (3) What are the physical/chemical forces that stabilize the pilus? (4) What mechanistic information is contained with the kinetics of pilus formation?

The following chapter presents a computational model for the predicted structure of the HrpA monomer and for the assembly of the Hrp pilus. Subsequent chapters show the use of several spectroscopic methods designed specifically to determine the structure and function of both HrpA and the Hrp pilus.

# II. Computational Modeling of HrpA

Currently, the structure of the Hrp pilus and the mechanism of its self-assembly are not well-understood. In this work, we have designed a computational, 3D model of the pilus to depict both the electrostatic and hydrophobic interactions that might initiate and stabilize the growth of the pilus *in vitro*. Spectroscopic methods can then be designed to test the validity of this model.

### II.A. Multiple Sequence Alignment (MSA)

The full-length, wild-type HrpA from *P. syringae* and *E. amylovora* were individually subjected to two iterations of PsiBLAST [2,3], respectively. Using the non-redundant database and an E-value cutoff of 10<sup>-6</sup> to obtain homologous sequences, 10 PsiBLAST hits were obtained for HrpA from *P. syringae*; additional iterations yielded no new hits. Lowering the E-value threshold to 10<sup>-3</sup>, 5 hits were obtained for HrpA from *E. amylovora*; additional iterations yielded no new hits. The final basis set included the 9 most identical sequences to *P. syringae* and the 5 sequences from *E. amylovora*, all derived from *Gammaproteobacteria*. These sequences were aligned using the best-validated multiple sequence alignment server, T-Coffee [34] and depicted using ESPript [14] (Figure 2.1). Residue conservation was assessed by the mean BLOSUM62 score among residues at a given position and by the sequence entropy

Entropy at position 
$$i = \sum p_k \log_2 p_k$$
 (1)

where  $p_k$  is the fraction of amino-acid type k at position i, where the summation spans all possible amino-acid types k. The lower the entropy, the higher the conservation at the position: a zero entropy implies that only one residue appears at that position,  $p_k = 1$ .

	1	10	20	30	40	50 60
PSPVM	HVAFAGI	TSKLTRLGRS.	VARVEGAROR	VNTVASNATL	OKNILLGI GE	SLEVENDA NA REEL SEANGER
PSPYTON	MVAFAGI	TSKLTNLGNS.	Vegycanto	VNTVASNATL	OKNILLGT CH	SLSVDNOAKASKESDANGAR
PSPVA						SLEVENOAKASKESDANGAR
PSPVD						SLSVDAGAKASKOSDANGAK
PSPVM 1						SLEVENDAKASTESDANGAR
PSPVTH						SLSVENOAKASTESDATCAS
PSPVTA						SLSVAMOTKAS EETDANGAR
HrpA PS						SLSLABONKAS NEMDIANGAO
PSPVO	RPAPPST	TASLTOAGTG!	ANGIRGALOG	ANTIASAANM	DENVIAGTORES	SLELAMONXAGNE MDANGA
ERW PYR	AL ALL DI	. obbigha. o				LLTSUSSSASTIESANGO
ERW AN						. SLTSASTSASETLESAMO
PERST			MEGILTOLME			PLASETSPRENTINGAMEN
ERN PC			V-9			LSQVASQAASOTLDTAMAG
HRPA ERMAN			V. V.			. SLIS STSASETLE SAMO
	70	40	*0	100	110	
PSPVM PSPVTOM PSPVA PSPVD	70 LEAMOAG LEAMOAG	60 ETHKROTHOV ETHKROTHOV ETHKROTHOV	NAIQAGKEDS	SMEKISATAT	NAKGISY	
PSPVA PSPVA PSPVD PSPVM_1		ETHKROTHOVE ETHKROTHOVE ETHKROTHOVE ETHKROTHOVE ETHKROTHOVE	NA DAGKEDS NA DAGKEDS NA DAGKEDS NA DAGKEDS	THE KISATAT THE KISATAT SHEKISATAT THE KISSTAT SHEKISATAT	NAKGISY NAKGISY NAKGISY NAKGISY NAKGISY	
PSPVA PSPVA PSPVD PSPVM_1 PSPVTH	LTAMOAC LTAMOAC LTAMOAC LTAMOAC LTAMOAC LTAMOAC	ETHEROTHOVE ETHEROTHOVE ETHEROTHOVE ETHEROTHOVE ETHEROTHOVE ETHEROTHOVE	NATOAGKEOS NATOAGKEOS NATOAGKEOS NATOAGKEOS NATOAGKEOS	THERESATAT THERESATAT SHEKISATAT THERESATAT THERESATAT SHEKISATAT THERESATAT THERESATAT	NAKGISY NAKGISY NAKGISY NAKGISY NAKGISY NAKGISY	
PSPVA PSPVA PSPVA PSPVA PSPVTA PSPVTA	LÍAHOAC LIAHOAC LIAHOAC LIAHOAC LIAHOAC LIAHOAC LIAHOAC	ETHEROTHOVE ETHEROTHOVE ETHEROTHOVE ETHEROTHOVE ETHEROTHOVE ETHEROTHOVE	NATOAGKEOS NATOAGKEOS NATOAGKEOS NATOAGKEOS NATOAGKEOS NATOAGKEOS NATOAGKEOS	THE KISATAT THE KISATAT SHEKISATAT THE KISSTAT SHEKISATAT THE KISATAT THE KISATAT THE KISATAT	NAKGISY NAKGISY NAKGISY NAKGISY NAKGISY NAKGISY NAKGISY	
PSPVTON PSPVA PSPVD PSPVM_1 PSPVTH PSPVTA RrpA_PS	LTAMOAC LTAMOAC LTAMOAC LTAMOAC LTAMOAC LTAMOAC	ETHEROTHOVE ETHEROTHOVE ETHEROTHOVE ETHEROTHOVE ETHEROTHOVE ETHEROTHOVE	NATOAGKEOS NATOAGKEOS NATOAGKEOS NATOAGKEOS NATOAGKEOS NATOAGKEOS NATEAGKEOS	THIKISATAT THIKISATAT THIKISATAT SHIKISATAT THIKISATAT THIKISATAT THIKISATAT THIKISATAT THIKISATAT THIKISATAT	NAKGISY NAKGISY NAKGISY NAKGISY NAKGISY NAKGISY NAKGISY	
PSPVTON PSPVA PSPVD PSPVM_1 PSPVTH PSPVTA RIPA_PS PSPVO	LÍAHOAC LIAHOAC LIAHOAC LIAHOAC LIAHOAC LIAHOAC LIAHOAC	ETHKROTHOU ETHKROTHOU ETHKROTHOU ETHKROTHOU ETHKROTHOU ETHKROTHOU EAGRATHOU EAGRATHOU ETRKROTHOU ETKROTHOU ETKROTHOU		THIRKISATAT THIRKISATAT SHIRKISATAT THIRKISATAT THIRKISATAT THIRKISATAQ THIRKISATAQ THIRKISATAQ THIRKISATAQ	NAKCISY NAKCISY NAKCISY NAKCISY NAKCISY NAKCISY NAKCISY NAKCISY NAKCISY NAKCISY NAKCISY	
PSPVTOM PSPVA PSPVD PSPVW_1 PSPVTA HrpA_PS PSPVO ERM_PYR	LÍAHOAC LIAHOAC LIAHOAC LIAHOAC LIAHOAC LIAHOAC LIAHOAC	ETHKROTMOV. ETHKROTMOV. ETHKROTMOV. ETHKROTMOV. ETHKROTMOV. ETHKROTMOV. ETHKROTMOV. ETHKROTMOV. ETKKROTMOV. ETKKROTMOV. AOASRHKMOT.	A CACACACACACACACACACACACACACACACACACAC	THINKISATAT THINKISATAT SHIKKISATAT THINKISATAT THINKISATAT THINKISATAT THINKISATAQ THINKISATAQ ANIMIKISATAQ	NAKGISY NAKGISY NAKGISY NAKGISY NAKGISY NAKGISY NAKGISY NAKGISY NAKGISY	
PSPVTON PSPVA PSPVD PSPVM_1 PSPVTH PSPVTA RIPA_PS PSPVO	LEAMOAC LUAMOAC LUAMOAC LUAMOAC LUAMOAC LUAMOAC LUAMOAE LUAMOAE LUAMOAE LUAMOAE LUAMOAE SLITESAN	ETHKROTMOV. ETHKROTMOV. ETHKROTMOV. ETHKROTMOV. ETHKROTMOV. ETHKROTMOV. ETRKROTMOV. ETRKROTMOV. ETRKROTMOV. ETRKROTMOV. ACASRMKMOT.		THINKISATAT THINKISATAT THINKISATAT THINKISATAT THINKISATAT THINKISATAT THINKISATAQ THINKISATAQ THINKISATAQ ASSISINSCHN	NAKGISY NAKGISY NAKGISY NAKGISY NAKGISY NAKGISY NAKGISY NAKGISY NAKGISY NAKGISY NAKGISY NAKGISY	
PSPVTOM PSPVA PSPVD PSPVW_1 PSPVTA HrpA_PS PSPVO ERM_PYR	LEAMOAC LUAMOAC LUAMOAC LUAMOAC LUAMOAC LUAMOAC LUAMOAE LUAMOAE LUAMOAE LUAMOAE LUAMOAE SLITESAN	ETHKROTMOV. ETHKROTMOV. ETHKROTMOV. ETHKROTMOV. ETHKROTMOV. ETHKROTMOV. ETHKROTMOV. ETHKROTMOV. ETKKROTMOV. ETKKROTMOV. AOASRHKMOT.		THINKISATAT THINKISATAT THINKISATAT THINKISATAT THINKISATAT THINKISATAT THINKISATAQ THINKISATAQ THINKISATAQ ASSISINSCHN	NAKGISY NAKGISY NAKGISY NAKGISY NAKGISY NAKGISY NAKGISY NAKGISY NAKGISY NAKGISY NAKGISY NAKGISY	
PSPVTOM PSPVA PSPVD 1 PSPVTH PSPVTA Hrpa PS PSPVO ERM PYR ERM AM	LEAMOAC LEAMOAC LEAMOAC LEAMOAC LEAMOAC LEAMOAC LEAMOAC LEAMOAE LEAMOAE SLITESAN SLITESAN SLITESAN	ETHKROTMOV. ETHKROTMOV. ETHKROTMOV. ETHKROTMOV. ETHKROTMOV. ETHKROTMOV. ETRKROTMOV. ETRKROTMOV. ETRKROTMOV. ETRKROTMOV. ACASRMKMOT.	MAIOA (RE 0 S A I (A C A C A C A C A C A C A C A C A C A	TM KKISATAT TM KKISATAT TM KKISATAT SM KKISATAT SM KKISATAT TM KKISATAT TM KKISATAT TM KKISATAT TM KKISATAO TM KKISATAO TM KKISATAO TM KKISATAO TM KKISATAO ASKSLMSGHM ASKSIMSGHM ASKSIMSGHM	NAKGISY NAKGISY NAKGISY NAKGISY NAKGISY NAKGISY NAKGISY NAKGISY NAKGISY AAKA OF	

Figure 2.1 Multiple Sequence Alignment (MSA) of HrpA from Pseudomonas syringae pv. maculicola (PSPVM), Pseudomonas syringae pv. tomato (PSPVTOM), Pseudomonas syringae pv. actinidiae (PSPVA), Pseudomonas syringae pv. delphinii (PSPVD), Pseudomonas syringae pv. magnoliae (PSPVM\_1), Pseudomonas syringae pv. theae (PSPVTH), Pseudomonas syringae pv. tagetis (PSPVTA), Pseudomonas syringae (PSPVTH), Pseudomonas syringae pv. tagetis (PSPVTA), Pseudomonas syringae (PSPVD), Erwinia pyrifoliae (ERW\_PYR), Erwinia amylovora (ERW\_PV), Erwinia emplovora (ERW\_PV), Pseudomonas syringae voi tagetis stewartii (PSSST), Pectobacterium carotovorum subsp. carotovorum (ERW\_PC). Highly conserved, moderately conserved, and unconserved residues are represented by an outlined grey background with a white letter, an outlined white background with a boldface black letter, and a colorless background with a black letter, respectively.

# II.B. Secondary-structure Predictions

Secondary-structure predictions were performed using the three best-validated [22] secondary-structure servers, PsiPRED [18, 29], SABLE2 [1], and SAM-T2K [19]. The results were visualized using our web-server <a href="http://proteins.msu.edu/Servers/Secondary\_Structure/visualize\_secondary\_structure\_pred">http://proteins.msu.edu/Servers/Secondary\_Structure/visualize\_secondary\_structure\_pred</a> ictions.html.

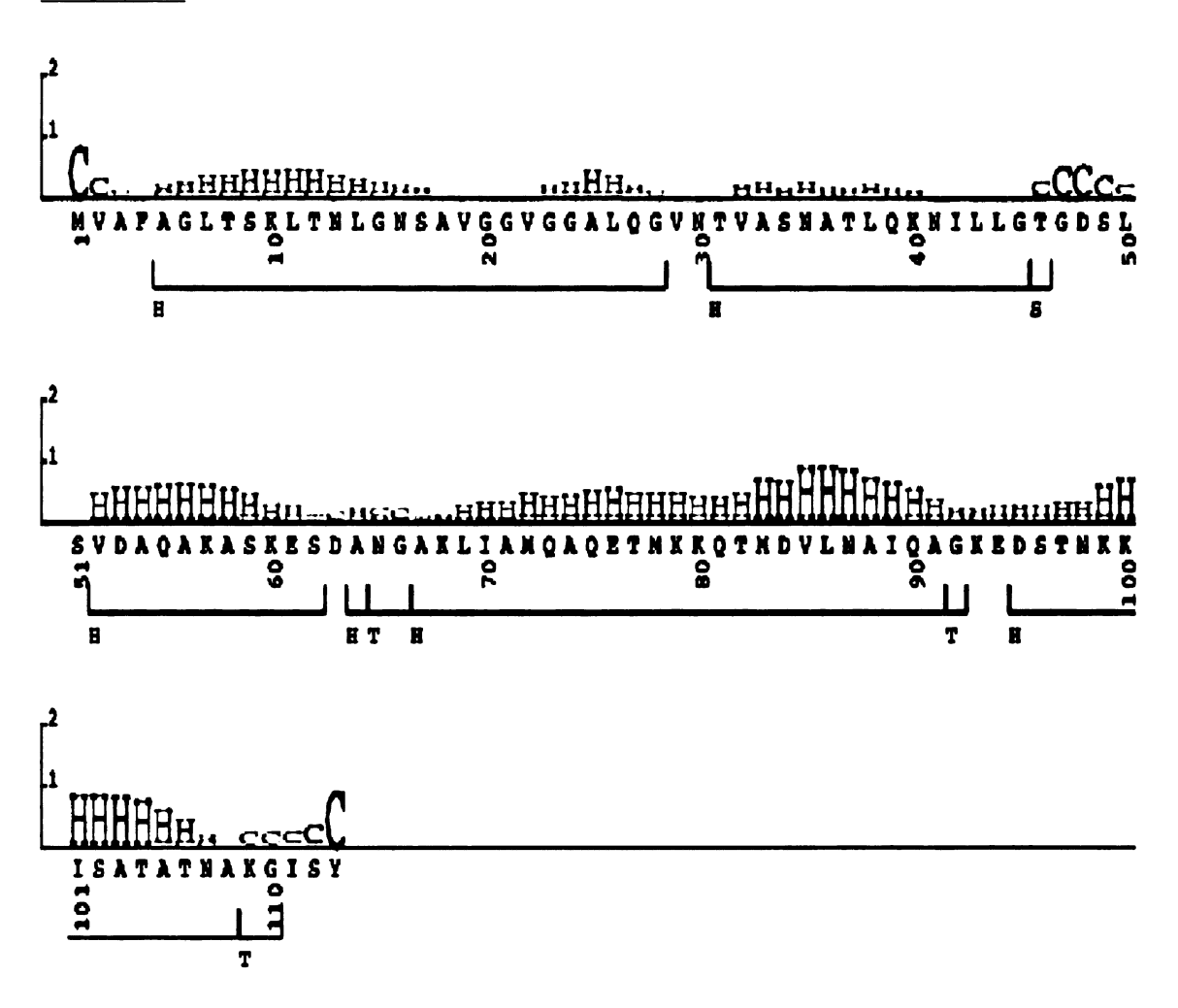


**Figure 2.2** Predicted secondary structure of HrpA from *P. syringae* using SAM-T2K, where H and C represent Helix and Coil, respectively, and the intensity relates to the probability.

The secondary-structure predictions generated by PsiPRED and SABLE2 were consistent with that of SAM-T2K (Figure 2.2), which shows the presence of distinct  $\alpha$ -helical regions.

# II.C. Three-dimensional Modeling of the Hrp Pilus

Jin et al. and Li et al. have shown, through immunocytochemistry, that the effector proteins, HrpZ and AvrPto, are extruded from the tip of the Hrp pilus, an observation which supports the conduit model [17, 24]. This observation also provides direct support for a shared mechanism in type III secretion and flagellar assembly, for the eight hrc genes involved in pilus assembly are homologous to those involved in flagellar assembly [10]. This hypothesis was experimentally confirmed by Li et al. who showed that newly produced HrpA proteins are added to the tip of the growing Hrp pilus [24].

In 2004, K. Namba *et al.* reported a plausible 3D structural model for the *Salmonella typhimurium* flagellum. This model was created using a partial structure obtained by X-ray diffraction and an image-reconstruction from electron cryomicroscopy [32,37]. Although the flagellin protein is much larger than the pilin protein, its N and C-termini associate as antiparallel  $\alpha$ -helices in the innermost core of the flagellum. These terminal  $\alpha$ -helices are the most closely corresponding parts of the flagellin to the HrpA pilin. In the Namba model, these helices are roughly parallel to the flagellar axis.

In this work, we combined our results from the MSA and the secondary-structure predictions along with the flagellar model to generate a putative model for the self-assembly of the Hrp pilus (Figure 2.3).

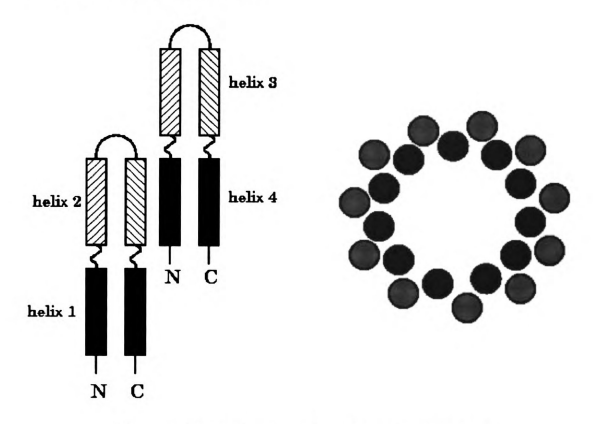


Figure 2.3 Model for the self-assembly of the Hrp pilus

According to this model, the folded form of the HrpA pilin in the pilus adopts an  $\alpha$ -helical hairpin conformation, with the turn centered on the TMKK (QASK) motif of HrpA from P. syringae (E. amylovora). The helices are arranged roughly parallel to the pilus axis, with the C-terminal half forming the inner wall and the N-terminal half the outer wall. Since, each C-terminal helix should contribute equally to the net dipole moment of the pilus, an electric field is produced within the pilus that is directed along its axis pointing from the tip to the base of the pilus (i.e. from the plant host cell to the outer

bacterial membrane). The electric field will help drive the transport of the negatively charged effector proteins toward the host cell (Figure 2.4). Being an  $\alpha$ -helix, the side chains of the C-terminal half should point from the base to the tip of the pilus (i.e. away from the bacterial cell and towards the host cell), thus inhibiting back-diffusion of the effector proteins.

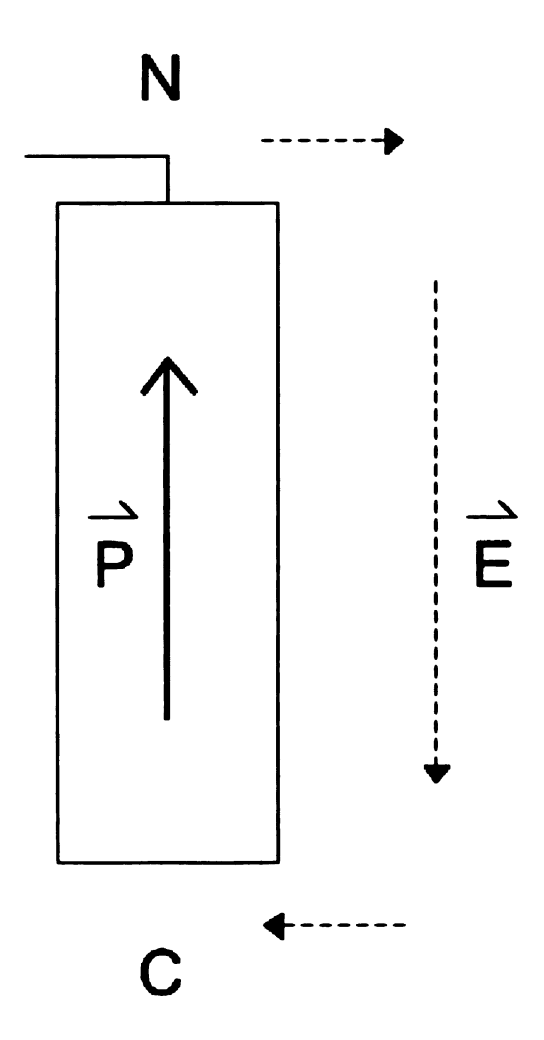


Figure 2.4 For a  $\alpha$ -helix, contributions from polarized amide groups along the peptide backbone generate a net dipole moment (P) which points from the C-terminus to the N-terminus, neglecting side chain contribution. The direction of the induced electric field (E) is depicted by the dashed arrows.

When combined with the MSA, this model allows us to identify clusters of interacting residues, since the helices of adjacent subunits are half-staggered. Using this reasoning,

we propose two clusters of interacting side chains for HrpA from *P. syringae*, one electrostatic and the other hydrophobic. The electrostatic cluster (Figure 2.5) consists of 7 residues from 3 subunits: K79, K80, D84, and N87 of subunit 1; D95, K99, and K100 of subunit 2; and finally, K109 and the C-terminal carboxylate of subunit 3. The hydrophobic cluster (Figure 2.5) consists of 7 residues from 2 subunits: 189, G92, and S96 of subunit 1 and A108, G110, I111, and Y113 of subunit 2.

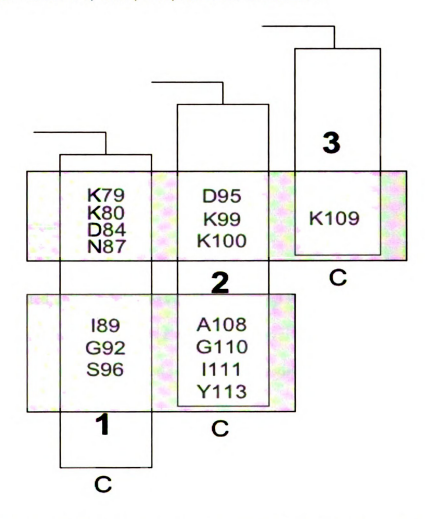


Figure 2.5 The electrostatic and hydrophobic clusters of the C-terminal helices of HrpA

# III. Protein Preparation

To test the computational model, the pilins must be expressed and purified for subsequent experimentation. The following sections show methods developed and optimized to express and purify the HrpA pilins from *Erwinia amylovora* and *Pseudomonas syringae* for physical and spectroscopic measurements. Methods for expressing isotopically labeled HrpA pilins from each of these plant pathogens are discussed, as well as thrombin digestion of the N-terminal (His)<sub>6</sub> tag on the purified truncated, wild-type HrpA from *P. syringae* for subsequent crystallization trials. Preparation of a novel GFP-tagged HrpA construct is also described.

#### III.A. Plasmid Constructs

As previously stated, this work focuses on two unrelated Hrp pilins from plant pathogens, Psuedomonas syringae pv. tomato and Erwinia amylovora. The two plasmids described below were prepared in the laboratories of Dr. D. Arvidson and Dr. G. Sundin of MSU, respectively.

## **III.A.i.** Truncated, Wild-type HrpA from *P. syringae pv. tomato* [DC3000]

Truncated HrpA (residues 41-115) from the DC3000 strain of *P. syringae pv. tomato* was cloned using the NdeI and HindIII restriction sites into a pET28b expression vector. This truncated sequence not only represents the portion of the protein that aligns with the full-

length *Erwinia amylovora* sequence, but is also observed to be the shortest naturally multimerizing sequence [36]. The construct was verified by DNA sequencing.

#### III.A.ii. Full-length, Wild-type HrpA from E. amylovora

The full-length HrpA from the Eal10 strain of *E. amylovora* was cloned using the NdeI and BamHI restriction sites into a pET28a expression vector from Novagen [45]. The construct was verified by DNA sequencing.

#### III.B. Expression of Wild-type HrpA Pilins

The pET28 expression vector codes for the *lac* repressor gene (*lac1*) and for antibiotic resistance to kanamycin. Isopropyl-beta-D-thiogalactoside (IPTG), a lactose analogue, induces the *lac* operon by initiating a conformational change in *lac1*. This induction enables the expression system to express the protein of interest.

Using sterile techniques, an aliquot of the BL21(DE3) Escherichia coli (E. coli) cells transformed with the HrpA expression vector was plated on an agar plate containing sterilized LB media and 50 µg/mL kanamycin, and incubated at 37°C for 24 hours. Several 15 mL sterile Corning conical tubes, each containing 5 mL of sterilized LB media and 50 µg/mL kanamycin, were inoculated with single colonies from the plate. These starter cultures were grown to a translucent consistency on a New Brunswick Scientific Series 25 Incubator shaker at 250 rpm and 37°C for 6 hours. These starter

cultures were utilized to innoculate 1 L shake flasks of the LB media described above. These 1 L cultures were grown to an OD<sub>600</sub> of 1.5-2.0 at 250 rpm and 37°C for 18 hours. These cultures were induced with 1 mM filter sterilized IPTG for 6 hours at 250 rpm and 37°C to obtain optimal expression of HrpA. The cells were harvested by centrifugation at 4°C. 1 L centrifuge bottles were spun at 4000 rpm in a Sorvall SLC-4000 rotor for 15 minutes. The supernatant was decanted and the resulting wet cell pellet was divided into 5-6 gram aliquots and stored at -80°C for the subsequent extraction and purification of HrpA.

III.C. Expression of the Truncated, Wild-type <sup>15</sup>N-labeled HrpA from P. syringae

The truncated, wild-type <sup>15</sup>N-labeled HrpA from *P. syringae* was expressed according to the protocol described in section III.B. with the following modifications. After the 1 L culture had reached an OD<sub>600</sub> of 1.0, it was pelleted by centrifugation at 4000 rpm in a Sorvall SLC-4000 rotor at 4°C for 15 minutes. The pellet was resuspended in 1 L of 1X M9 minimal medium [40] containing 50 µg/mL kanamycin and 1 g/L of <sup>15</sup>N-labeled ammonium chloride. The resulting culture was incubated with shaking at 37°C and 1 mM IPTG was immediately added to induce expression of the isotopically labeled HrpA. After a 6 hour induction period, the cells were harvested by centrifugation as above.

# III.D. Expression of Single-Residue-Labeled HrpA from P. syringae

The truncated, wild-type single-residue-labeled HrpA from *P. syringae* was expressed according to the modified protocol described in section III.C with the following modification. To accomplish single-residue labeling (e.g. 1-<sup>13</sup>C or <sup>15</sup>N-labeled alanine), 100 mg of the isotopically labeled amino acid of interest (section **V.F**) were introduced to the 1 L culture after the media switch and just prior to induction with 1 mM IPTG.

## III.E. Purification of HrpA Pilins

The pET28 expression vector includes an N-terminal hexahistidine [(His)6] tag and a thrombin cleavage site (Leu-Val-Pro-Arg-Gly-Ser) immediately N-terminal to the HrpA insert. Our standard purification protocol exploits the (His)6 tag.

The 5-6 gram aliquots of wet cells were thawed and resuspended in 40 mL of Nickel A (NiA) buffer (Appendix) in the presence of two EDTA-free protease inhibitor tablets. Cell lysis was performed by pulse sonication at 50 W and the resulting lysate was incubated on ice. The lysate was transferred to 50 mL Oak Ridge centrifuge tubes and pelleted by centrifugation, using a Sorvall RC5C Plus centrifuge and a SS-34 rotor, at 11,000 rpm at 4°C for 20 minutes. The supernatant was heat-treated at 70°C to remove protein impurities and then re-centrifuged at 12,000 rpm. The supernatant was retained and kept on ice.

Extraction and isolation of the HrpA is facilitated by (His)<sub>6</sub> tag, which has an inherent affinity for chelating to Ni(II). The first stage of purification is accomplished by a Ni-affinity column chromatography. An FPLC column was packed with 15 mL of Ni-NTA agarose and washed, by gravity filtration, with three column volumes of the 20 mM imidazole NiA buffer. 120 mL of lysate supernatant were allowed to bind to the column by gravity filtration. The column was washed with three column volumes of the following buffers: 1) NiA, 2) NiA + 6M Urea, and 3) NiA + 600 mM NaCl (Appendix). The column was installed onto a Pharmacia Biotech FPLC system for purification. The His-tagged HrpA was eluted with a gradient of imidazole, contained in NiB buffer (Appendix) according to the following program on the Pharmacia Biotech Programmer GP-250 Plus (Table 3.1)

Table 3.1 Gradient elution scheme from 0% to 100% NiB buffer

Volume (Ml)	Function	Value
0	Concentration % NiB	0
0	mL/min	0.4
40	Concentration % NiB	100
40	mL/min	0.4
45	Concentration % NiB	100
45	mL/min	0.4

The fractions were collected according to the following Table 3.2.

**Table 3.2** Composition of % NiB in the eluted fractions

Fraction #	% NiB
1	
1	0-50%
2	50-55%
3	55-60%
4	60-65%
5	65-70%
6	70-75%
7	75-80%
8	80-85%
9	85-90%
10	90-95%
11	95-100%
12	>100% volume

The concentration of HrpA in each fraction was determined using a photometric BCA assay. This assay extrapolates the protein concentration from a standard curve of the absorbances at 562 nm of known quantities of BSA. Consistent protein yields of ~30 mg/L of culture were obtained for both HrpA constructs.

Each fraction found to contain significant HrpA was concentrated by centrifugation using an Eppendorf Centrifuge 5810R and 4 mL Amicon 5000 molecular weight cut-off (MWCO) concentrators. The fractions were centrifuged at 4000 rpm for 20 minutes at 4°C. 13 µL aliquots of each fraction were used to generate samples for SDS-PAGE. SDS-PAGE samples were prepared according to Table 3.3.

Table 3.3 SDS-PAGE sample preparation

13 µL HrpA Elution Fractions
5 μL 4x Sample Loading Buffer
2 μL 10x Reducing Agent

These samples were heated for 10 min at 70°C and loaded onto 12% Bis/Tris acrylamide gels from Invitrogen. The electrophoresis was run at 200 mV for 45 minutes. The gels were the stained with Coomassie Blue stain overnight. Upon de-staining, the following results were obtained (Figures 3.1 a-b).

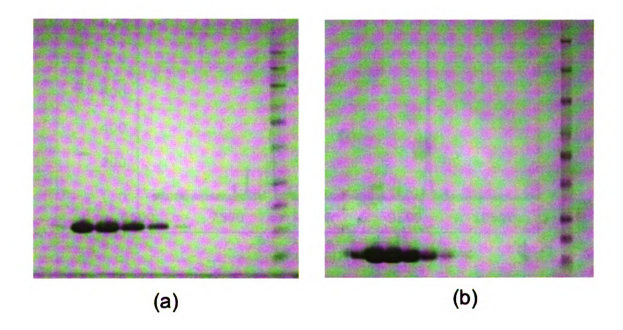
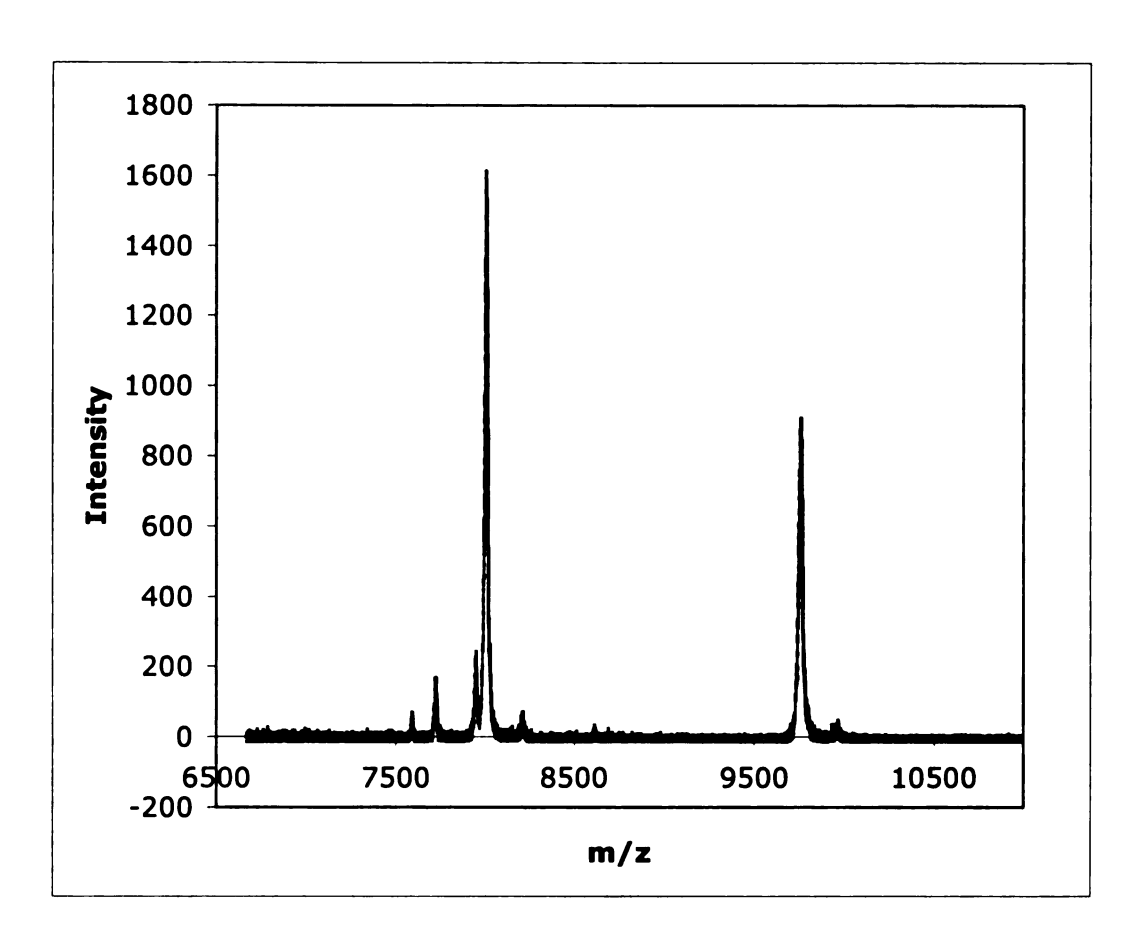


Figure 3.1 Coomassie-stained SDS-PAGE gel of purified HrpA from (a) *P. syringae* and (b) *E. amylovora* 

The presence of HrpA was confirmed by N-terminal sequencing, MALDI-TOF-MS (Figure 3.2), and chemiluminescent Western Blot analysis using an Invitrogen WesternBreeze kit with a primary antibody for the N-terminal (His)6 tag.



**Figure 3.2** MALDI-TOF-MS spectrum of the truncated, wild-type HrpA from P. syringae. The peak centered at 9.8 kDa represents the truncated, wild-type HrpA and the peak centered at 7.9 kDa is a consistently observed degradation product of the HrpA.

The fractions containing the 95% pure HrpA were combined and concentrated to 2 mL aliquots for FPLC injection. Further purification and characterization were accomplished by size exclusion chromatography according to the system parameters given in Table 3.4.

**Table 3.4** Size exclusion gel filtration system parameters

Parameter	Value
Column	HiPrep 26/60 Sephacryl S100
Flow Rate	1.3 mL/min
Equilibrate w/	0.00 Ml
Empty Loop w/	100.00 Ml
Fraction Size	5.00 M1
Length of Elution	1.1

The Amersham Sciences HiPrep 26/60 Sephacryl S-100 column was calibrated using bovine pancreatic ribonuclease A, chymotrypsinogen A, ovalbumin, and albumin by plotting the logarithm of either the hydrodynamic radius (calculated from the PDB structures 7rsa, 1cgi, 1ova, and 1ao6, respectively) or molecular weight versus elution volume. A typical size exclusion chromatogram for the HrpA from *P. syringae* is given in Figure 3.3. The elution was performed with a 15 mM Tris-HCl and 100 mM NaCl buffer at pH 7.5.

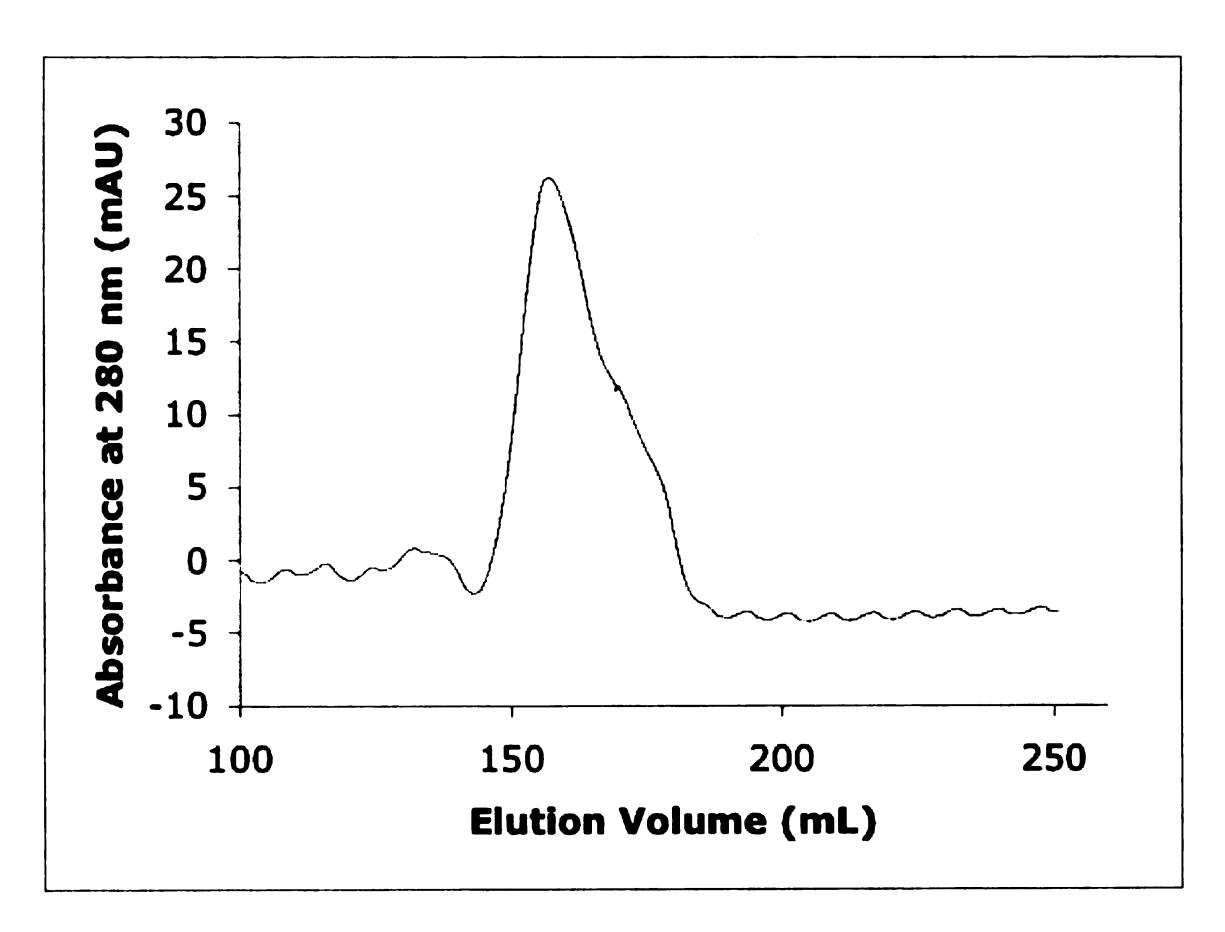


Figure 3.3 Typical size exclusion chromatogram for HrpA from P. syringae

The fundamental equation used to determine the effective molecular weight from the elution volume was derived from the above calibration to be

Elution Volume – Void Volume = 
$$-43.9 \ln (\text{mol. wt.}) + 208.25$$
 (2)

According to Equation (2), the effective molecular weight of HrpA having an elution peak centered at 156.862 mL was 28.9 kDa. The discrepancy observed in the effective and calculated molecular weights suggests that the protein is at least partially unstructured. Fractions 13-18 were retained because they spanned the breadth of the peak centered at 156.862 mL. These fractions were concentrated to ~20 mg/mL and stored at -20°C to serve as HrpA stock solutions.

# III.F. Cleavage of the N-terminal (His)<sub>6</sub> Tag on HrpA from P. syringae

Thrombin cleavage of the N-terminal 17-residue His-tag was deemed crucial for protein crystallization and to control for the contributions of the N-terminus to pilus assembly. The following thrombin digestion protocol was developed and optimized for efficiency and yield.

Thrombin was dissolved in 1x Thrombin Digestion buffer at pH 8.4 (Appendix) to a concentration of 1 unit/ $\mu$ L. This pH was chosen because it enables high thrombin activity and because it is below the isoelectric point (pI ~ 8.77) of the cleaved HrpA, thus ensuring solubility. Thrombin digestion was performed by combining the following

components into a 15 mL Corning conical tube: (1) 30 mg of HrpA, (2) thrombin at 5 units/mg of HrpA from *P. syringae*, and (3) 1x Thrombin Digestion buffer in 3:1 volume-to-volume ratio with HrpA for solubility. The reaction conical was placed on a New Brunswick Scientific InnOva 2000 platform shaker for 2 hours at 25°C. PMSF was added to a final concentration of 1 mM to inhibit thrombin activity. The reaction mixture was concentrated to 2 mL for subsequent size exclusion chromatography (Figure 3.4) as described above. This chromatography was employed to separate the thrombin and the (His)<sub>6</sub> tag from the cleaved HrpA. SDS-PAGE analysis was performed to monitor the progress of digestion at several times (Figure 3.5).

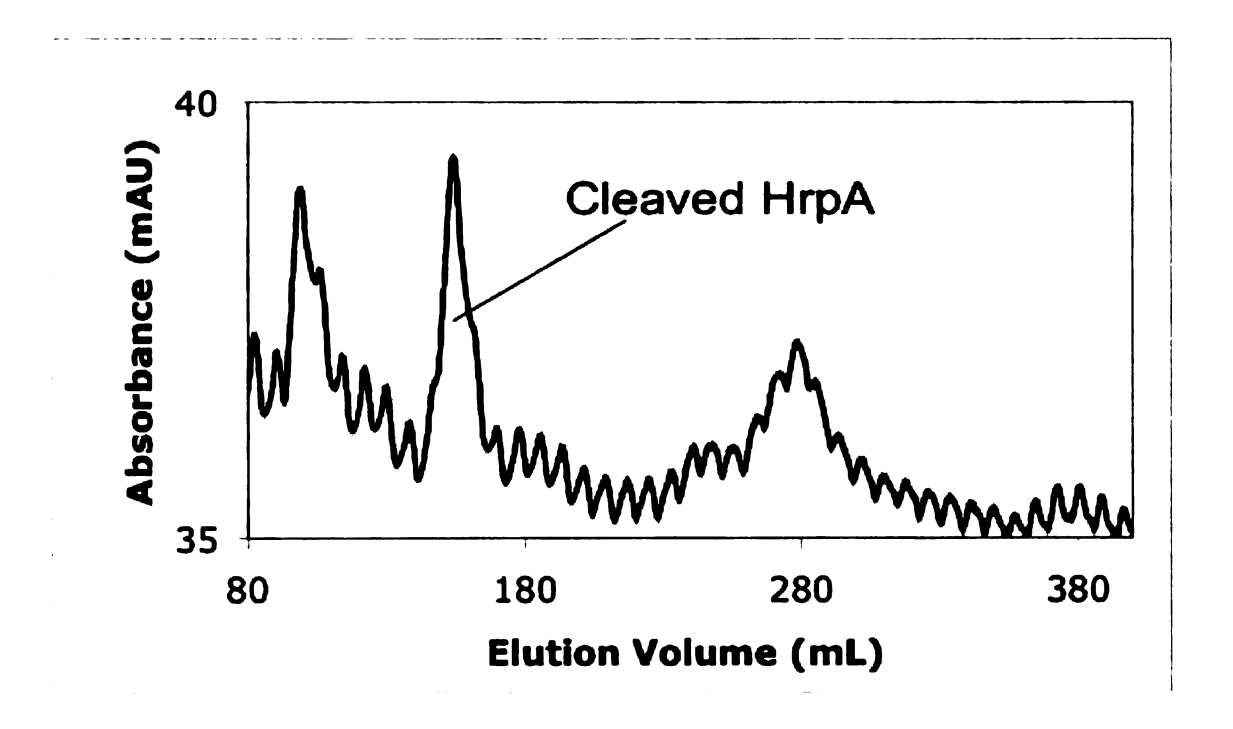


Figure 3.4 Size exclusion chromatogram for isolation of cleaved HrpA

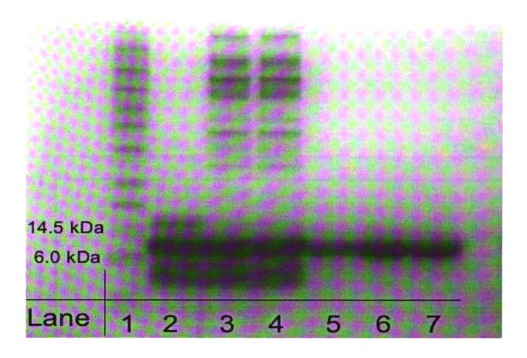


Figure 3.5 SDS-PAGE gel depicting the time evolution of the thrombin digestion. Lane 1 contains molecular weight standards. Lane 2 contains HrpA diluted in the 1X cleavage buffer pH 8.4. The band at 14.5 kDa represents the uncleaved HrpA and the band at ~9 kDa represents the consistently observed degradation product of HrpA that is consistent in weight with the (His)6 tag cleaved HrpA. Lanes 3 and 4 contains the contents from Lane 2 in the presence of thrombin (5 units/mg) at time t=0 and t=2 hours, respectively. Lanes 5, 6, and 7 represent purified (His)6 tag cleaved HrpA collected from size exclusion fractions 10-12.

The digestion was confirmed by three methods: chemiluminescent Western Blot analysis with a primary antibody for the N-terminal (His)<sub>6</sub> tag, N-terminal sequencing, and HPLC/MALDI-TOF-MS (Figure 3.6-7). The N-terminal sequencing showed the presence of 2 predominant species: (1) GSHMNILLG... with a molecular weight of 7.9 kDa and (2) MNILLG... with a molecular weight of 7.7 kDa.

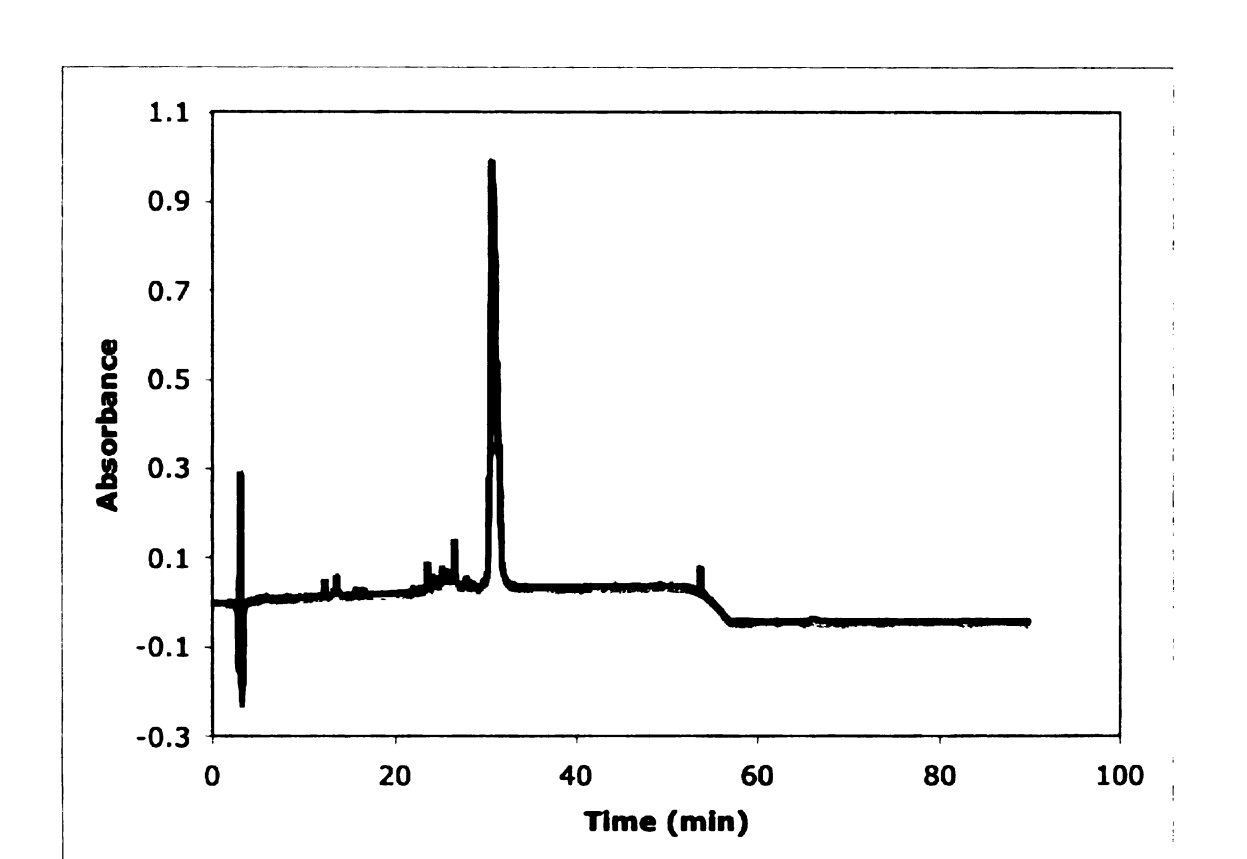


Figure 3.6 HPLC chromatogram of purified, cleaved HrpA from P. syringae



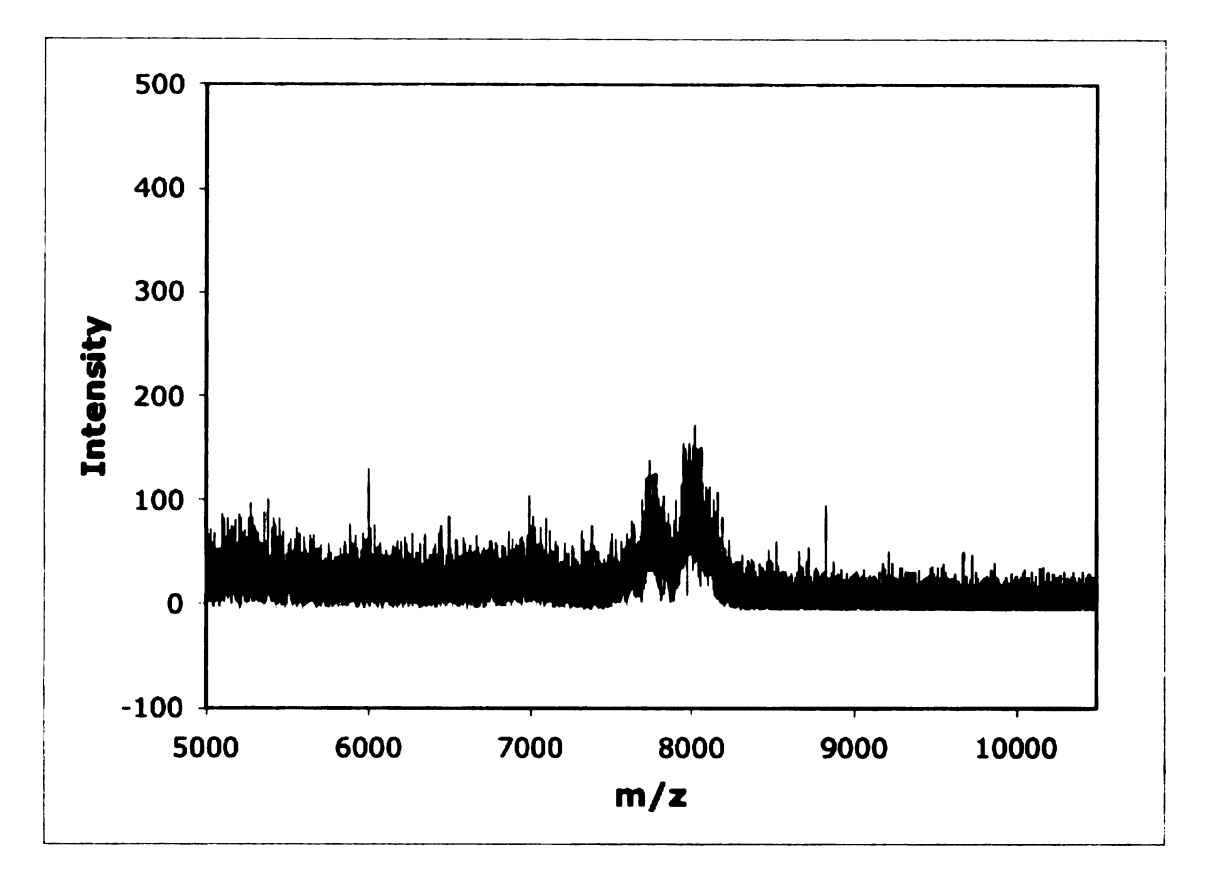


Figure 3.7 MALDI-TOF-MS spectrum of cleaved HrpA from P. syringae

The spectrum obtained from MALDI-TOF-MS confirmed the digestion of HrpA and the results from N-terminal sequencing, as mass peaks were observed at 7.7 kDa and 7.9 kDa. From these coincident pieces of data, it was determined that the thrombin digestion was successful in preparing the (His)<sub>6</sub> tag cleaved form of HrpA with high purity.

#### IV. In Vitro Preparation of the Hrp Pilus

The experimental determination of the structure and function of HrpA depends on isolating stable forms of both its monomeric and multimeric states. Spectroscopic probes of these two forms will provide insight not only into the structure and folding of HrpA, but also into the formation of the Hrp pilus.

#### IV.A. Two Forms of HrpA: Monomer and Multimer

It has been hypothesized that, in the bacterial cytosol, the full-length HrpA pilin exists as a mostly unstructured monomer linked in a chaperone complex [33]. Upon reaching the membrane-embedded base, the monomer dissociates from the native chaperone complex. This event is essential for pilus formation because only unstructured proteins can fit through the inner diameter (2 nm) to translocate. When the monomer reaches the tip of the growing pilus, it adopts a stable fold and adds to the assembly [24]. The resulting non-covalent multimer of HrpA, termed the Hrp pilus, serves as a conduit for bacterial effector proteins. The following work attempts to probe the mechanism for this self-assembly.

To probe the self-assembly of HrpA, it was necessary to develop a means for reliably producing the pilus *in vitro*. Roiné *et al.* have successfully shown that the Hrp pilus can be prepared *in vitro* from purified HrpA [36]. He *et al.* have shown that increasing the pH from 5.0 to 7.5 induces pilus formation at pH>6.5 [23].

We have performed a more systematic study of co-solvents and their effects on Hrp pilus formation. The secondary structure predictions presented in section II.B show that the stable folding of HrpA should be predominantly α-helical. The use of neutral helix-favoring co-solvents, such as 2,2,2-trifluoroethanol (TFE) would be a reasonable approach to induce the folding of monomeric HrpA [39]. Also, at relatively low pH (pH<6.0), the surfaces of the cleaved and uncleaved HrpA monomers are positively charged, for the isoelectric points are 8.77 and 9.6, respectively. Thus, it has been hypothesized that the use of well-chosen anions might stabilize the electrostatic interactions of the pilin and lower the free energy of the system enough to drive pilus formation.

Our study shows that pilus formation is selective for helix-favoring co-solvents and for the lyotropic anions of the Hofmeister series [4]. The denaturing effects of chaotropic anions, even those existing within the same family as stabilizing lyotropic anions (i.e. halide salts), are manifested in the absence of pili. The fact that HrpA does not self-assemble in the presence of chaotropic anions suggests that the driving force for pilus formation is the combination of the stabilization of electrostatic interactions within the HrpA monomer and the hydrophobic interactions existing between adjacent monomers.

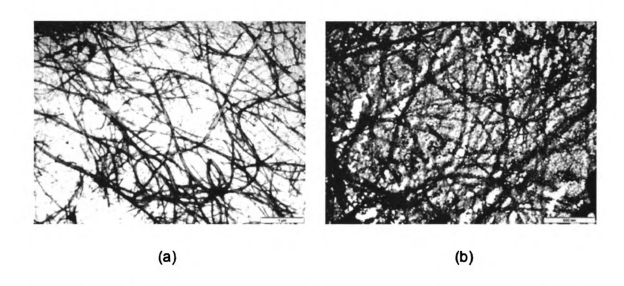
## IV.A.i. 2,2,2-trifluoroethanol (TFE)

TFE across the concentration range of 10-20% (v/v) is a helix-favoring co-solvent [39]. TFE likely induces  $\alpha$ -helical structure by disrupting the solvation sphere of the

unstructured protein, thus making it more likely that the amide hydrogens will form intramolecular hydrogen-bonds.

To test the effects of TFE on Hrp pilus formation, 100 μL of 20 mg/mL cleaved and uncleaved monomeric HrpA were exchanged from a pH 7.5 buffer containing 15 mM Tris-HCl and 100 mM NaCl to a pH 5.5 buffer containing 10% (v/v) TFE and 50 mM NaH<sub>2</sub>PO<sub>4</sub>. Buffer exchange was accomplished in two repetitive stages of 50-fold dilution in the 10% TFE buffer followed by concentration to the initial volume in 5 mL Amicon 5000 MWCO centrifuge tubes. The resulting 100 μL were transferred to a 0.5 mL Eppendorf tube and frozen for 24 hours at -20°C. Upon thawing to 25°C, the samples exhibited a high viscosity consistent with pilus formation.

These samples were plated on copper grids, negatively stained with 2% aqueous phosphotungstic acid, and examined using transmission electron microscopy (TEM) at the Michigan State University Center for Advanced Microscopy. Conventional light/dark field images by electron scattering were obtained using a JEOL (Japan Electron Optics Laboratories) 100CXII microscope with the help of Dr. Alicia Pastor-Lecha (Figures 4.1 a,b).



Figures 4.1 (a,b) TEM images of *in vitro* Hrp pilus assembly for (a) uncleaved and (b) (His)<sub>6</sub> tag cleaved wild-type, truncated HrpA from *P. syringae* in the presence of TFE.

These images verify that this protocol successfully generated pili at pH 5.5, a result that disagrees with that of He *et al.* who found that pilus formation is induced only upon increasing the pH above 6.5. The ability to produce pili at this relatively low pH has enabled the examination of the electrostatic contributions to pilus formation. The presence of pili in both the cleaved and uncleaved samples has proven that the N-terminal (His)<sub>6</sub> tag does not play any role in the self-assembly process.

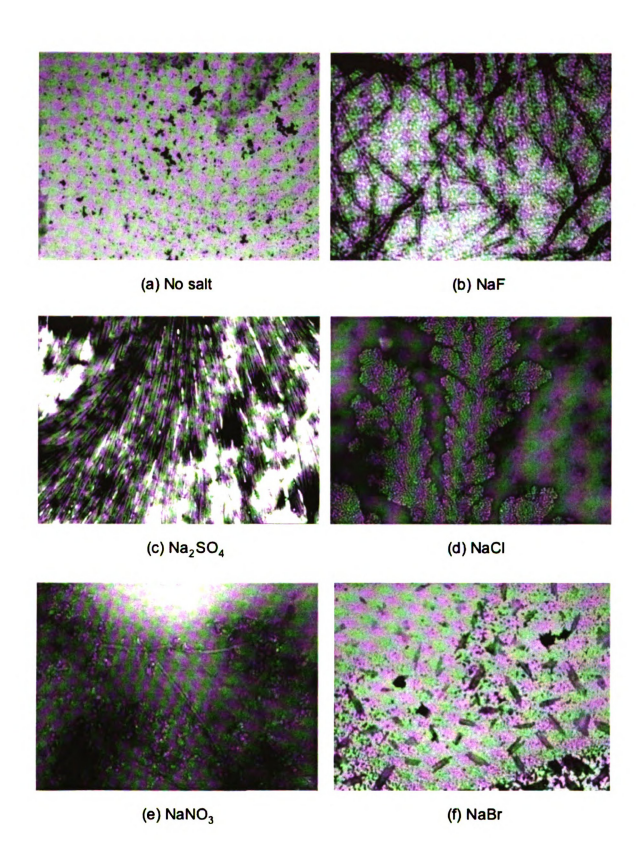
#### IV.A.ii. Salts

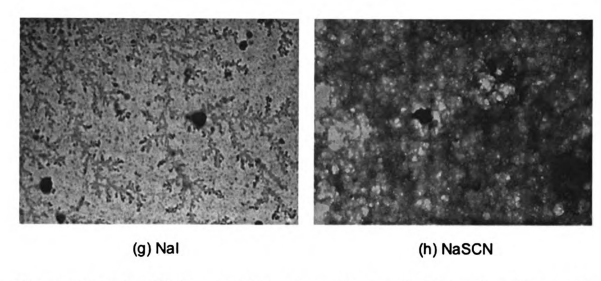
The previously observed dependence of pilus formation on pH suggests that electrostatic repulsion between the HrpA monomers contributes significantly to the free energy of pilus formation. Hence, we hypothesized that anions would stabilize the positively charged surface of monomeric HrpA at pH 5.5 by Manning-type condensation [27], in

which ions are quasi-permanently bound to a linear charge density, such as that of the Hrp pilus. A set of anions was selected to examine the range of lyotropic to chaotropic anions depicted in the Hofmeister series [4].

50 mM NaH<sub>2</sub>PO<sub>4</sub> buffers at pH 5.5 were doped with 300 mM quantities of the following salts: NaF, Na<sub>2</sub>SO<sub>4</sub>, NaCl, NaNO<sub>3</sub>, NaBr, NaI, and NaSCN. The sample preparation described in section **IV.A.i** was followed for each buffer, and the resulting 100 μL were transferred to 0.5 mL Eppendorf tubes and frozen for 24 hours at -20°C. Upon thawing to 25°C, viscosity was observed only in the buffers containing 300 mM NaF, NaCl, NaNO<sub>3</sub>, and Na<sub>2</sub>SO<sub>4</sub>. 20% dilutions were prepared for TEM according to the above freeze/thaw cycle.

The samples were plated on copper grids and negatively stained with 2% aqueous phosphotungstic acid for TEM. Conventional light/dark field images by electron scattering were obtained (Figures 4.2 a-h).





Figures 4.2 (a-h) TEM images of truncated, wild-type HrpA from *P. syringae* in the presence of 50 mM NaH<sub>2</sub>PO<sub>4</sub> buffer pH 5.5 with (a) no salt (b) 300 mM NaF, (c) 300 mM NaSO<sub>4</sub>, (d) 300 mM NaCl, (e) 300 mM NaNO<sub>3</sub>, (f) 300 mM NaBr, (g) 300 mM Nal, and (h) 300 mM NaSCN.

The samples containing the halide salts closely follow the lyotropic to chaotropic nature of the Hofmeister series [4]. The sample containing F ions induced the formation of pili having well-defined inner and outer diameters, 2 nm and 8 nm, respectively. The Cl containing buffer elicited a "coral reef"-like structure, implying a moderate disorder to the structure. The Br and I containing buffers showed no structural forms in comparison with the phosphate buffer control. The buffer containing the fully denaturing anion, SCN, also showed no structural forms when compared with the control. According to the Hofmeister series, SO<sub>4</sub> consoften display similar lyotropic effects to F ions and NO<sub>3</sub> ions are reportedly similar to Cl ions. The results of this work are consistent with the known behaviors of these ions, as the NO<sub>3</sub> and SO<sub>4</sub> buffers induced the formation of pili and "raft"-like arrangements of pili, respectively. The

ability of SO<sub>4</sub><sup>2-</sup> to form "raft"-like arrangements of pili may result from its divalent nature, being able to coordinate with two pili simultaneously.

#### IV.A.iii. Stable Multimers of Uniform Dimensions

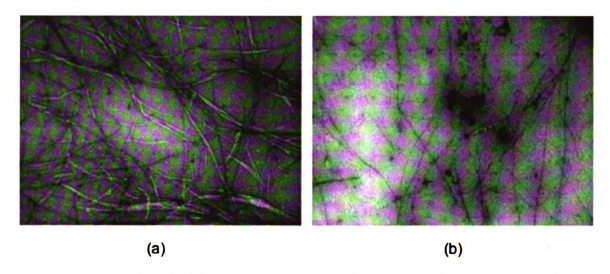
To probe the folding kinetics of HrpA or to obtain definitive secondary/tertiary structural information via solid-state NMR, electron cryomicroscopy, or electron fiber diffraction, it is desirable to produce stable multimers of uniform length. We hypothesized that this would be feasible through polyanion driven Manning-type condensation. Two well-chosen poly-anions were selected: ADP and the Dickerson-Drew dodecamer of DNA. ADP was chosen to provide insight as to the validity of this hypothesis. The Dickerson-Drew dodecamer has a unique palindromic sequence of 5'-CGCGAATTCGCG-3' [9]. The reason for selecting the palindromic dodecamer of double-stranded DNA was two-fold: (1) its polyanionic structure has consistent and uniform length and (2) the outer diameter of the double-helix was slightly smaller than the inner diameter of the pili observed above (Figure 4.2 a).

#### IV.A.iii.a. Adenosine Diphosphate (ADP)

50 mM NaH<sub>2</sub>PO<sub>4</sub> buffer at pH 5.5 was doped with 278 mM ADP. The sample preparation described in section **IV.A.i** was followed for the ADP-doped buffer. The resulting 100 μL were transferred to a 0.5 mL Eppendorf tube and frozen for 24 hours at -20°C. Upon thawing to 25°C, the sample exhibited a high viscosity consistent with pilus

formation. A 20% dilution was prepared for TEM according to the above freeze/thaw cycle.

The sample was plated on copper grids and negatively stained with 2% aqueous phosphotungstic acid for TEM. Conventional light/dark field images by electron scattering were obtained (Figures 4.3 a.b).



**Figures 4.3 (a,b)** TEM images of truncated, wild-type HrpA from *P. syringae* in the presence of 50 mM NaH<sub>2</sub>PO<sub>4</sub> buffer pH 5.5 doped with ADP.

The observation of pili in this sample exhibited evidence to support the hypothesis that polyanion driven Manning-type condensation was reasonable for the HrpA system.

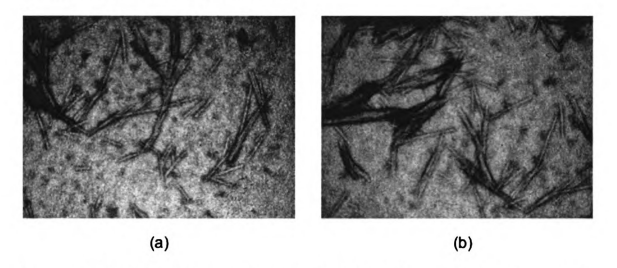
#### IV.A.iii.b. Dickerson-Drew Dodecamer of DNA

100 μL of 30 mg/mL uncleaved monomeric HrpA were exchanged from a pH 7.5 buffer containing 15 mM Tris-HCl and 100 mM NaCl to a pH 5.5 buffer containing 50 mM

NaH $_2$ PO $_4$ . The sample preparation described in section IV.A.i was followed, and the resulting 100  $\mu$ L were transferred to a 0.5 mL Eppendorf tube.

920 nanomoles of lyophilized Dickerson-Drew dodecamer were dissolved in 100  $\mu$ L Tris-EDTA (TE) buffer (Appendix). The resulting DNA solution was displaced into the 100  $\mu$ L of buffer exchanged HrpA until a final concentration of 4 mM DNA was achieved. The resulting mixture was frozen at -20°C for 24 hours. Upon thawing to 25°C, a white precipitate was observed within the sample, which we hypothesized could signify the presence of a large number of small pili. A 10% dilution was prepared for TEM according to the above freeze/thaw cycle.

The sample was plated on copper grids and negatively stained with 2% aqueous phosphotungstic acid for TEM. Conventional light/dark field images by electron scattering were obtained (Figures 4.4 a-b).



**Figures 4.4 (a-b)** TEM images of truncated, wild-type HrpA from *P. syringae* in the presence of 50 mM NaH<sub>2</sub>PO<sub>4</sub> buffer pH 5.5 doped with the Dickerson-Drew dodecamer of DNA.

From these images, it was determined that the pili adopted stable multimers having a 2 nm inner diameter, an 8 nm outer diameter, and a longest dimension ranging from 40 to 160 nm. Knowing that the dodecamer is approximately 4 nm in its longest dimension, it was estimated that the smallest observable pilus condenses onto 10 units of DNA. From these images, it was interpreted that the rigidity of the DNA only supports pilus growth to the terminal endpoint at 160 nm. This terminal length is likely the point at which bending and torsional forces, as depicted in Figures 4.1-4.3, affect pilus elongation.

#### V. Secondary and Tertiary Structure of Monomeric and Multimeric HrpA

General hydrodynamic and spectroscopic methods were utilized to probe the 2° and 3° structure of HrpA. Analytical ultracentrifugation (AUC) and size exclusion chromatography are hydrodynamic techniques that were used to answer the following two questions: (1) Is HrpA monomeric or multimeric under native conditions? (2) Is monomeric HrpA folded under native conditions? Thermal melt (TM) UV, circular dichroism (CD), and liquid-state NMR spectroscopies provided complementary techniques for determining the answer to the question regarding the folding state of HrpA. CD and solid-state NMR (SSNMR) spectroscopies were employed to probe the 2° structure of multimeric HrpA. Finally, thermal melt UV spectroscopy was also used to probe the unfolding transition of multimeric HrpA.

The hydrodynamic techniques showed that, under native conditions, HrpA exists as a mostly disordered monomer. This result was further supported by the data obtained from the complementary spectroscopic methods, TM analysis, CD, and liquid-state NMR. Structural analysis of multimeric HrpA, by CD and SSNMR, showed that upon self-assembly into the Hrp pilus, HrpA adopts a predominantly  $\alpha$ -helical structure. A discussion of these hydrodynamic and spectroscopic techniques and of the interpretation of the above results appears in the subsequent sections.

### V.A. Analytical Ultracentrifugation

Analytical ultracentrifugation (AUC) is a hydrodynamic tool that can assay the mass, density, and hydrodynamic volume of proteins under biologically relevant conditions [22]. For studying proteins, the concentration is usually assayed by absorption at 280 nm due to the tryptophan and tyrosine residues; however, other spectroscopic probes of concentration can be used, such as fluorescence, refractrometry, and absorption at other wavelengths (e.g. 215 nm). Real-time monitoring of the sedimentation of these biomolecules in a centrifugal field enables extraction of both hydrodynamic and thermodynamic information unique to the system. This is accomplished through two complementary methods: (1) sedimentation *velocity* (SV) and (2) sedimentation *equilibrium* (SE) [22].

In SV, the application of a strong centrifugal force causes the depletion of protein at the meniscus and the formation of a concentration boundary that moves toward the base of the centrifuge cell with time [22]. Analysis of the concentration boundary velocity yields the sedimentation coefficient, s, of the protein. The s-value is determined by the Svedberg equation:

$$s = \frac{\mu}{\omega^2 r} = \frac{M(1 - \nu \rho)}{N_A f} \tag{3}$$

where  $\mu$  is the radial velocity of the protein,  $\omega$  is the angular velocity of the rotor, r is the radial position of the boundary,  $\omega^2 r$  is the centrifugal acceleration, M is the molar mass, v

is the partial specific volume of the solute (i.e. protein),  $\rho$  is the solution density,  $N_A$  is Avagadro's number and f is the frictional coefficient [22]. The measured sedimentation coefficient, s, is directly proportional to the buoyant mass of the protein by

$$M_b = M(1 - \nu \rho) \tag{4}$$

where  $M_b$  is the buoyant mass. Through this relation, SV is sensitive to the protein mass and shape; thus, it enables one to distinguish multimeric states within the solution.

In SE, the centrifugal force is applied to establish an equilibrium between sedimentation and diffusion [22]. A lesser centrifugal force is utilized to ensure an adequate equilibration time of ~5 days. At equilibrium, the observed concentration distribution conforms to a Boltzmann distribution given by

$$C_{eq}(R) \sim \exp\left[\frac{M_b \omega^2 R^2}{2k_B T}\right] \tag{5}$$

where R is the radius,  $\omega$  is the angular velocity of the rotor,  $k_B$  is Boltzmann's constant, T is the temperature in Kelvin, and  $M_b$  is the buoyant mass from Equation (4). In comparison with SV, the SE method is only sensitive to the protein mass and multimeric states are differentiated by multiple distributions.

In this work, SV and SE data were collected for the wild-type, truncated HrpA from P. syringae on a Beckman XLI analytical centrifuge. The samples for each experiment consisted of FPLC-purified HrpA (1 mg/mL) in 450  $\mu$ L of 50 mM NaH<sub>2</sub>PO<sub>4</sub>, 300 mM NaCl at pH 5.5. The sample for SV was aliquotted to a centrifuge cell with quartz windows and centrifuged at 60000 rpm with scans of absorbance at 230 nm recorded every ten minutes for 12 hours at 4°C. One sedimenting species was observed having a sedimentation coefficient of 0.97 Svedbergs that was determined by linear fitting of the logarithm of the boundary position versus  $\omega^2 t$  (Figure 5.1), where t is the time in seconds and  $\omega$  is the rotational speed in radians/sec; the boundary position was calculated by the second-moment method [7, 13].

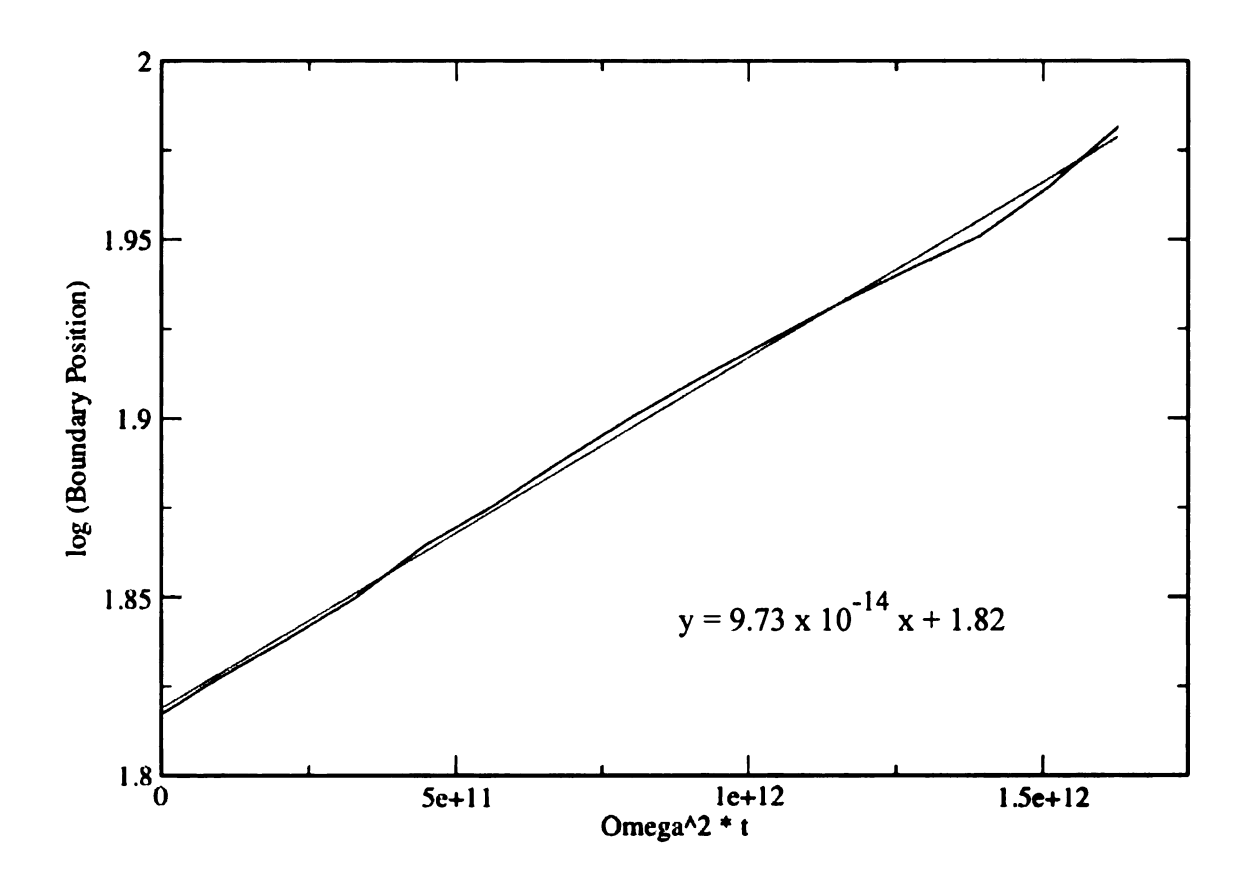


Figure 5.1 Sedimentation velocity of truncated, wild-type HrpA from P. syringae

The buoyant mass (M<sub>b</sub>) of HrpA was calculated to be 1.2 kDa, assuming a solution viscosity equal to that of water at 20°C, a protein solvation of 0.3 g/g, a solution density of 1 mg/mL, and a protein specific volume of 0.73 mL/mg [7].

The sample for SE was centrifuged at 10000 rpm for five days at 4°C. A buoyant mass of 1.8 kDa was obtained from the slope of the linear fit of the logarithm of the final concentration versus  $\omega^2 r^2/2k_BT$  (Figure 5.2), where r is the radius,  $k_B$  is Boltzmann's constant, and T is the temperature in Kelvin.

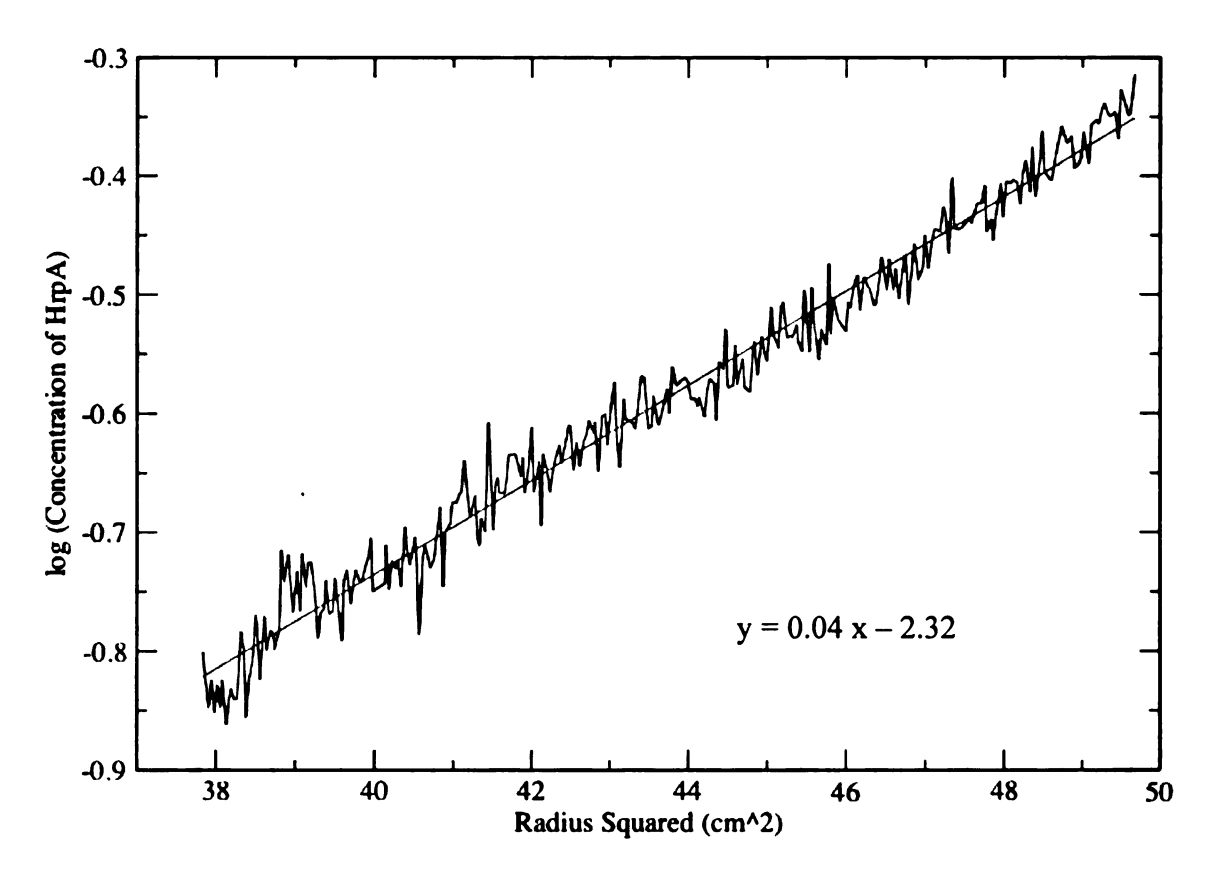


Figure 5.2 Sedimentation equilibrium of truncated, wild-type HrpA from P. syringae

The observed molecular weight was obtained from the relationship between the buoyant mass and molar mass given by Equation (4), assuming a solution density of 1.0 mg/mL and a protein partial specific volume of 0.73 mL/mg [7]. The observed molecular weight for the truncated, wild-type HrpA from *P. syringae* was determined to be 6.69 kDa. Given that the monomeric weight is known to be 9.8 kDa from MALDI-TOF-MS (section III.E), we can estimate the protein partial specific volume to be 0.8156 mL/mg, which is consistent with being unstructured.

#### **V.B.** Size Exclusion Chromatography

Size exclusion chromatography can be utilized both as a means of protein purification and as a means of obtaining hydrodynamic properties of the protein of interest. This technique provides insight into the hydrodynamic radius, the effective molar mass, and the state of folding of the protein.

Size exclusion chromatography was performed according to section III.E. on an Amersham Sciences HiPrep 26/60 S-100 HR sephacryl column calibrated with bovine pancreatic ribonuclease A, chymotrypsinogen A, ovalbumin, and albumin by plotting the logarithm of either the hydrodynamic radius (calculated from the PDB structures 7rsa, 1cgi, 1ova, and 1ao6, respectively) or molecular weight versus elution volume.

Through analysis of Figure 3.4 by Equation (1), the effective molecular weight of HrpA having an elution peak centered at 156.862 mL was calculated to be 28.9 kDa. The discrepancy observed in the effective molecular weight and theoretical molecular weight (9.6 kDa) suggests that the protein is unstructured. The higher observed molecular weight correlates with the increased amount of friction experienced by an unfolded protein in comparison with a folded protein.

# V.C. Solution-state 2D-NMR and HN-Heteronuclear Single Quantum Correlation (HN-HSQC)

For small soluble proteins (<10 kDa), solution-state 2D-NMR provides an excellent set of experiments for determining both folding and structure. The HN-HSQC pulse sequence enables one to observe each of these fundamental frequencies as a correlation between <sup>15</sup>N and <sup>1</sup>H chemical shifts [26]. The distribution of <sup>1</sup>H chemical shifts is directly related to the foldedness or unfoldedness of the protein of interest. A large dispersion of <sup>1</sup>H chemical shifts (4-5 ppm) is indicative of a folded protein, while a narrow dispersion (<2 ppm) indicates an unfolded protein. This incongruity in chemical shift ranges is derived from the differences in local fields experienced by an amide proton in a folded versus unfolded state. In the unfolded state, the amide protons are sufficiently exposed to the solvent system and, thus, share a similar chemical environment. However, in the folded state, amide protons may experience very different chemical environments. In this work, HN-HSQC was utilized for analysis of the state of folding of monomeric HrpA from *P. syringae*.

<sup>15</sup>N-labeled wild-type, truncated HrpA from *P. syringae* was concentrated to 1 mM within a minimal salt buffer, consisting of 10 mM NaH<sub>2</sub>PO<sub>4</sub> at pH 7.5 and 10% D<sub>2</sub>O. An HN-HSQC spectrum was generated on a Varian INOVA 600 MHz spectrometer at 25°C using the standard probe and pulse sequence. 1024 t<sub>2</sub> scans were collected and signal averaged over 2 hours to ensure adequate baseline resolution (Figure 5.3).

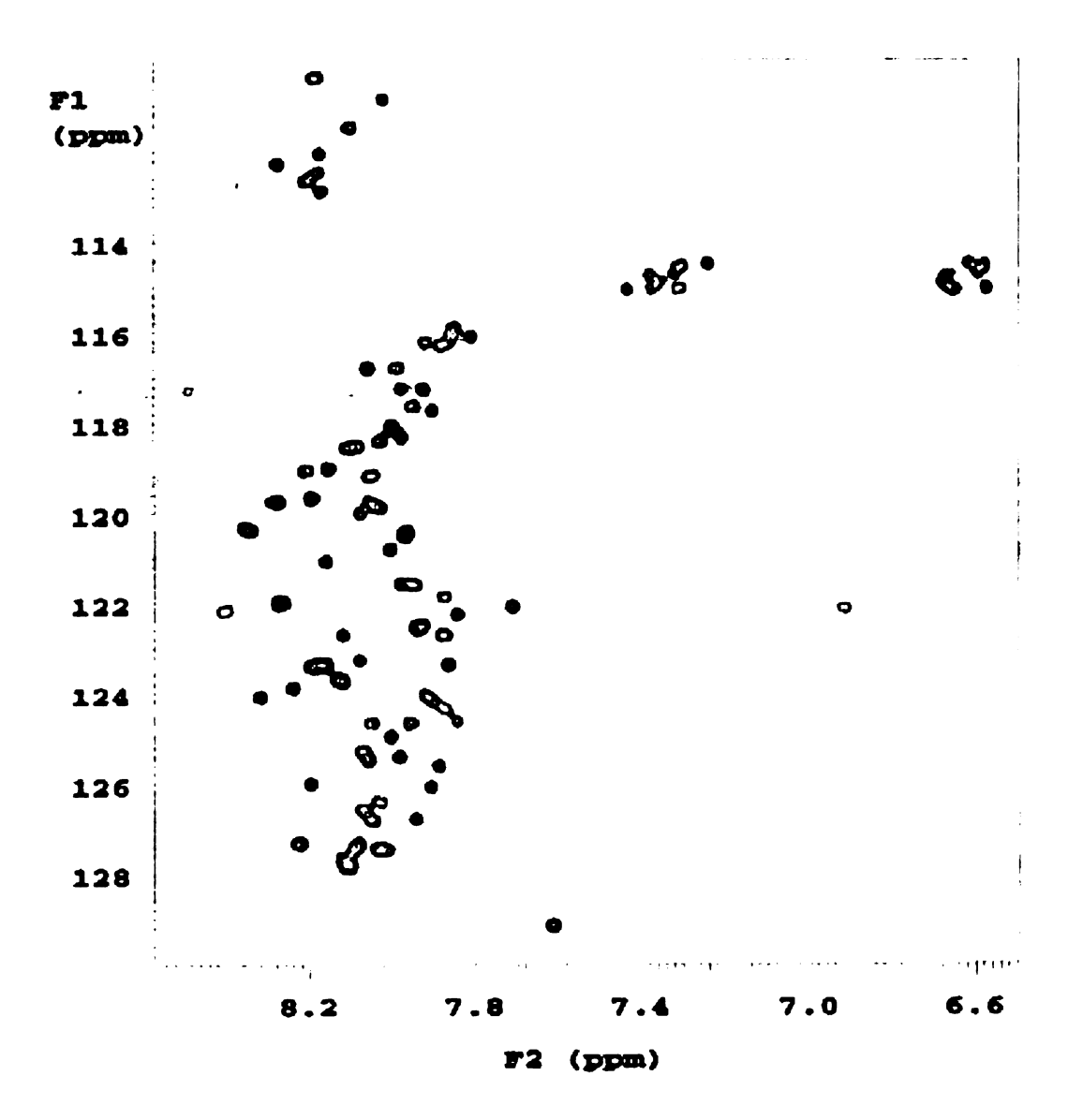


**Figure 5.3** HSQC spectrum of <sup>15</sup>N-labeled truncated, wild-type HrpA from *P. syringae*. F1 and F2 correspond to <sup>15</sup>N and <sup>1</sup>H chemical shifts, respectively.

The observed narrow dispersion of <sup>1</sup>H chemical shifts (~0.6 ppm) provided another piece of evidence in support of the hypothesis that the HrpA monomer is natively unstructured.

## V.D. Thermal Folding Transitions by UV Spectroscopy

Determining the thermal stability of the folding of proteins containing aromatic residues is facilitated by the application of thermal melt (TM) UV spectroscopy. Through monitoring the absorbance at 287 nm, one is able to observe changes in folding through detection of the red-shifted fluctuations for the  $\pi \rightarrow \pi^*$  transition of aromatic residues (e.g. tyrosine for HrpA from *P. syringae*), a class of 280 nm chromophores. If the protein were folded, the aromatic residue would not be exposed to the solvent, in contrast, if the protein were unfolded the residue is completely exposed to the solvent system. The absorbance signal for the unfolded protein would be blue-shifted and less intense because of solvent quenching effects (Figure 5.4).

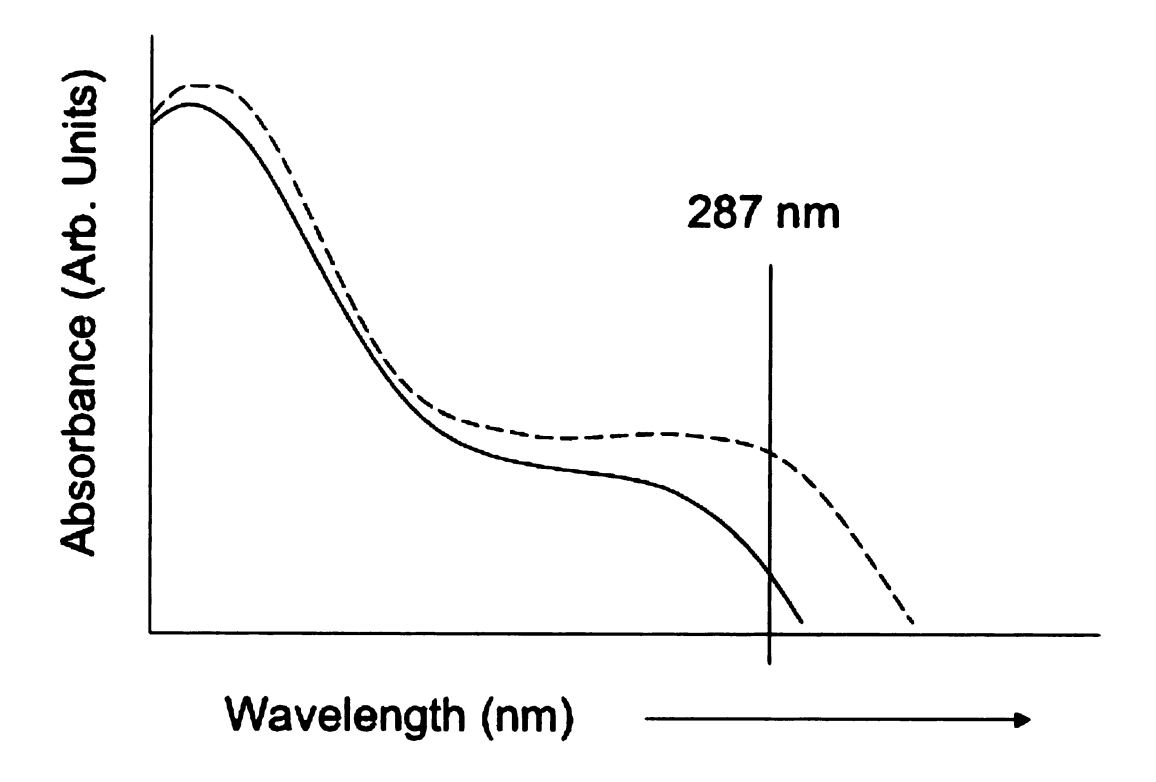


Figure 5.4 Protein folding is observed by monitoring the absorbance differences exhibited by the tyrosine chromophore at 287 nm as the tyrosine transitions from being folded, or unexposed to the solvent (dotted line) to being unfolded, or exposed to the solvent (solid line)

The sample is taken across a reversible temperature ramp that is designed to denature and possibly refold the protein of interest. Values for the thermal unfolding transition and the enthalpy of folding are extracted from fitting these data to the simple two-state folding transition with constant heat capacity model given by

$$-\frac{\Delta G}{RT} = \frac{\Delta S}{R} - \frac{\Delta H}{RT} = \left(\frac{\Delta H_m}{RT_m}\right) * \left(1 - \frac{T_m}{T}\right) \tag{6}$$

where  $T_m$  and  $\Delta H_m$  represent the melting temperature and the folding enthalpy, respectively [35].

The thermal unfolding transition for the wild-type, truncated HrpA from *P. syringae* was monitored by absorbance at 287 nm on a Shimadzu UV-1700 spectrophotometer under computer control. HrpA was diluted to 1 mg/mL in 20 mM Mes, 100 mM NaH<sub>2</sub>PO<sub>4</sub> and 10 mM NaF at pH 6.0. The sample was monitored along a reversible temperature ramp from 2°-70°C and then back to 2°C using a Shimadzu S-1700 thermoelectric (Peltier) cell holder coupled to a ThermoForma Model 2602 circulating water bath; a nitrogen atmosphere was maintained to minimize condensation on cell windows. For analysis purposes, the absorbance at 287 nm was normalized with the simultaneously collected absorbance at 280 nm (Figure 5.5).

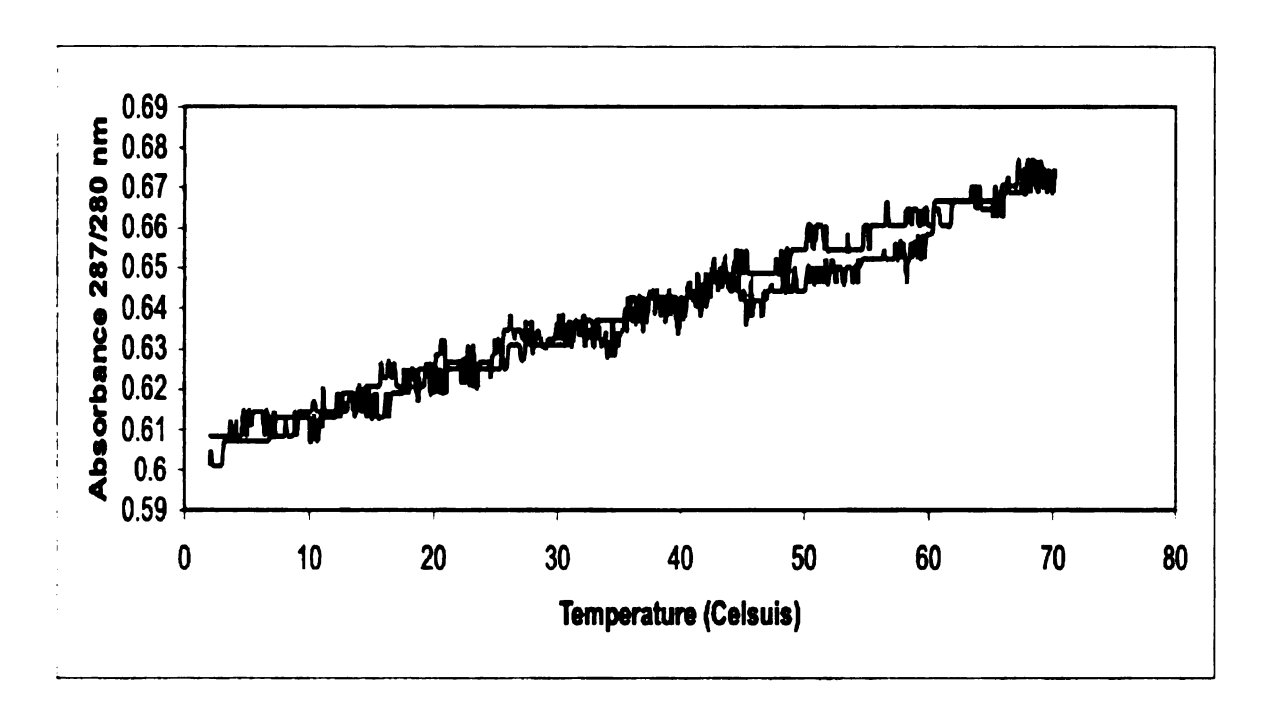


Figure 5.5 Thermal melt analysis for the truncated, wild-type HrpA monomer from *P. syringae* 

The absence of change in absorbance at 287 nm signifies that, under native conditions, monomeric HrpA is unstructured.

From the EM data, it was known that buffer condition of 10% TFE in 50 mM NaH<sub>2</sub>PO<sub>4</sub> at pH 5.5 supported pilus formation in both the His-tag cleaved and uncleaved forms of the wild-type, truncated HrpA from *P. syringae*. Ten-fold dilution in fresh buffer was performed on the 10% TFE buffered samples that had been previously prepared for EM to yield working volumes of concentration 2 mg/mL for TM analysis. These samples were frozen at -20°C for 24 hours to maintain intact pili post-dilution. TM data were recorded according to the protocol from above (Figures 5.6-7)

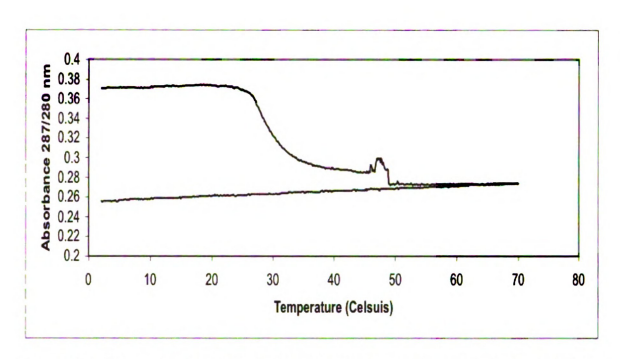
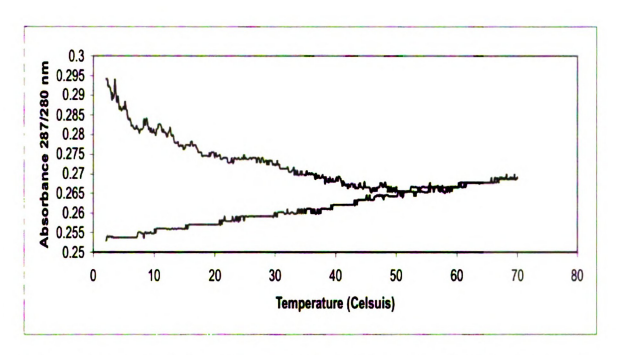


Figure 5.6 Thermal melt analysis for the uncleaved truncated, wild-type Hrp pilus from *P. syringae* 



**Figure 5.7** Thermal melt analysis for the (His)<sub>6</sub> tag cleaved truncated, wild-type Hrp pilus from *P. syringae*.

Thermal melting of the Hrp pilus exhibited an irreversible unfolding transition at 30°C.

The noticeable difference existing between the cleaved and uncleaved traces was thought

to be related to the difference in stability of the pili upon dilution. Thus, there is clearly a spectroscopic difference between the unstructured HrpA monomer and the folded Hrp pilus. Given that there is only 1 aromatic residue, the C-terminal tyrosine, this residue is likely to be buried in the pilus

#### V.E. Circular Dichroism (CD)

Plane-polarized light comprises two circularly polarized components of equal magnitude, one rotating clockwise (dextrorotary) and one rotating counter-clockwise (levorotary). A CD signal is generated when unequal absorption of these two components occurs as the radiation passes through a sample that possesses a chiral chromophore, such as a protein. The unequal absorption reorders the plane-polarized light into elliptically polarized light [20]. Far-UV CD (170 -250 nm) is sensitive to the 2° structure of proteins and is widely utilized as a spectroscopic means to estimate the relative percentages of 2° structure. In this work, CD was employed to examine the 2° structure of both the monomer and multimer of the wild-type, truncated HrpA from *P. syringae*.

CD spectra were generated on a JASCO J-810 spectropolarimeter according to the system parameters outline in Table 5.1.

**Table 5.1** JASCO J-810 acquisition parameters

System Parameter	Value
Scanning Mode	Continuous
Scanning Range	180-250 nm
Scanning Speed	2 nm/min
Band Width	1 nm
# of Scans	5

The temperature was controlled using a Hellma 165-QS water-jacketed, 1-cm cuvette that was coupled to a ThermoNeslab Model RTE111 circulating water bath.

1 mL solutions containing a 10 μM final concentration of monomeric HrpA were prepared in each of the following buffer conditions: (1) 50 mM NaH<sub>2</sub>PO<sub>4</sub> at pH 5.5, (2) 10% TFE in 50 mM NaH<sub>2</sub>PO<sub>4</sub> at pH 5.5, and (3) 10, 25, 50, 100, 150, 300, and 600 mM NaF in 50 mM NaH<sub>2</sub>PO<sub>4</sub> at pH 5.5. The resulting CD spectra acquired at 5°C are given in Figures 5.8 (a-c).

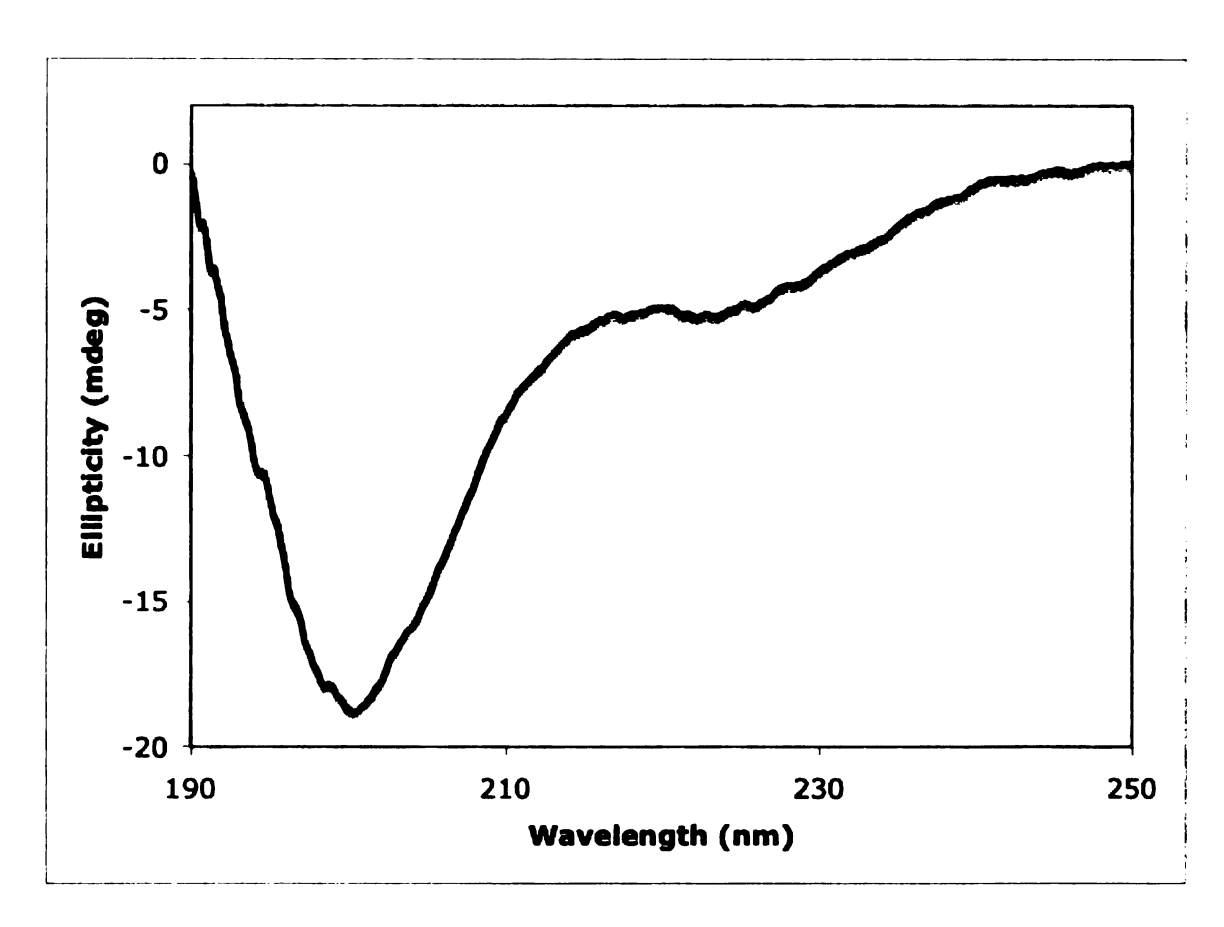


Figure 5.8 (a) CD spectrum of the truncated, wild-type HrpA monomer from P. syringae in 50 mM NaH<sub>2</sub>PO<sub>4</sub> buffer at pH 5.5

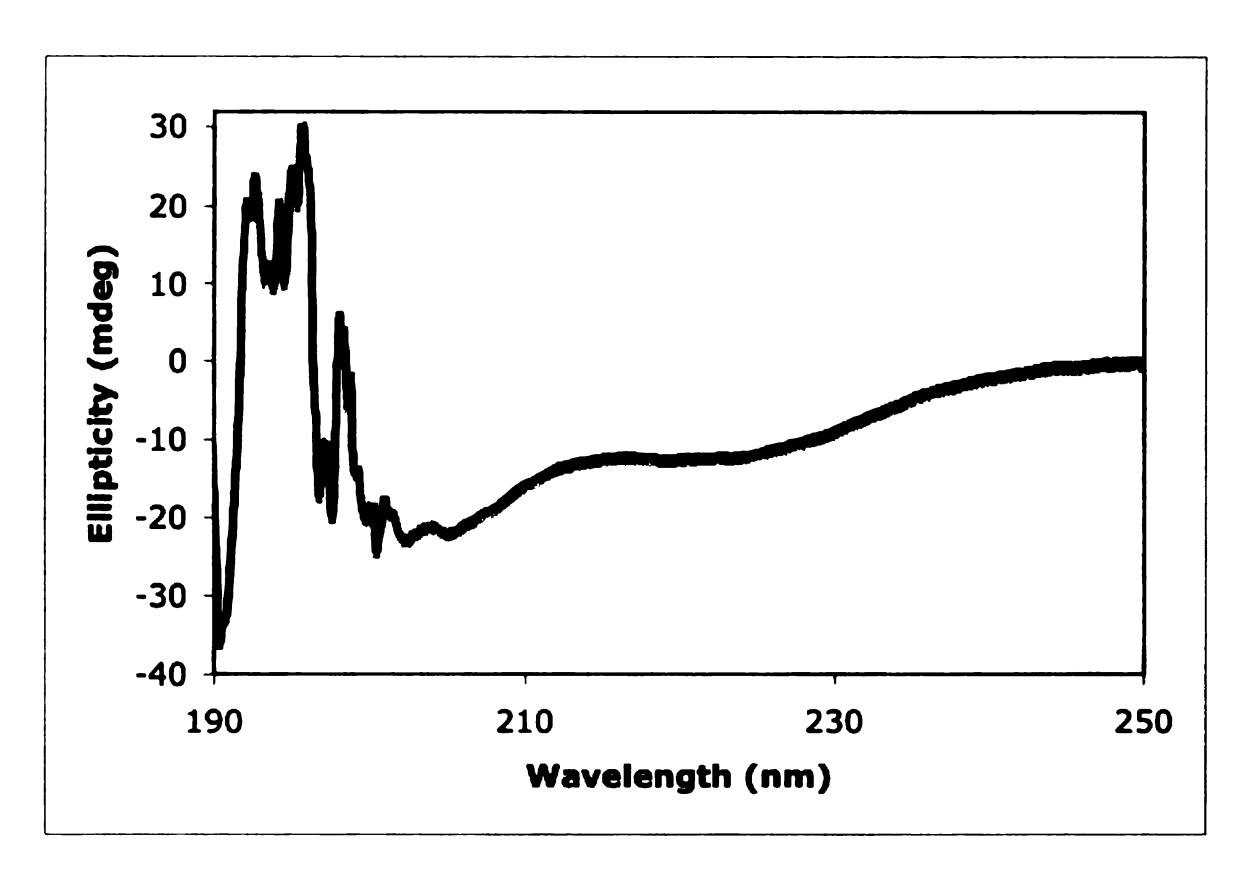


Figure 5.8 (b) CD spectrum of the truncated, wild-type HrpA monomer from P. syringae in 10% TFE and 50 mM NaH<sub>2</sub>PO<sub>4</sub> buffer at pH 5.5.

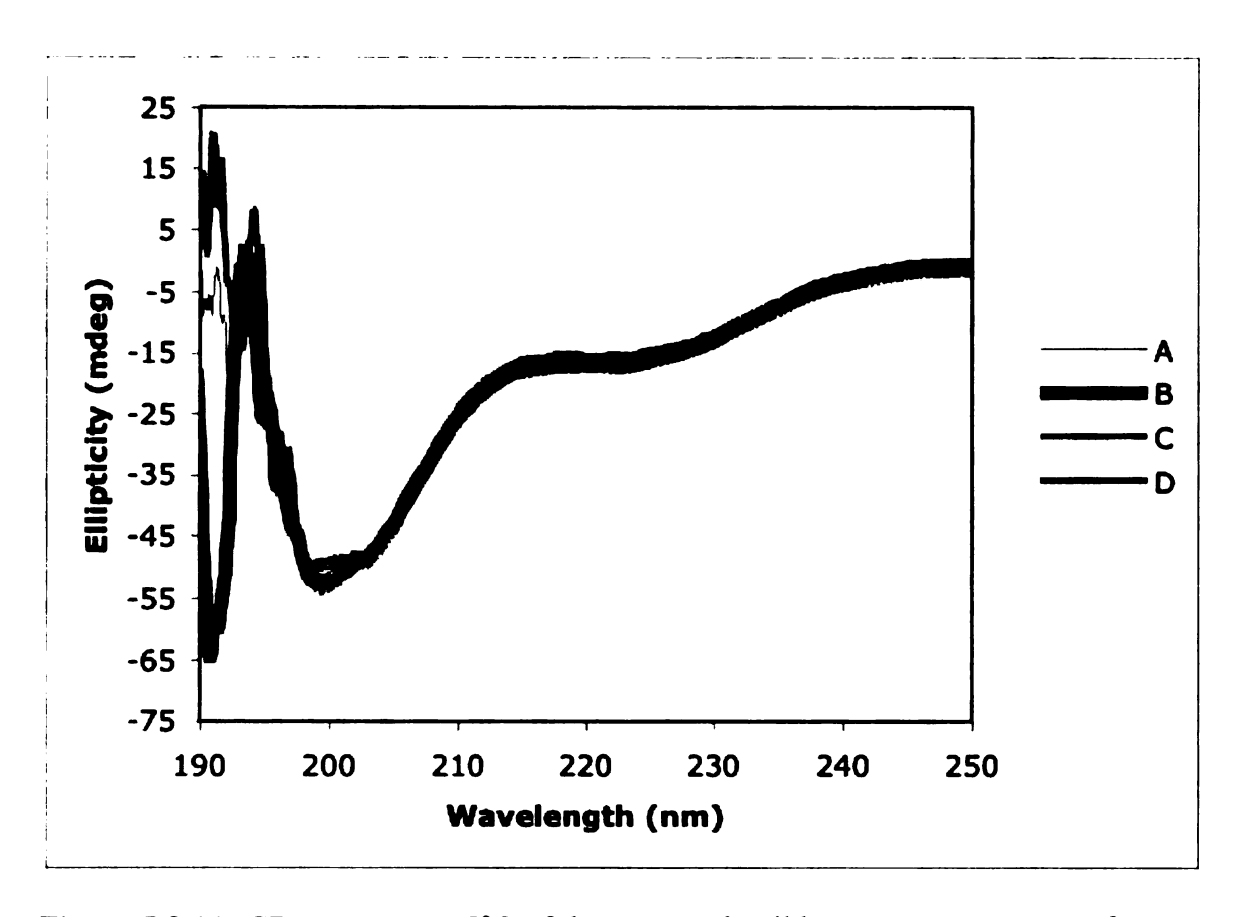


Figure 5.8 (c) CD spectrum at 5°C of the truncated, wild-type HrpA monomer from *P. syringae* in 50 mM NaH<sub>2</sub>PO<sub>4</sub> buffer pH5.5 with (A) 25 mM NaF, (B) 100 mM NaF, (C) 300 mM NaF, and (D) 600 mM NaF.

The CD spectra (Figures 5.8 (a-c)) of the wild-type, truncated HrpA monomer from P. syringae were observed to follow the trace characteristic of a random coil [20], having a

single minimum at 204 nm. This is consistent with the monomer being unstructured under native conditions.

Following the protocol for preparation of pili described in section **IV.A.i-ii**, 100 μL samples were prepared and diluted to 1 mL in the following buffer conditions: (1) 10% TFE in 50 mM NaH<sub>2</sub>PO<sub>4</sub> at pH 5.5 and (2) 1, 5, 10, 25, 50, 75, 100, 150, and 300 mM NaF in 50 mM NaH<sub>2</sub>PO<sub>4</sub> at pH 5.5. The resulting CD spectra acquired at 5°C are given in Figures 5.9 (a-b).

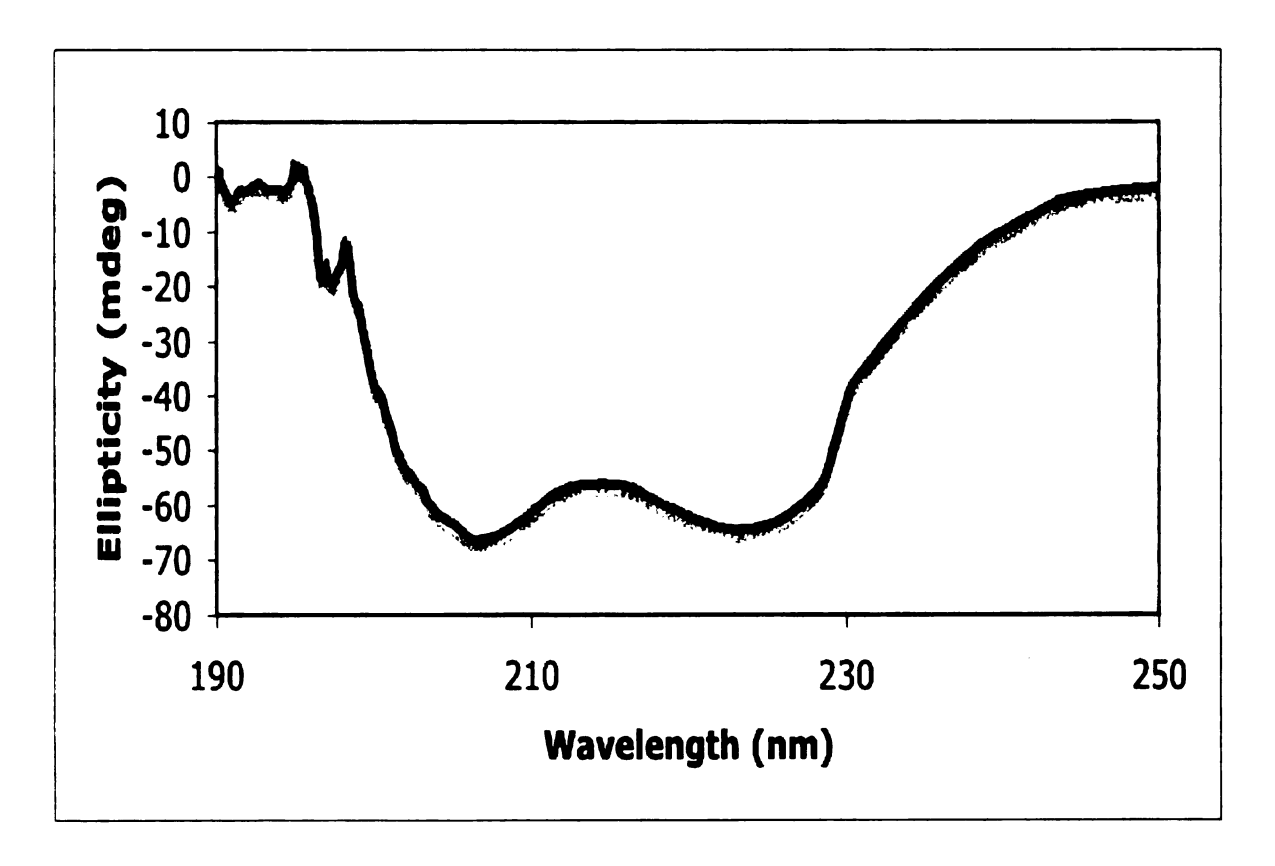
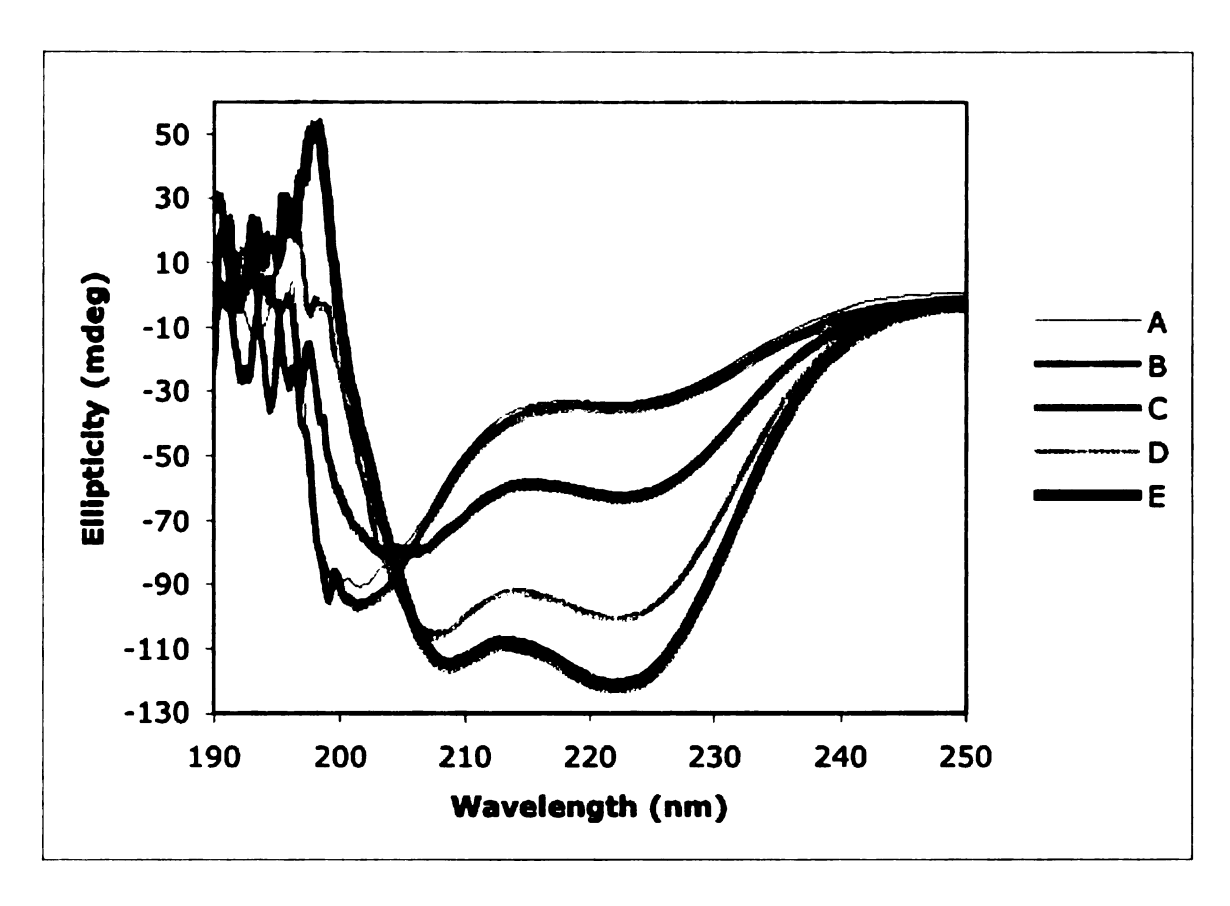


Figure 5.9 (a) CD spectrum at 5°C of the truncated, wild-type HrpA from *P. syringae* incorporated into the pilus in the presence of 10% TFE in 50 mM NaH<sub>2</sub>PO<sub>4</sub> buffer at pH 5.5



**Figure 5.9 (b)** CD spectrum at 5°C of the truncated, wild-type HrpA from *P. syringae* incorporated into the pilus in the presence 50 mM NaH<sub>2</sub>PO<sub>4</sub> buffer at pH 5.5 containing (A) no salt, (B) 10 mM NaF, (C) 50 mM NaF, (D) 100 mM NaF, and (E) 150 mM NaF.

Under conditions identified by EM to support pilus formation, the CD spectra (Figures 5.9 (a-b)) were consistent with that of a folded protein [20], having a double minimum at 208 and 222 nm, which is consistent with the predicted  $\alpha$ -helical 2° structure presented in section II. The results support the hypothesis that the monomer is natively unstructured, but then folds upon incorporation in the pilus.

The thermal stability of pilus was monitored for the above solution of pili prepared with 300 mM NaF and 50 mM NaH<sub>2</sub>PO<sub>4</sub> buffer at pH 5.5. CD spectra were acquired every

5°C across a reversible temperature ramp from 5-60°C and then back to 5°C (Figures 5.10 a-b).

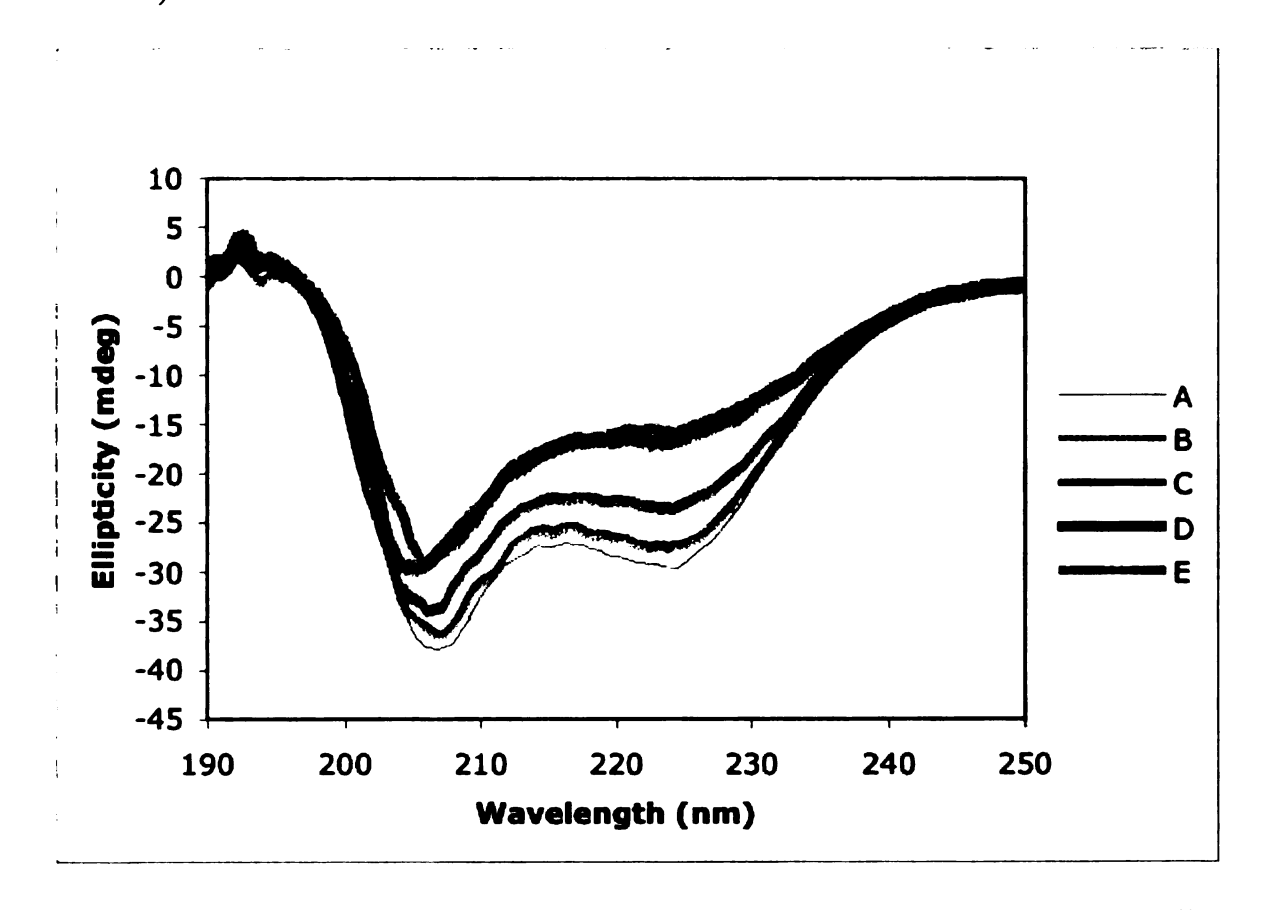


Figure 5.10 (a) Increasing temperature ramp from 5-60°C and its associated pilus stability observed at (A) 5°C, (B) 10°C, (C) 20°C, (D), 40°C, and (E) 60°C.

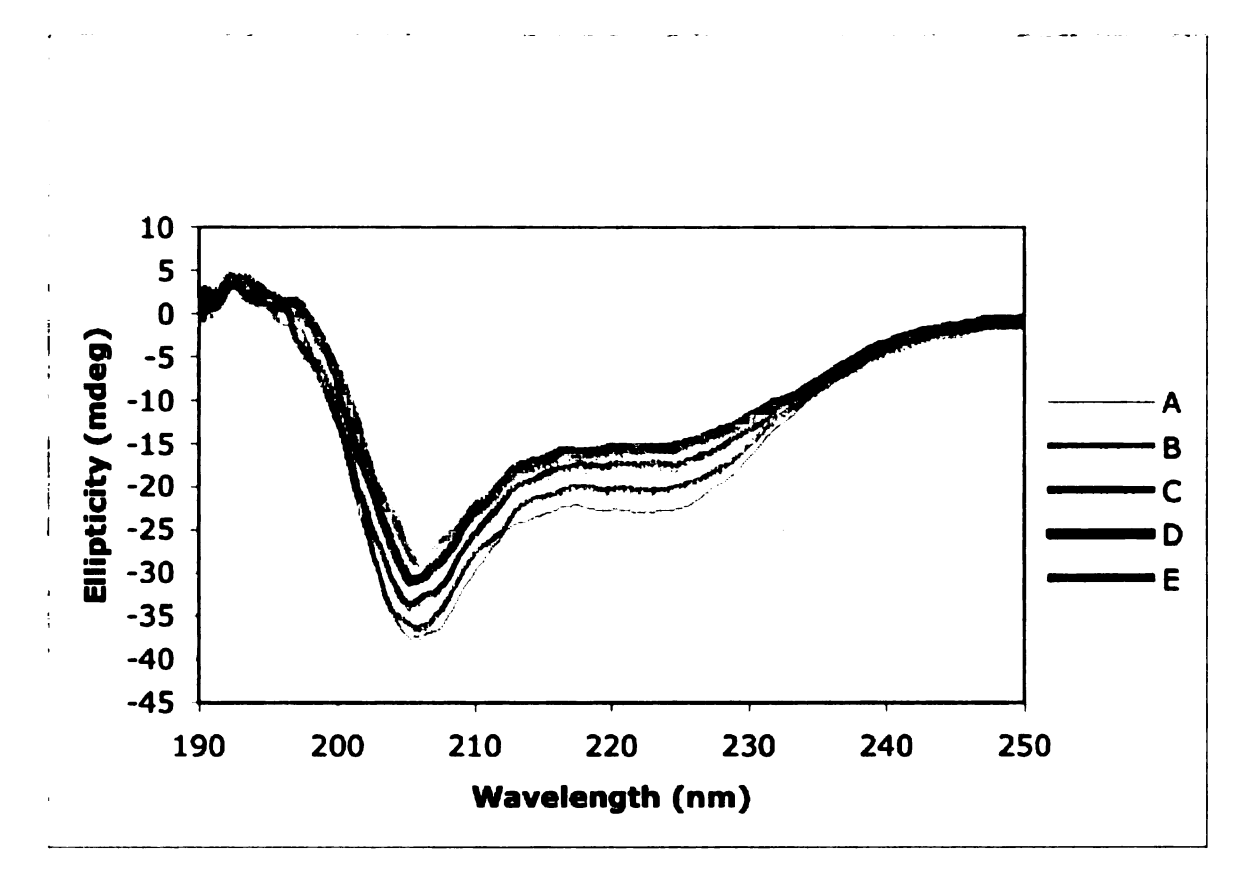


Figure 5.10 (b) Decreasing temperature ramp from 60-5°C and the refolding of the dissociated pilus at (A) 5°C, (B) 10°C, (C) 20°C, (D), 40°C, and (E) 60°C.

In agreement with the TM analysis of the unfolding of the pilus presented in section **V.D**, the CD data show a thermal unfolding transition at ~30°C and an irreversible unfolding of the pilus.

## V.F. Solid-state NMR (SSNMR)

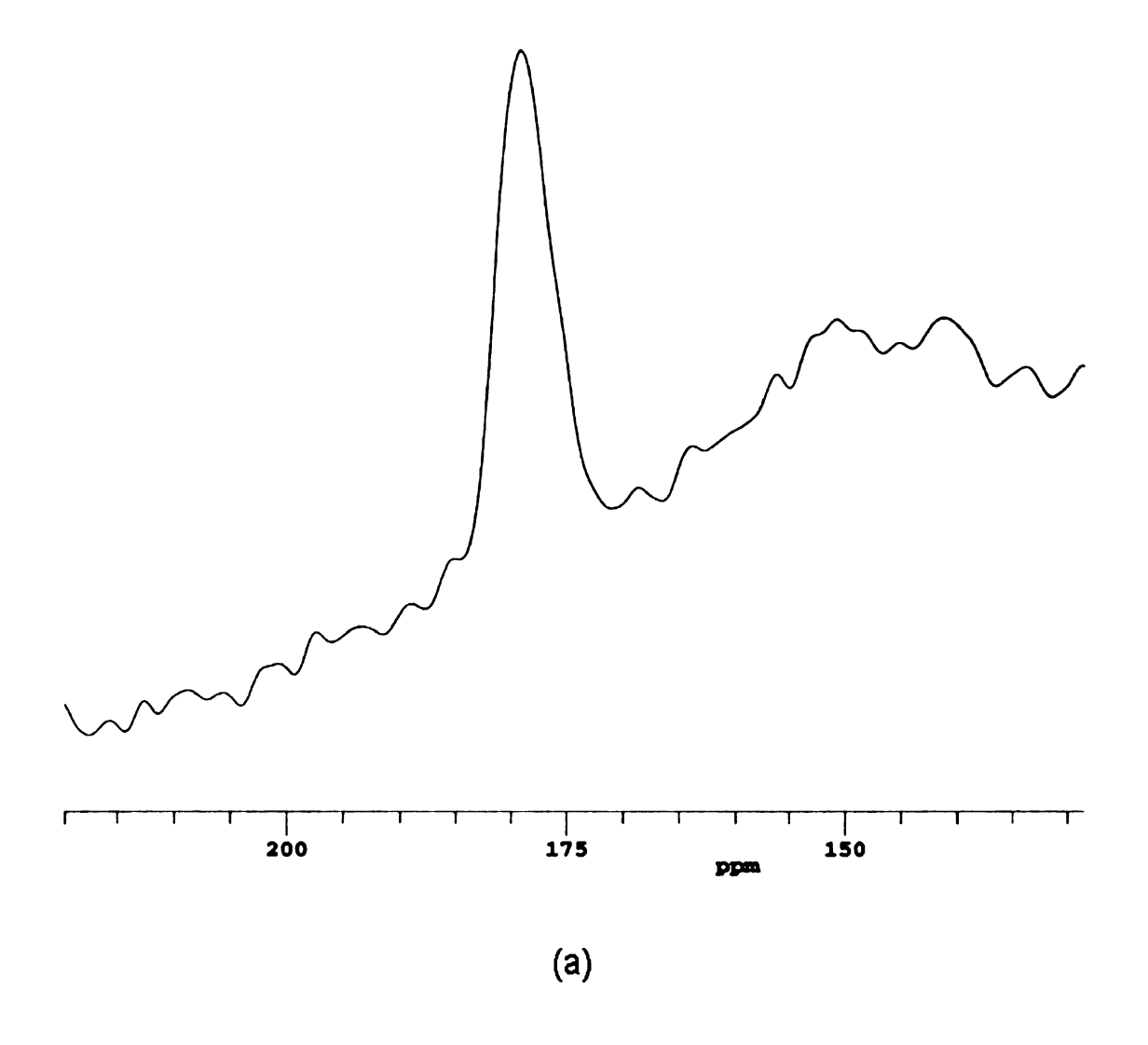
For membrane proteins or large soluble proteins (>100 kDa), Magic Angle Spinning (MAS) solid-state NMR provides structural biochemists with a means for obtaining information about local secondary structure. Taking advantage of the bacterial expression host's ability to incorporate a single 1-13C labeled amino acid during

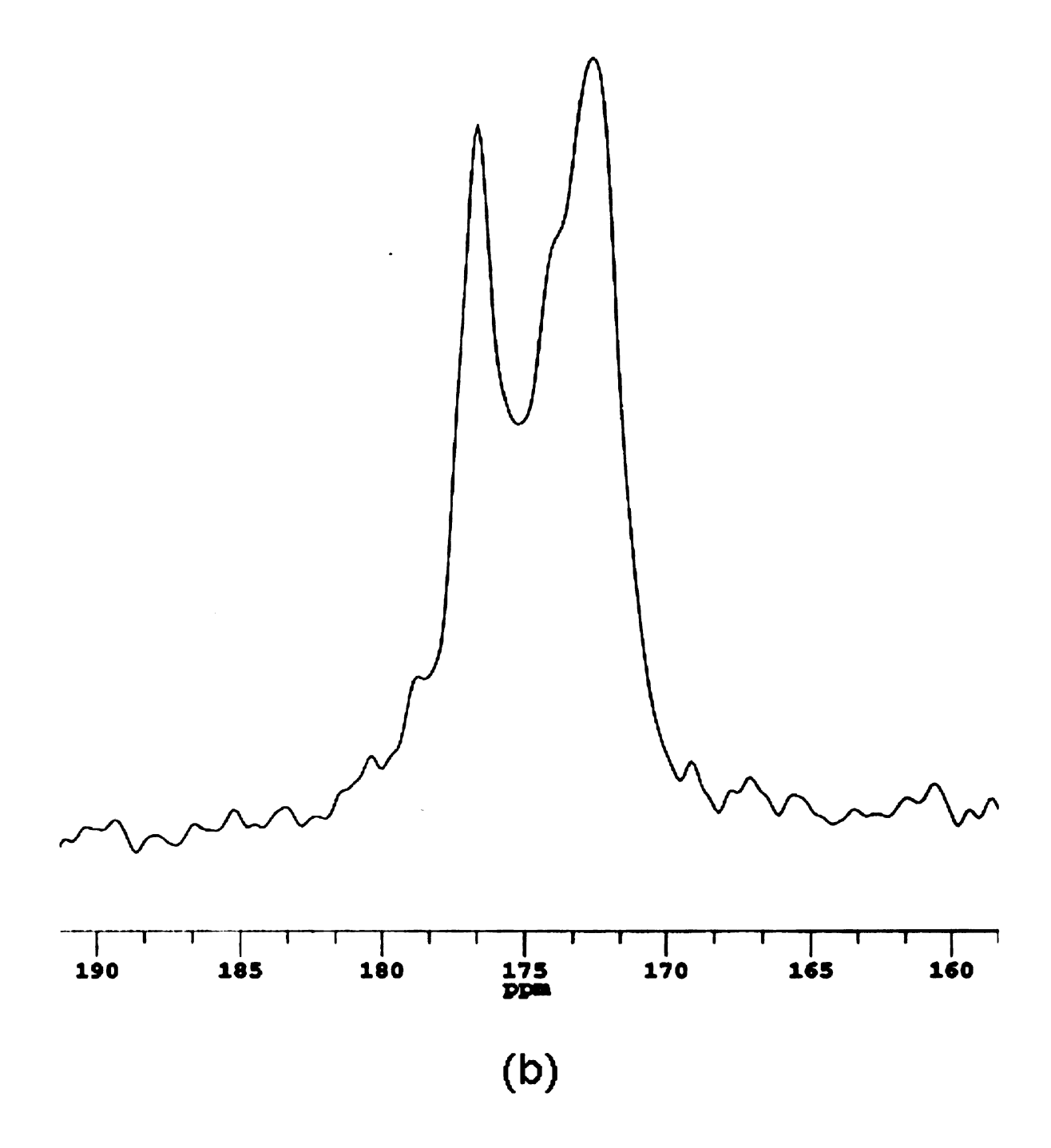
induction has facilitated the extraction of such information. Here, MAS is utilized to average out dipolar couplings and chemical shift anisotropies (CSAs) to generate nearly isotropic chemical shifts.

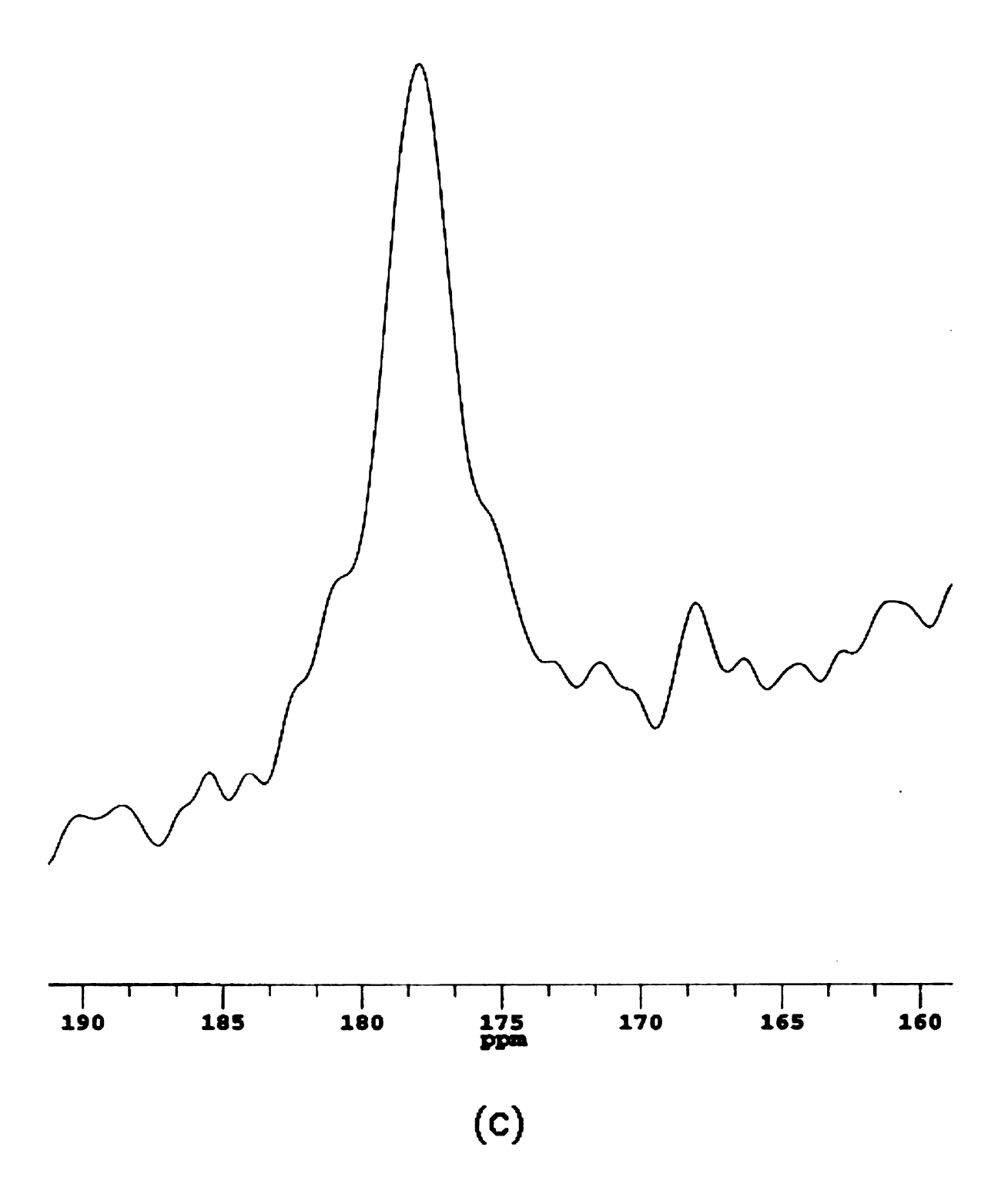
<sup>13</sup>C chemical shift (CS) measurements by cross-polarization (CP) MAS experiments enable one to probe local conformation at specific residues using the known correlation of CSs with local 2° structure [43]. The 1D-CPMAS experiment is a blanket approach to obtaining 2° structure because of the inability to label only one amino acid and the inherent line broadening associated with SSNMR. Simply stated, if the incorporated amino acid has more than one occurrence within the sequence, the resulting peak will represent a distribution of the CSs contributed by each residue. For nearly homologous proteins, this experiment presents an inexpensive and efficient means of extracting 2° structure for significant portions of the sequences.

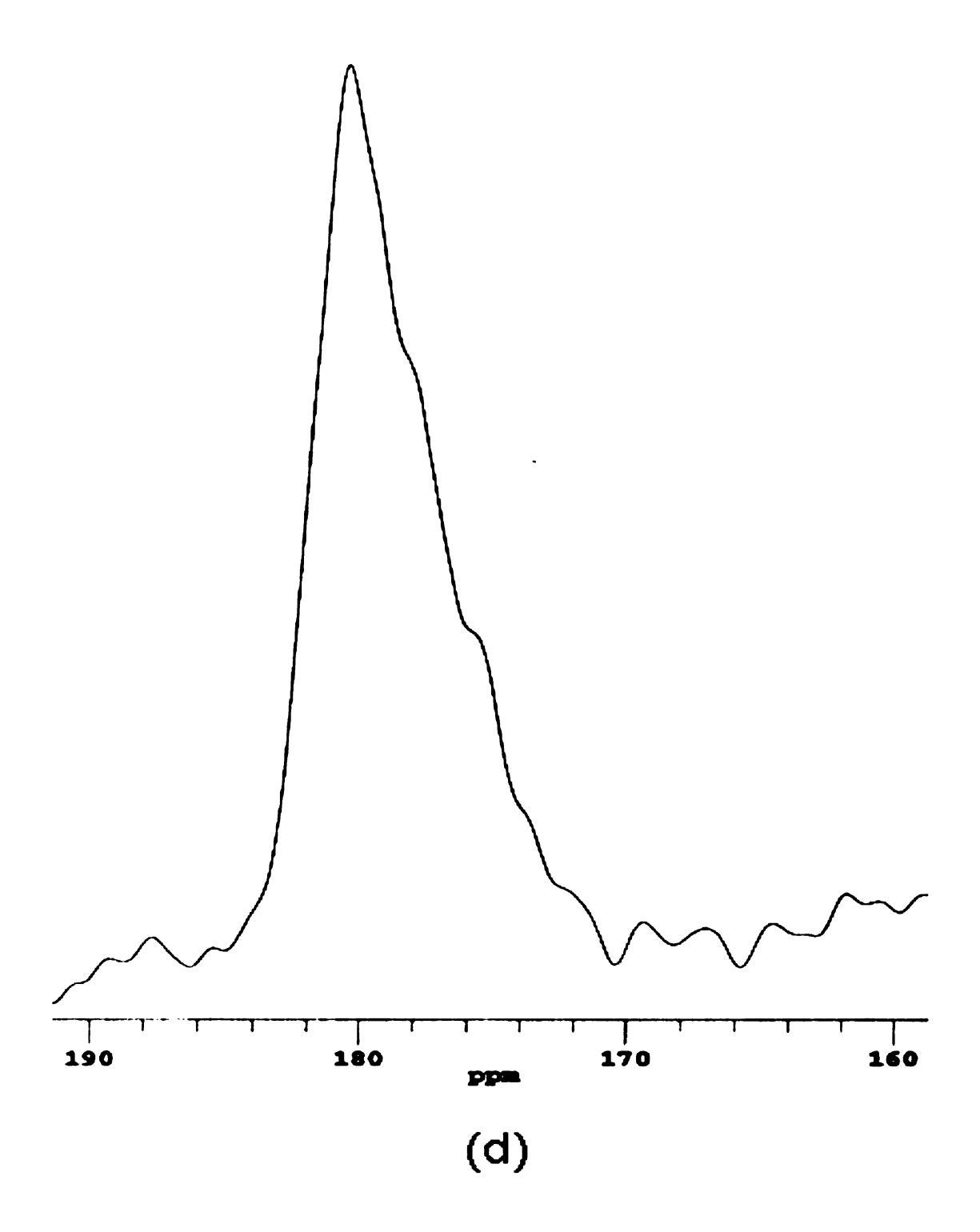
The rotational-echo double resonance (REDOR) filtering sequence [15] is a robust technique that enables one to obtain the 2° structure of a single, unique residue. Through backbone labeling of an existing unique pair of adjacent residues (e.g. <sup>13</sup>C=O and the adjacent <sup>15</sup>N-H), one utilizes this filtering sequence to examine the <sup>13</sup>C CS of only one residue. This information can then be directly compared to computational predictions of 2° structure to examine validity of the model of interest.

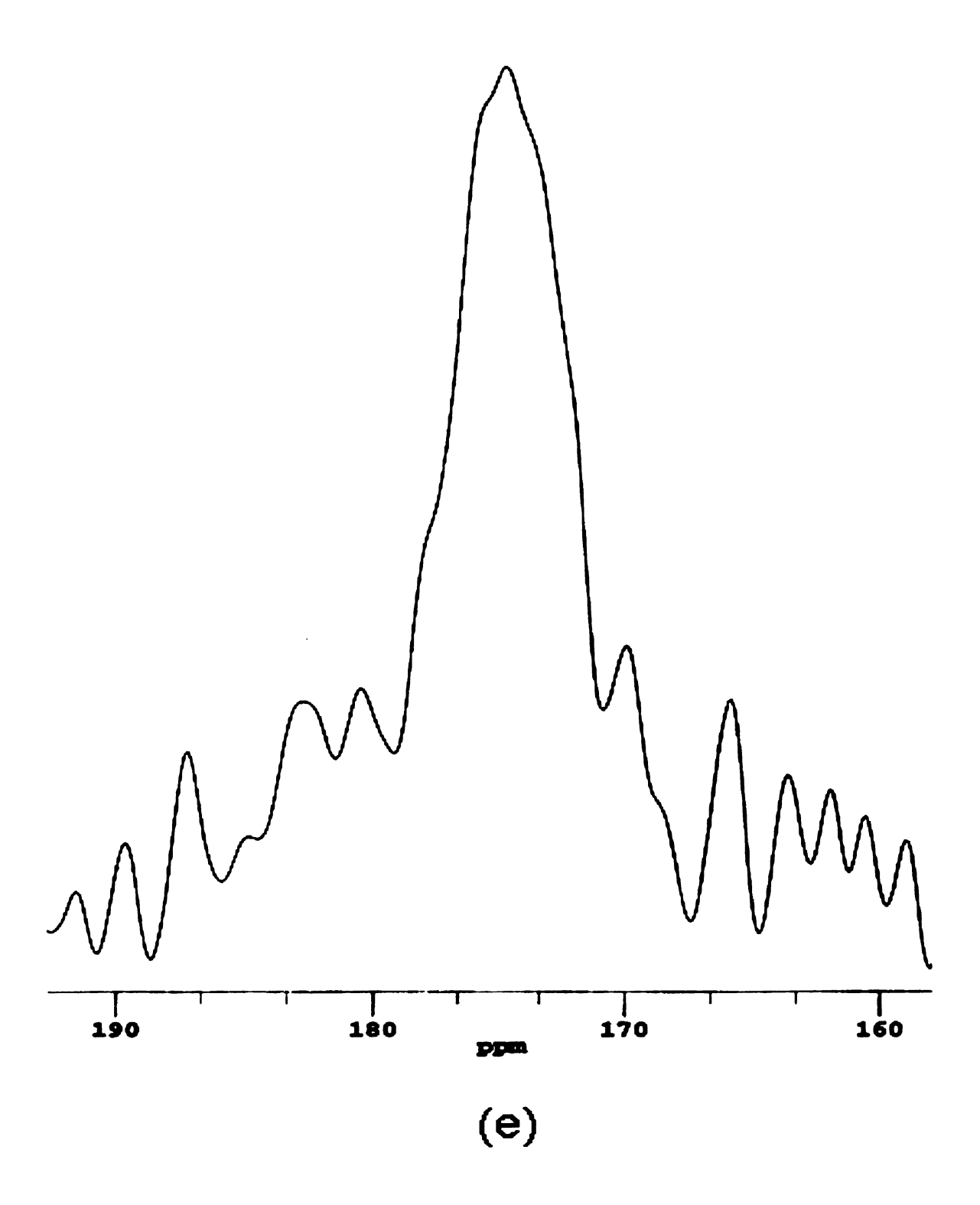
In this work, the contributions of both CPMAS and REDOR were examined on a Varian 400 MHz solid-state NMR spectrometer for comparison to the 2° structure predictions presented in section II.B. Pili formation was induced (as in section IV.A) for isotopically labeled HrpA from both P. syringae and E. amylovora (as in sections III.C and III.D). For CPMAS, HrpA from P. syringae was expressed with <sup>13</sup>C=O labeled Ala, Gly, Met, or Lys, and HrpA from E. amylovora was expressed with <sup>13</sup>C=O labeled Leu, Ala, or Gly (Figure 5.10). For REDOR, HrpA from P. syringae was expressed with <sup>13</sup>C=O Leu and  $^{15}$ N Ile to establish labeling of the Leu29/Ile30 unique residue pair (Figure 5.10). 40  $\mu$ L of the viscous samples were pipetted into a 2/3 volume 4 mm Teflon rotor. A quasi-solid was formed by slow-spinning (500 Hz) the rotor at -80°C in a 4 mm HCX probe. The spinning speed for the CPMAS and REDOR experiments was then ramped slowly to 8 kHz and the <sup>1</sup>H decoupling field was set at 100 kHz for the duration of acquisition. The resulting data were processed and phased (Figures 5.11 (a-g) and 5.12).

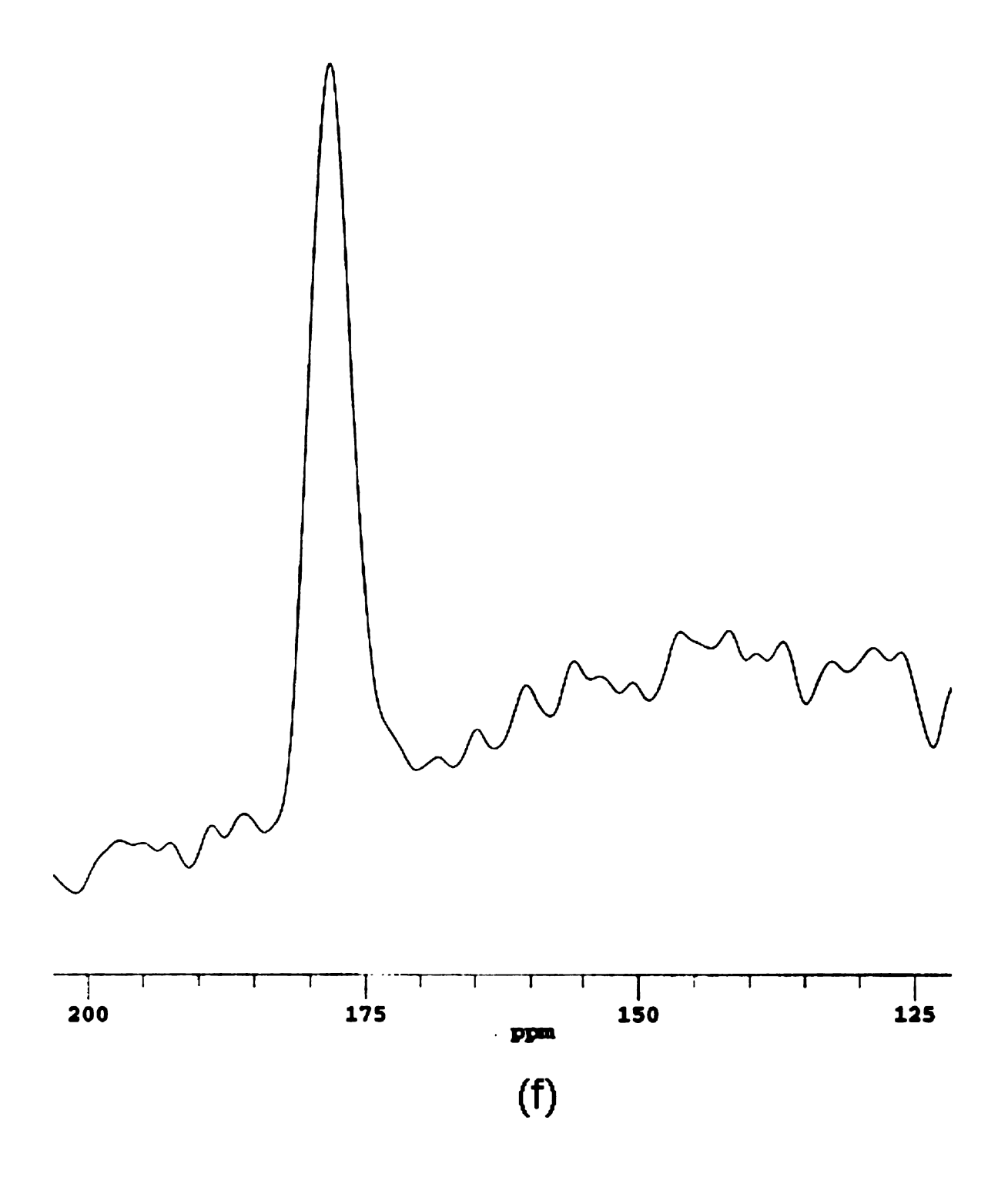


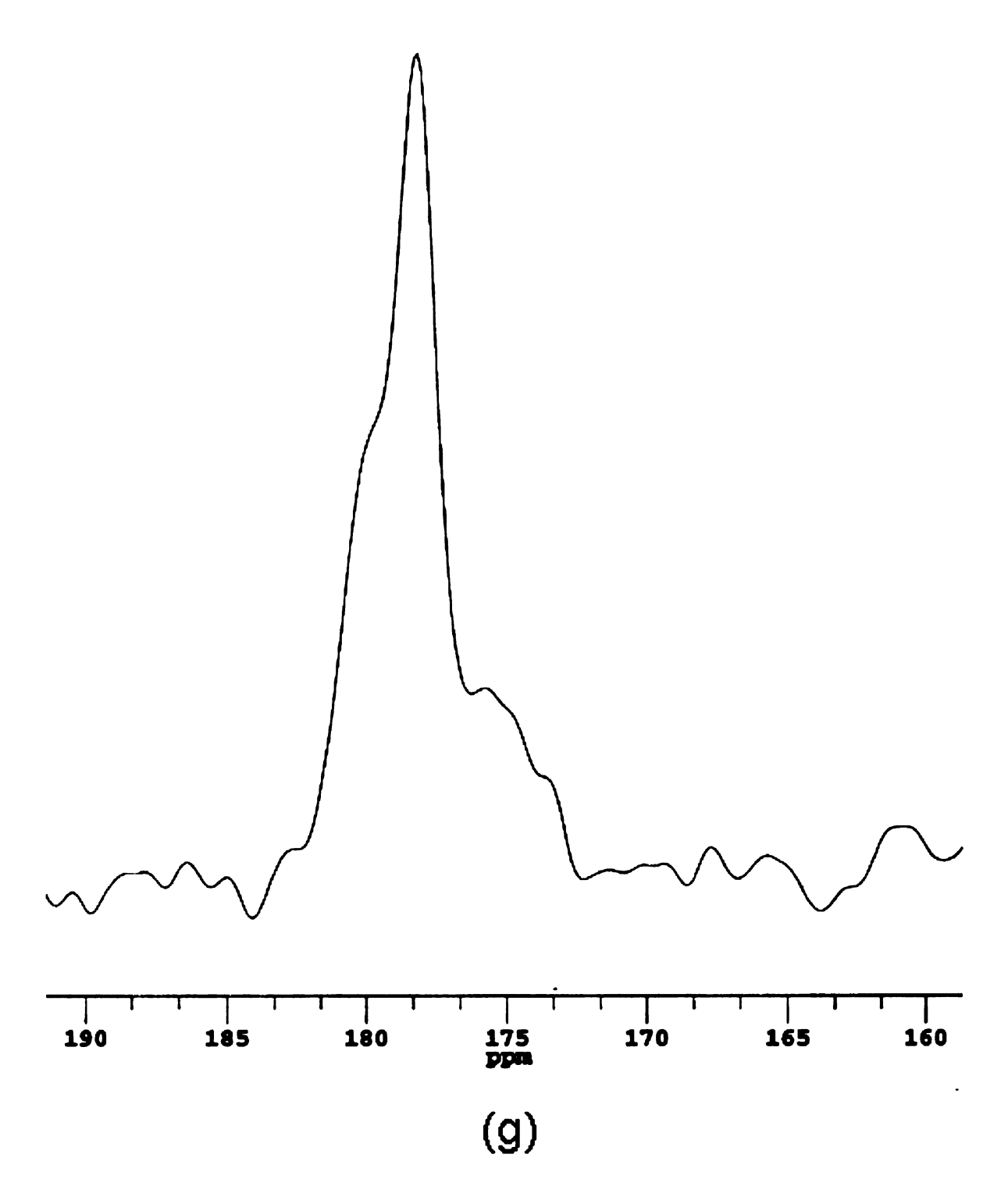












**Figures 5.11 (a-g)** CPMAS signals for single isotopically labeled, truncated, wild-type HrpA from *E. amylovora* (a-c) and *P. syringae* (d-g) pili. HrpA from *E. amylovora* was labeled with <sup>13</sup>C=O (a) Ala, (b) Gly, and (c) Leu, and HrpA from *P. syringae* was labeled with <sup>13</sup>C=O (d) Ala, (e) Gly, (f) Lys, and (g) Met.

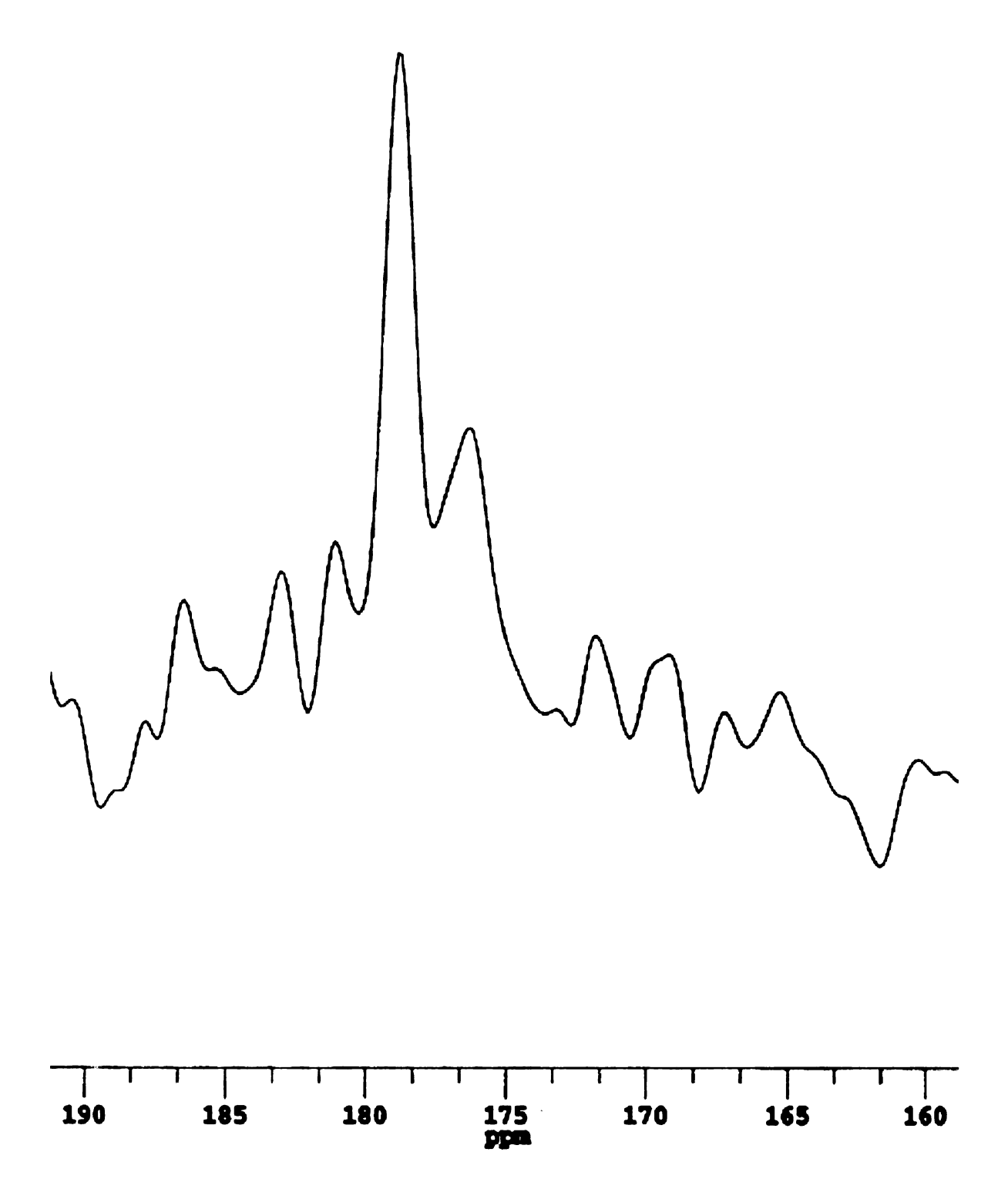


Figure 5.12 REDOR-filtered signal from the 1-<sup>13</sup>C Ile-<sup>15</sup>N Leu unique pair in the truncated, wild-type HrpA from *P. syringae* prepared pili.

Our isotopic labeling scheme exploited the homology of these two HrpA pilins and enabled us to obtain complementary, local  $2^{\circ}$  structure information spanning the majority of the individual sequences (Figure 5.13). The CS analysis of these spectra was correlated with the table of known carbonyl shifts [43]. The observed CSs show the HrpA from both strains to be predominantly  $\alpha$ -helical at the sites of the above residues. These results are consistent with the local  $2^{\circ}$  structure predictions for these residues and the presented CD data (Figures 5.8-10).

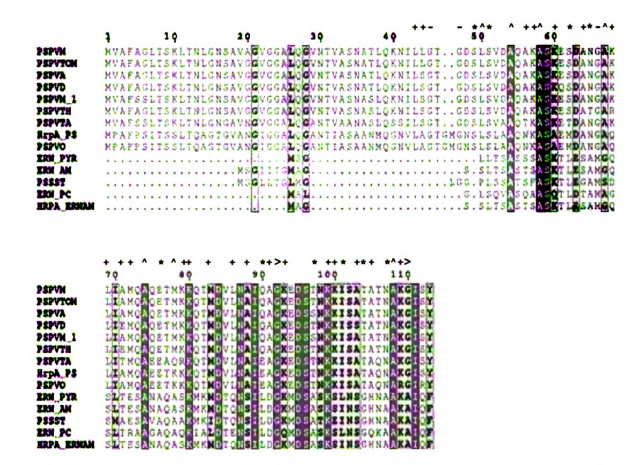


Figure 5.13 Local  $2^{\circ}$  structure information of multimeric HrpA by homology. For HrpA from *E. amylovora*, the "\*" and the "·" indicate residues involved in (1) an α-helix and (2) an α-helix or β-sheet, respectively. For HrpA from *P. syringae*, the "+" indicates residues involved in an α-helix. The "·" indicates residues involved in an α-helix that occur at the same position in both sequences. Finally, the "·" indicates residues having the same sequence position in both pilins, but are involved in (1) an α-helix or (2) an α-helix or β-sheet in *P. syringae* or *E. amylovora*, respectively.

#### VI. Conclusions

This work addresses the following topics: (1) the structure of monomeric and multimeric HrpA, (2) the physical interactions stabilizing the self-assembly of HrpA, (3) the agreement between the computational predictions and experimental observations, (4) methods for preparing stable multimers of uniform length, and (5) methods for disrupting pili to help guide development of small-molecule inhibitors. Through the use of various co-solvents and sundry hydrodynamic and spectroscopic methods, a series of complementary sets of data were obtained for interpretation and comparison to the computational model identified in section II.

Taken together, the data show that HrpA is intrinsically disordered as a monomer under native conditions but, upon self-assembly *in vitro* into the Hrp pilus, adopts stable  $2^{\circ}$  structure that is predominantly  $\alpha$ -helical. These results are consistent with both the computational model of self-assembly and the biological hypothesis for infection mediated by type III secretion systems. EM images of the Hrp pili assembled *in vitro* suggest that they are stable multimers of uniform outer diameter that could function as a conduit for Gram-negative bacterial effector proteins *in vivo*. HrpA appears to self-assemble only at pH values below its isoelectric point (i.e. when the HrpA monomer is positively charged). However, the self-assembly can be inhibited by lowering the pH far enough; for example, the pili will form *in vitro* at pH 7, but not at pH 5 [23]. This suggests that overcoming electrostatic repulsion is a key step in pilus formation. Since HrpA assembles into a long hollow cylinder of uniformly positive charge density,

Manning-type condensation of anions [27] within the cylinder will possibly occur to stabilize the electrostatic interactions. It is evident that hydrophobic interactions are also important for association, since different anions can promote or inhibit pilus formation *in vitro* according to the Hofmeister series [4].

#### VII. Works in Progress

We have shown that, in pilus formation, folding is coupled to the association of the pilin subunits. In future work, we intend to investigate the kinetics of this process (and its reversal) as well as performing further structural studies. Kinetics will be probed by fluorescence spectroscopy targeting the chromophore on the C-terminal aromatic residue, as described below. Structural studies will be approached by several methods. First, an N-terminal GFP-tagged HrpA construct is being prepared to be expressed and purified for fluorescence microscopy and TEM studies. This will allow us to monitor self-assembly optically and to determine the number of monomers per unit length within the pilus. Secondly, proline mutations of conserved residues predicted to have  $\alpha$ -helical 2° structure will provide information about residues thought to be important in pilus formation. Thirdly, X-ray crystallography has the potential to yield atomic-resolution, 3D structures for the wild-type, truncated HrpA and the co-crystallizable GFP-tagged HrpA. Finally, multimers of both the wild-type, truncated HrpA and the GFP-tagged HrpA will be investigated by electron fiber diffraction to obtain high-resolution, 3D structural information with respect to HrpA within the Hrp pilus.

## VII.A. Unfolding/Dissociation Kinetics of Multimeric HrpA from P. syringae

The truncated, wild-type HrpA from *P. syringae* has a single aromatic residue, a tyrosine, located at its C-terminus. The rate of unfolding of the truncated, wild-type multimer of HrpA from *P. syringae* will be determined by fluorescence spectroscopy. Through

monitoring the solvent quenching of the tyrosine fluorophore, the rate constant associated with this first-order process will be determined. The unfolding will be prompted by the presence of denaturants, either guanidine-HCl (Gdn-HCl) or urea, across the range of concentrations 0-6M. The Arrhenius behavior of the observed rate constant will also be monitored to determine the activation energy (E<sub>a</sub>) associated with the unfolding transition of the multimer.

A simple thermal unfolding experiment was designed to determine whether the rate of unfolding occurred on a time-scale measurable by our instrumentation. Through manual control of the Shimadzu UV-1700 spectrophotometer with the Peltier cell holder set to the observed unfolding transition temperature of 30°C (section V.D), preliminary kinetics data were collected on a multimeric HrpA sample as prepared previously for TM analysis in section V.D. The rate of unfolding was monitored as the change in absorbance at 287 nm with elapsed time. A plot of absorbance versus time (Figure 7.1) was generated and fit with the first-order exponential decay function given by

$$A(t) = A_0 \exp\left(-\frac{t}{\tau}\right) \tag{7}$$

where  $A_0$  is a pre-exponential factor, t is time, and  $\boldsymbol{\tau}$  is the lifetime.

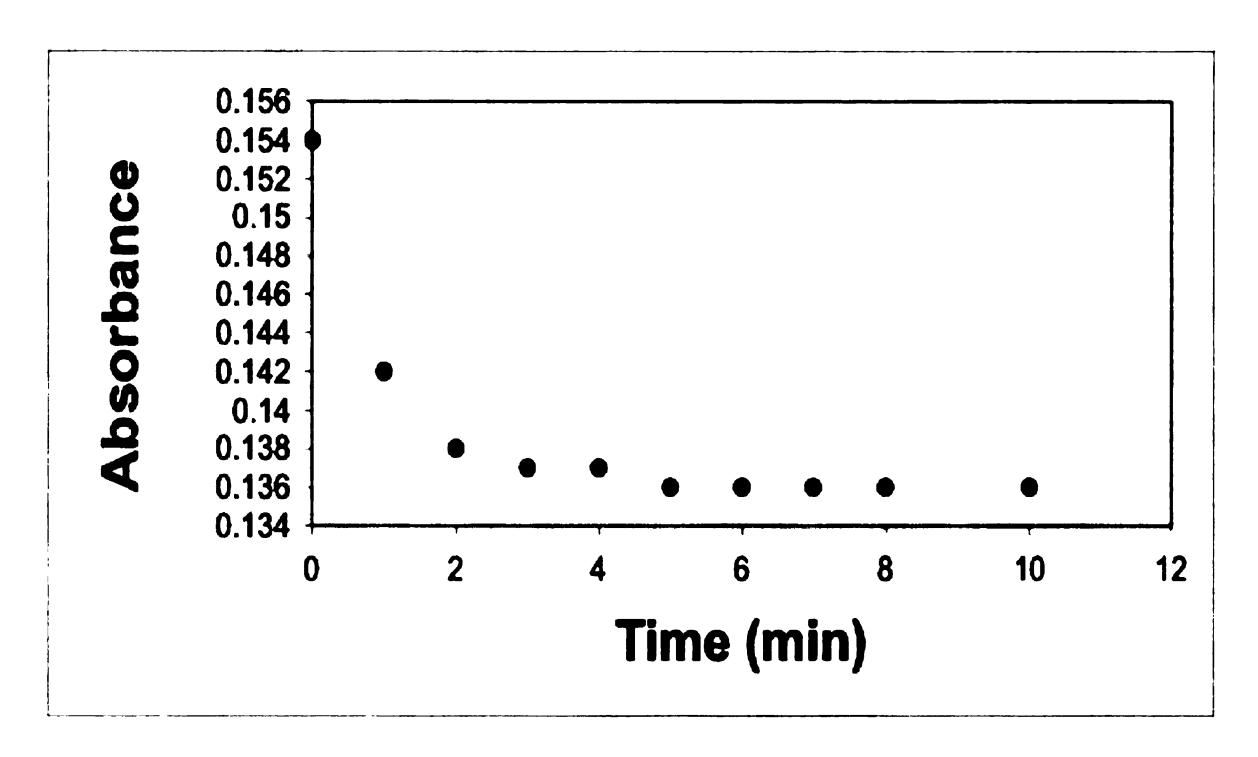


Figure 7.1 First-order exponential decay of Hrp pilus unfolding

The lifetime derived from the fit was 59 seconds. This result shows that the previously described fluorescence measurements are feasible, for the rate of unfolding of the HrpA multimer occurs on a time-scale detectable by the instrument.

VII.B. Preparation, Expression, Purification, and Fluorescence Microscopy of an N-terminal GFP-tagged HrpA Construct

The Invitrogen pRSETb expression vector [46] containing a (His)<sub>6</sub> tag, an enterokinase (EK) cleavage site, and the BamHI fragment of the green-enhanced S65T mutant GFP on the N-terminus, was donated generously by the laboratory of Dr. S. Ferguson-Miller. Using a Stratagene QuikChange site-directed mutagenesis kit, the C-terminal TAATAA stop codon sequence was mutated to TAGCAA to enable expression of a subsequent C-

terminal protein insert, and the NdeI restriction site of the pET28b expression vector N-terminal to the truncated, wild-type HrpA from *P. syringae* to the XhoI restriction site. The HrpA insert will be cloned into the pRSETb expression vector using the XhoI and HindIII restriction sites. This N-terminal GFP-tagged HrpA construct will be verified by DNA sequencing.

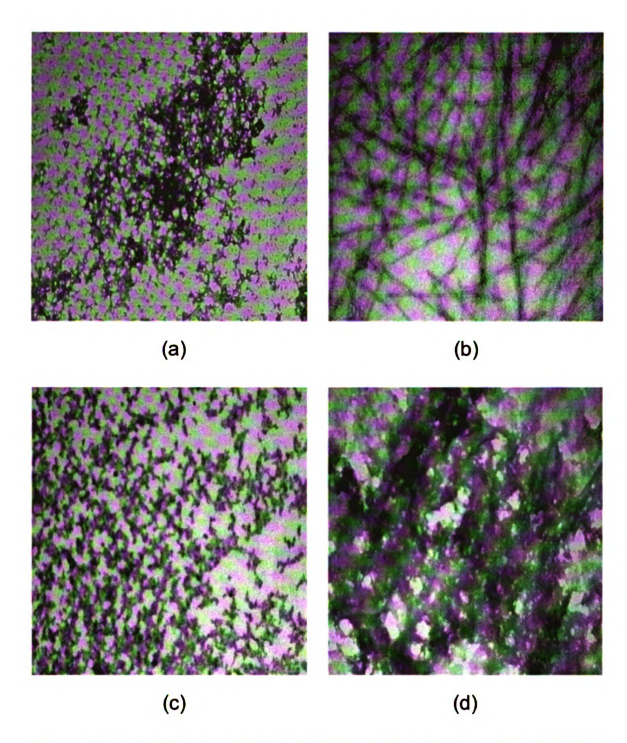
The GFP-tagged HrpA construct will be expressed by BL21:\(\lambda\)DE3 \(E.\) coli cells and purified according to the protocol outlined in section III. The monomeric form of the GFP-tagged HrpA complex is hypothesized to facilitate protein crystallization efforts. The use of GFP as a co-crystallizing agent could yield a crystal whose diffraction pattern is easily solved by molecular replacement of the GFP, a protein of known structure. In vitro preparation of multimeric HrpA will be verified by TEM. The resulting multimeric sample will be utilized by two methods. First, the sample will be examined by fluorescence microscopy. This experiment has the potential for determination of the number of HrpA monomers present within a stable multimer of specified length. And second, this multimer might facilitate high-resolution, 3D structure determination of HrpA, within the pilus, by fiber diffraction utilizing the oversampling method [30, 31], as described below. GFP would serve as a molecular replacement tool during analysis.

#### VII.C. Proline Mutations

Collectively,  $2^{\circ}$  structure predictions, TEM, CD, and SSNMR have provided evidence that shows the existence of  $\alpha$ -helical structure in HrpA when assembled in the pilus. It

was hypothesized that a disturbance in the  $\alpha$ -helical structure of HrpA would cause a dissociation of the pilus into its unstructured, monomeric subunits. It is well-understood that prolines disrupt  $\alpha$ -helices [38]. A series of proline mutants were selected for several highly conserved and predicted  $\alpha$ -helical residues, as well as a residue that rests in the random coil structure of the turn of the hairpin fold, in the truncated, wild-type HrpA from *P. syringae*. A54P and A64P reside near the N-terminus, D84P represents the turn of the predicted hairpin fold, and I89P and I101P reside near the C-terminus. These mutants were generated using a Stratagene QuikChange Site-directed Mutagenesis kit and verified by DNA sequencing.

Mutants I89P and I101P were expressed in BL21:λDE3 E. coli cells and purified according to the protocol outlined in Chapter 3. Samples containing either 100% mutant HrpA or a 1:1 molar equivalent mixture of the mutant and wild-type were prepared for each mutant, according to the protocol for in vitro pilus preparation presented in Chapter 4. The samples were plated on copper grids and negative stained with 2% aqueous phosphotungstic acid for TEM. Conventional light/dark field images by electron scattering were obtained (Figures 7.2 a-d).



Figures 7.2 (a-d) TEM images of (a) 189P mutant HrpA, (b) 1:1 molar ratio of 189P mutant and truncated, wild-type HrpA, (c) 1101P mutant HrpA, and (d) 1:1 molar ratio of 1101P mutant and truncated, wild-type HrpA in the presence of 50 mM NaH<sub>2</sub>PO<sub>4</sub> buffer pH 5.5 with 300 mM NaF.

As predicted, the samples containing pure I89P and I101P exhibited a negative result for pilus formation. The samples containing these mutants doped with wild-type HrpA were not so consistent. The sample of I89P doped with wild-type HrpA showed a positive result for pilus formation, as the formation of pili was not thwarted. By contrast, the sample of I101P doped with wild-type HrpA exhibited a dominant negative result for pilus formation.

One interpretation of these results is that the I101P mutant is able to associate with the wild-type pilus and inhibit its growth, however, the I89P mutant is neither able to self-assemble into the pilus nor associate with the wild-type pilus. To test the validity of this interpretation, it is necessary to check whether the I101P HrpA can be incorporated into the wild-type pilus. Preparation of samples containing both I101P HrpA and the GFP-tagged HrpA will hopefully provide insight into this process. The will enable a more definitive interpretation of the above TEM results. Applying the combination of TEM and fluorescence microscopy will show whether the wild-type, in fact, associates with the mutant.

Exploring the remaining mutants, in the manner described above, might provide some insight as to which residues are crucial to pilus formation and stability. The results of these experiments have the potential to guide development of small-molecule inhibitors that might render this TTSA ineffective.

VII.D. Atomic-resolution Structural Studies: X-ray Crystallography and Electron Fiber

Diffraction

An atomic-resolution structure of folded HrpA would be useful in determining the residues critical for folding and association. Several structure determination methods and their associated preliminary work will be discussed in the subsequent sections.

VII.D.i. Crystallization of Monomeric HrpA and X-ray Diffraction

Protein crystallization and X-ray diffraction has the potential to yield atomic-resolution three-dimensional structures of soluble proteins. Since crystallization requires that the protein of interest be well-structured and folded, the unstructured HrpA monomer seems unlikely to crystallize. It is not, however, beyond the realm of possibilities for the crystallization of such a protein to occur. There could exist a set of conditions that would induce HrpA to adopt some stable and folded intermediate state that would crystallize.

To pursue this possibility, we undertook preliminary crystallization trials of the truncated, wild-type HrpA from *P. syringae*. The (His)<sub>6</sub> tag cleaved form of the truncated, wild-type HrpA was purified and concentrated to 10 mg/mL in 15 mM Tris-HCl, 100 mM NaCl at pH 7.5 for crystallization condition screening. A Douglas Instruments Oryx-4 crystallization robot coupled to an XYZV Plateloader was used to set up sitting-drop vapor diffusion across the conditions contained within the Synergy screen [25] and

Hampton Screens I and II, provided by Hampton Research, Inc. 2  $\mu$ L drops, containing 50% protein stock solution, were prepared to sit on a pedestal in a closed, vapor diffusion chamber having a well-solution of 75  $\mu$ L of the respective crystallizing agents. The conditions were incubated at 5°C to assist in stabilizing the formation of  $\alpha$ -helices. The drops were visualized with a Leica MZ 12 stereoscope and possible crystal hits were recorded. After two days, conditions containing (1) 200 mM ammonium sulfate and 30% PEG 4000 (Figure 7.3) and (2) 200 mM ammonium sulfate and 30% PEG 8000 (not shown) yielded similar needle-like crystals that stained positively as protein crystals with the application of Izit dye.

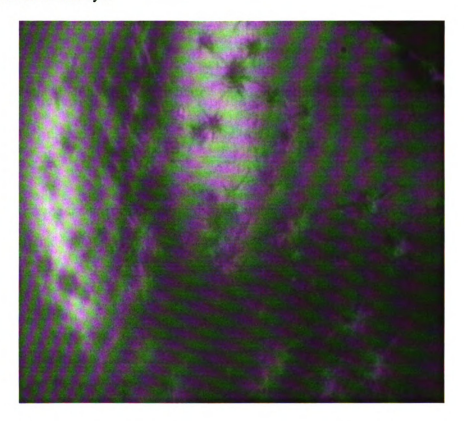


Figure 7.3 Photograph of needle-like crystals of (His)<sub>6</sub> tag cleaved, truncated, wild-type HrpA from *P. syringae* obtained after two days of incubation at 5°C in 200 mM ammonium sulfate and 30% PEG 4000.

These conditions showed very rapid, clustered crystal growth from a large number of nucleation sites. Current work focuses on optimizing these conditions to obtain diffraction quality crystals for structural analysis.

#### VII.E. Fiber Diffraction Studies of Multimeric HrpA

X-ray crystallography can provide atomic-resolution 3D structures of biomolecules only if they are crystallized. For non-crystalline macromolecules or biomolecular assemblies (e.g. fibrils), 3D structure determination is often an arduous task that requires many spectroscopic tools. J. Miao et al. have shown that phase retrieval from oversampled diffraction patterns of selected noncrystalline biological systems is feasible [30]. This method is believed to be able to open the door for high-resolution, 3D structure determination of complex and noncrystalline biological specimens [31]. In this work, we wish to examine the feasibility of introducing either X-ray or electron beam fiber diffraction as a means for determining the 3D high-resolution structure of the Hrp pilus as prepared in vitro.

We hypothesized that either pili or noncrystalline pilus-like intermediates could be prepared in a condition similar to the monomeric crystallization conditions presented in Figure 7.3. 100  $\mu$ L of 20 mg/mL uncleaved monomeric HrpA were exchanged from a pH 7.5 buffer containing 15 mM Tris-HCl and 100 mM NaCl to an aqueous solution of 200 mM ammonium sulfate. Buffer exchange was accomplished in two repetitive stages of 50-fold dilution in the phosphate buffer followed by concentration to the initial volume

in 5 mL Amicon 5000 MWCO centrifuge tubes. The resulting 50  $\mu$ L were transferred to a 0.5 mL Eppendorf tube. 72  $\mu$ L of 50% (w/v) PEG 4000 was pipetted to the HrpA solution to yield a final concentration of 30% (w/v). The resulting mixture was transferred to a 0.5 mL Eppendorf tube and frozen for 24 hours at -20°C. Upon thawing to 25°C, the sample developed an inherent viscosity. A 10% dilution was prepared for TEM according to the above freeze thaw cycle.

The unstained sample was plated on a copper grid for TEM analysis of its contents.

Conventional light/dark field images by electron scattering were obtained (Figure 7.4).



Figure 7.4 TEM image for truncated, wild-type HrpA from *P. syringae* in the presence of 200 mM ammonium sulfate and 30% PEG 4000.

The sample area presented in Figure 7.4 was subjected to the incident electron beam. A diffraction pattern was collected prior to ablation of the sample area (Figure 7.5).

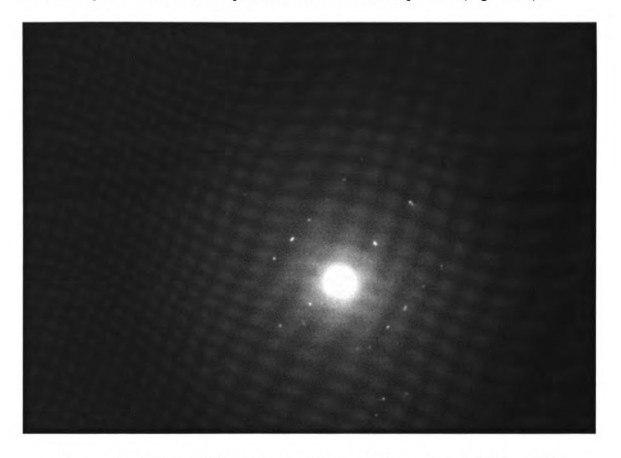


Figure 7.5 Electron diffraction image for the TEM sample area in Figure 7.4

This preliminary result shows that obtaining structural information from electron and/or X-ray fiber diffraction is possible. Current work focuses on extracting phase information and diffraction coefficients from this diffraction pattern to eventually index and characterize HrpA.

Appendix

## Appendix. Buffers and Stock Solutions

## NiA buffer:

50 mM NaH <sub>2</sub> PO <sub>4</sub>
300 mM NaCl
20 mM Imidazole
5 mM β-Mercaptoethanol
2 EDTA-free Protease Inhibitor tablets
pH 8.0

## NiA + 6 M Urea buffer:

50 mM NaH <sub>2</sub> PO <sub>4</sub>
300 mM NaCl
20 mM Imidazole
5 mM β-Mercaptoethanol
6 M Urea
2 EDTA-free Protease Inhibitor tablets
pH 8.0

## NiA + 600 mM NaCl buffer:

50 mM NaH <sub>2</sub> PO <sub>4</sub>
300 mM NaCl
20 mM Imidazole
5 mM β-Mercaptoethanol
600 mM NaCl
2 EDTA-free Protease Inhibitor tablets
pH 8.0

## NiB buffer:

50 mM NaH <sub>2</sub> PO <sub>4</sub>
300 mM NaCl
300 mM Imidazole
5 mM β-Mercaptoethanol
2 EDTA-free Protease Inhibitor tablets
pH 8.0

# 1 X Thrombin Cleavage buffer:

20 mM Tris-HCl	
150 mM NaCl	
2.5 mM CaCl <sub>2</sub>	
pH 8.4	

## Sterile Tris-EDTA (TE) buffer:

10 mM Tris-HCl	
1 mM EDTA	
pH 8.0	

## 5 X M9 Salts

30 g NaH <sub>2</sub> PO <sub>4</sub>
15 g KH <sub>2</sub> PO <sub>4</sub>
5 g NH <sub>4</sub> Cl
2.5 g NaCl
15 mg CaCl <sub>2</sub>
Autoclave to sterilize

## 1 X M9 Minimal Media

200 mL 5 X M9 Salts
1 mM Sterile MgSO <sub>4</sub>
0.2% (v/v) Sterile Glucose
Antibiotic
Dilute to 1 L with Sterile H <sub>2</sub> O

#### **BIBLIOGRAPHY**

- 1. Adamczak, R., Porollo, A., and Meller, J. (2005) Combining prediction of secondary structure and solvent accessibility in proteins. *Proteins: Struct. Funct. Genet.* **59**, 467-475.
- 2. Altschul, S.F., Gish, W., Miller, W., Myers, E.W., and Lipman, D.J. (1990) Basic Local Alignment Search Tool. J. Mol. Biol. 215, 403-410.
- 3. Altschul, S.F., Madden, T.L., Schaffer, A.A., Zhang, J.H., Zhang, Z. Miller, W., and Lipman, D.J. (1997) Gapped BLAST and PSI-BLAST: a new generation of protein database search algorithms. *Nucl. Acids Res.* 25, 3389-3402.
- 4. Baldwin, R.L. (1996) How Hofmeister ion interactions affect protein stability. *Biophys. J.* 71, 2056-2063.
- 5. Brown, I.R., Mansfield, J.W., Taira, S., Roine, E., and Romantschuk, M. (2001) Immunocytochemical localization of HrpA and HrpZ supports a role for the Hrp pilus in the transfer of effector proteins from Pseudomonas syringae pv. tomato across the host plant cell wall. *Mol. Plant Microbe Interact.* 14(3), 394-404.
- 6. Buttner, D. and Bonas, U. (2002) Port of entry the type III secretion translocon. *TRENDS in Microbiol.* **10**(4), 186-192.
- 7. Cantor, C.R. and Schimmel, P.R. Biophysical Chemistry. Part II. Techniques for the Study of Biological Structure and Function. W.H. Freeman, New York, 1980.
- 8. Cornelis, G.R. (2000) Type III secretion: a bacterial device for close combat with cells of their eukaryotic host. *Phil. Trans. R. Soc. Lond. B.* 355, 681-693.
- 9. Dickerson, R.E. and Drew, H.R. (1981) Structure of a B-DNA dodecamer: II Influence of base sequence on helix structure. *J. Mol. Biol.* 149, 761-786.
- 10. Emerson, S.U., Tokuyasu, K., and Simon, M. (1970) Bacterial flagella: polarity of elongation. *Science*. **169**, 190-192.
- 11. Espinosa, A., and Alfano, J.R. (2004) Disabling surveillance: bacterial type III secretion system effectors that suppress innate immunity. *Cell. Microbiol.* 6(11), 1027-1040.
- 12. Ghosh, P. (2004) Process of protein transport by the type III secretion system. *Microbiol. Mol. Biol. Rev.* 68(4), 771-795.

- 13. Goldberg, R.J. (1953) Sedimentation in the ultracentrifuge. J. Phys. Chem. 57, 194-202.
- 14. Gouet, P., Robert, X., and Courcelle, E. (2003) ESPript/ENDscript: extracting and rendering sequence and 3D information from atomic structures of proteins. *Nucl. Acids Res.* 31, 3320-3323.
- 15. Gullion, T. and Schaefer, J. (1989) Rotational-echo double-resonance NMR. J. Mag. Reson. 81, 196-200.
- 16. He, S.Y., Nomura, K., and Whitman, T.S. (2004) Type III protein secretion mechanism in mammalian and plant pathogens. *Biochimica et Biophysica Acta*. **1694**, 181-206.
- 17. Jin, Q. and He, S.Y. (2001) Role of the Hrp pilus in type III protein secretion in Pseudomonas syringae. *Science*. **294**, 2556-2558.
- 18. Jones, D.T., (1999) Protein secondary structure prediction based on position-specific scoring matrices. *J. Mol. Biol.* 292, 195-202.
- 19. Karplus, K., Karchin, R., Barrett, C., Tu, S., Cline, M., Diekhans, M., Grate, L., Casper, J., and Hughey, R. (2001) What is the value added by humen intervention in protein structure prediction? *Proteins: Struct. Funct. Genet.* Suppl. 5., 86-91.
- 20. Kelly, S.M., Jess, T.J., and Price, N.C. (2005) How to study proteins by circular dichroism. *Biochimica. et Biophysica Acta.* 1751, 119-139.
- 21. Koh, I.Y.Y., Eyrich, V.A., Marti-Renom, M.A., Przybylski, D., Madhusudhan, M.S., Eswar, N., Grana, O., Pazos, F., Valencia, A., Sali, A., and Rost, B. (2003) EVA: evaluation of protein structure prediction servers. *Nucl. Acids Res.* 31, 3311-3315.
- 22. Lebowitz, J., Lewis, M.S., and Schuck, P. (2002) Modern analytical ultracentrifugation in protein science: a tutorial review. *Protein Sci.* 11, 2067-2079.
- 23. Lee, Y.H., Kolade, O.O., Nomura, K., Arvidson, D.N., and He. S.Y. (2005) Use of dominant-negative HrpA mutants to dissect Hrp pilus assembly and type III secretion in *Pseudomonas syringae pv. tomato. J. Biol. Chem.* **280**(22), 21409-21417.
- 24. Li, C., Brown, I., Mansfield, J., Stevens, C., Boureau, T., Romantschuk, M., and Taira, S. (2002) The Hrp pilus of Pseudomonas syringae elongates from its tip and acts as a conduit for translocation of the effector protein HrpZ. *EMBO J.* 21(8), 1909-1915.
- 25. Majeed, S., Ofek, G., Belachew, A., Huang, C., Zhou, T., and Kwong, P.D. (2003) Enhancing protein crystallization through precipitant synergy. *Structure*. **11**, 1061-1070.

- 26. Mandal, P.K. and Majumdar, A. (2004) A comprehensive discussion of HSQC and HMQC pulse sequences. *Concepts Magn. Reson. Part A*, **20**A(1) 1–23.
- 27. Manning, G.S. (1969) Limiting laws and counterion condensation in polyelectrolyte solutions I. Colligative properties. *J. Chem. Phys.* **51**(3), 924-933.
- 28. Marlovits, T.C., Kubori, T., Sukhan, A., Thomas, D.R., Galan, J.E., and Unger, V.M. (2004) Structural insights inot the assembly of the type III secretion needle complex. *Science*. **306**, 1040-1042.
- 29. McGuffin, L.J., Bryson, K., and Jones, D.T. (2000) The PSIPRED protein structure prediction server. *Bioinformatics*. **16**, 404-405.
- 30. Miao, J., Ishikawa, T., Anderson, E.H., and Hodgson, K.O. (2003) Phase retrieval of diffraction patterns from noncrystalline samples using the oversampling method. *Phys. Rev. B.* 67, 174104-(1-6).
- 31. Miao, J., Kirz, J., and Sayre, D. (2000) The oversampling phasing method. Acta Cryst. **D56**, 1312-1315.
- 32. Mimori-Kiyosue, Y., Yamashita, I., Fujiyoshi, Y., Yamaguchi, S., and Namba, K. (1998) Role of the outermost subdomain of *salmonella* flagellin in the filament structure revealed by electron cryomicroscopy. *J. Mol. Biol.* **284**, 521-530.
- 33. Mota, L.J., Sorg, I., and Cornelis, G.R. (2005) Type III secretion: the bacteria-eukaryotic cell express. *FEMS Microbiol. Lett.* **252**, 1-10.
- 34. Notredame, C., Higgins, D.G., and Heringa, J. (2000) T-Coffee: a novel method for fast and accurate multiple sequence alignment. J. Mol. Biol. 302, 205-217.
- 35. Privalov, P.L. and Gill, S.J. (1998) Stability of protein structure and hydrophobic interaction. Adv. Protein. Chem. 39, 191-234.
- 36. Roine, E., Saarinen, J., Kalkkinen, N., and Romantschuk, M. (1997) Purified HrpA of Pseudomonas syringae pv. tomato DC3000 reassembles into pili. *FEBS. Lett.* 417, 168-172.
- 37. Samatey, F.A., Matsunami, H., Imada, K., Nagashima, S., Shaikh, T.R., Thomas, D.R., Chen, J.Z., DeRosier, D.J., Kitao, A., and Namba, K. (2004) Structure of the bacterial flagellar hook and implication for the molecular universal joint mechanism. *Nature*. 431, 1062-1068.
- 38. Schulman, B.A. and Kim, P.S. (1996) Proline scanning mutagenesis of a molten globule reveals noncooperative formation of a protein's overall topology. *Nat. Struct. Biol.* 3, 682-687.

- 39. Shiraki, K., Nishikawa, K., and Goto, Y. (1995) Trifluoroethanol-induced stabilization of the α-helical structure of β-Lactoglobulin: implication for non-hierarchical protein folding. *J. Mol. Biol.* **245**, 180-194.
- 40. Short Protocols in Molecular Biology, vol 1. Edited by Ausubel, F.M., Brent, R., Kingston, R.E., Moore, D.D., Seidman, J.G., Smith, J.A. and Struhl, K., John Wiley and Sons, 2002, p.1-2.
- 41. Sigle, W. (2005) Analytical transmission electron microscopy. *Annu. Rev. Mater. Res.* 35, 239-314.
- 42. Tampakaki, A.P., Fadouloglou, V.E., Gazi, A.D., Panopoulos, N.J., and Kokkinidis, M. (2004) Conserved features of type III secretion. *Cell. Microbiol.* 6(9), 805-816.
- 43. Wishart, D.S., Sykes, B.D., and Richards, F.M. (1991) Relationship between nuclear magnetic resonance chemical shift and protein secondary structure. *J. Mol. Biol.* 222, 311-333.
- 44. Yip, C.K. and Strynadka, N.C.J. (2006) New structural insights into the bacterial type III secretion system. *TRENDS in Biochemical Sciences*. **31**(4), 223-230.
- 45. <a href="http://www.novagen.com">http://www.novagen.com</a> (last accessed June 2006)
- 46. http://www.invitrogen.com (last accessed June 2006)

1
•
•

